Endogenous activity regulates the early development of adult-born neurons in the mouse olfactory bulb

Thesis submitted as requirement to fulfill the degree

„Doctor of Philosophy" (Ph.D.)

at the

Faculty of Medicine

Eberhard Karls University

Tübingen

by
Kaizhen Li

from
Shandong, China

June 2018

Oral defense date: 25.07.2018

Dean: Professor Dr. I. B. Autenrieth
1. Reviewer: Professor Dr. Olga Garaschuk
2. Reviewer: Professor Dr. Stefan Liebau

Table of contents

List of abbreviations

ANOVA	analysis of variance
AUC	area under the curve
BDNF	brain-derived neurotrophic factor
BW	body weight
CREB	cAMP response element-binding protein
DPI	days post injection
FOV	field of view
GABA	gamma-aminobutyric acid
GC	granule cell
GCL	granule cell layer
GFP	green fluorescent protein
GL	glomerular layer
i.m.	intramuscular injection
i.p.	intraperitoneal injection
IQR	interquartile range
JGC	juxtaglomerular cell
Kir	inward-rectifier potassium channel
Kv	voltage gated potassium channel
NeuN	neuronal nuclear antigen
NMDA	N-methyl-D-aspartic acid
OB	olfactory bulb
OD	odor deprivation
PBS	phosphate-buffered saline
pCREB	phosphorylated cAMP response element-binding protein
PFA	paraformaldehyde
PMT	photomultiplier
ROI	region of interest
RMS	rostral migratory stream
SEM	standard error of the mean
SVZ	subventricular zone
TDBL	total dendritic branch length
TH	tyrosine hydroxylase
TTX	tetrodotoxin
WPRE	woodchuck hepatitis virus posttranscriptional regulatory element
$\Delta R/R$	relative change in Twitch-2B ratio over time

1. Introduction

1.1 Adult neurogenesis in the mouse olfactory bulb

For many decades neuroscientists believed that post-embryonic brain is very stable and nothing will change (Cajal, 1914). In 1965, Altman and Das provided the first anatomical evidence for the presence of newly generated dentate granule cells in the postnatal rat hippocampus (Altman and Das, 1965). Afterward, Altman firstly described that the rostral migratory stream (RMS) located between the subventricular zone (SVZ) and the olfactory bulb (OB) also contains proliferating cells (Altman, 1969). The development of DNA incorporating and immunohistological techniques combined with confocal microscopy resulted in a burst of findings over adult neurogenesis which is mainly located in the subgranular zone of the dentate gyrus in the hippocampus and the SVZ of the lateral ventricles. A growing body of evidence pointed towards adult neurogenesis occurring in birds, mice, rats, monkeys and other species (Bond et al., 2015; Goldman and Nottebohm, 1983; Gould et al., 1998; Lledo et al., 2006; Lois and Alvarez-Buylla, 1994; Luskin, 1993; Zhao et al., 2008). However, whether adult neurogenesis exists in the human brain is still under debate. Three major studies showed the existence of adult neurogenesis in human hippocampus (Boldrini et al., 2018; Eriksson et al., 1998; Spalding et al., 2013), whereas two other studies proposed that adult neurogenesis in the human brain was not present or extremely low (Dennis et al., 2016; Sorrells et al., 2018). The direct *in vivo* proof for adult-born neurons in the human brain is needed. Adult neurogenesis in rodents is implicated in memory formation, e.g. pattern separation and encoding temporal context (for a review, see Aimone et al., 2014). Decoding the functional role of neurogenesis will provide us with fundamental knowledge about the olfactory and hippocampal systems and help to develop cell replacement therapy for human neurological diseases.

Olfaction provides information about danger, foods, reproductive status, social partners and triggers vital innate and learned behavioral responses. The olfactory system is of great importance to rodents. The rodent OB is a highly plastic brain region involved in the early processing of olfactory information and contains multiple layers and various types of neurons. Olfactory sensory neurons in the olfactory epithelium project their axons into the glomeruli of the OB and synapse onto the apical dendrites of glutamatergic mitral cells and tufted cells which send olfaction information to piriform cortex. Adult neurogenesis continuously adds new interneurons, juxtaglomerular cells (JGCs) and granule cells (GCs), into the OB circuits to modulate the activity of mitral and tufted cells. After birth in SVZ, adult-born neurons migrate along the RMS and arrive in the olfactory bulb 4-6 days later (Lois and Alvarez-Buylla, 1994), where they differentiate into local interneurons (Bagley et al., 2007; Lledo et al., 2006, 2004; Ming and Song, 2011; Zhao et al., 2008) (Figure 1). This long march of adult-born neurons is composed by tangential migration in the RMS, radial migration in the granule cell layer (GCL) and lateral migration in the glomerular layer (GL) (Liang et al., 2016).
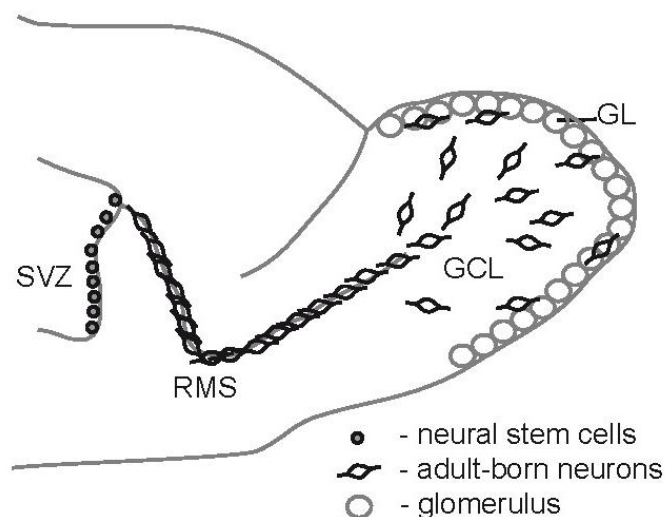

Figure 1. Schematic diagram illustrating adult neurogenesis in the mouse SVZ and OB. The neural stem cells in the SVZ give rise to adult-born neurons, which migrate tangentially along the RMS and radially in the OB. The Immature adult-born neurons differentiate into two

major types of interneurons: GCs integrating into the GCL and JGCs integrating into the GL. GCs, granule cells; JGCs, juxtaglomerular cells; GCL, granule cell layer; GL, glomerular layer; RMS, rostral migratory stream; SVZ, subventricular zone.

The majority of adult-born neurons integrate into the GCL becoming adult-born GCs, whereas 5-10% of cells migrate further to the GL becoming adult-born JGCs (Lledo et al., 2008; Lois and Alvarez-Buylla, 1994). Adult-born GCs gain simple unbranched dendrites before the stop of migration and then fully mature dendritic morphology during 15-30 days after birth (Petreanu and Alvarez-Buylla, 2002; Sailor et al., 2016). Adult-born JGCs take ~1.5 months to be morphologically mature and have the most dendritic branch numbers and intersections and longest branch length at about 45 days of age (Livneh and Mizrahi, 2011; Mizrahi, 2007). Although thousands of adult-born neurons reach the rodent OB every day, the size of the OB does not substantially change throughout life (Kaplan et al., 1985; Petreanu and Alvarez-Buylla, 2002). Approximately 50% of adult-born neurons undergo programmed cell death after arriving in the OB (Petreanu and Alvarez-Buylla, 2002; Winner et al., 2002).

So far, the mechanisms of the migration, differentiation, and survival of adult-born neurons into the pre-existing OB circuitry remain unclear. JGCs locate in the superficial layer of the OB and allow for studying the *in vivo* development of adult-born neurons. Our previous work has demonstrated that the adult-born JGCs have a unique radial-to-lateral switch in migration patterns when reaching the GL (Figure 2). All adult-born neurons are similar in their migratory behaviors in RMS and GCL, whereas the adult-born JGCs continue lateral migration in GL. This unique long-distance lateral migration has characteristic temporal (stop-and-go) and spatial (migratory, unidirectional or multidirectional) patterns, with a clear cell age-dependent decrease in the migration speed (Liang et al., 2016). The adult-born JGCs are highly mobile during the first week after arriving in the GL and all ceased moving at around 4 weeks of age. During this 3-4

weeks period which is also named as "pre-integration phase", the adult-born JGCs are vigorously migrating and likely seeking integration targets. Yet, the mechanism of this lateral migration of adult-born JGCs is still not elucidated.
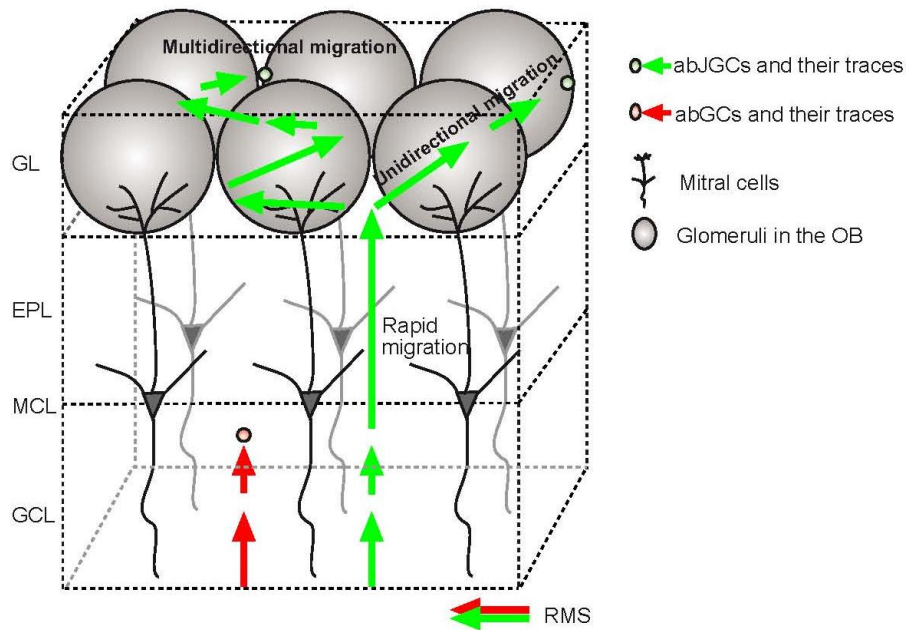
Figure 2. A model of the migration of the adult-born neurons in the OB. The adult-born GCs migrate purely radially (red arrows). Whereas GCs slow down to integrate into the GCL, the JGCs speed up to quickly traverse EPL. When reaching the GL, the adult-born JGCs switch to lateral migration, moving either unidirectionally or multidirectionally (green arrows). They gradually slow down, integrating some 1-2 glomeruli away from their initial entry site (modified from Liang et al., 2016).

1.2 The role of neuronal activity in the development of adult-born neurons

Neuronal activity is critical for sculpting the intricate circuits of the nervous system during development of perinatal brain and refinement and maintenance of adult brain. Neural activity occurs in primary sensory areas in two forms: endogenous (spontaneous) activity independent of sensory input and sensory-driven activity (Zhang and Poo, 2001). Endogenous activity is generated by the nervous system itself before the sensory input is available and

represents a hallmark of the developing nervous system (Hanganu-Opatz, 2010; Penn and Shatz, 1999). Endogenous activity and related or concomitant intracellular Ca^{2+} signaling are abundant during perinatal development and are well known for their key roles in neuronal proliferation, migration, differentiation, and wiring (Spitzer, 2006). Once sensory input becomes available, sensory-driven activity starts to shape neuronal connections and functions. Both types of neuronal activity regulate the development of neural circuits and nervous system.

1.2.1 Endogenous neuronal activity

During perinatal neurogenesis, when immature neurons start to develop voltage-dependent ion channels and sensory input is not available, endogenous activity controls the formation of the developing neural networks, e.g. the proliferation of neural stem and progenitor cells, the migration, the morphological development and the initial integration of immature neurons (Luhmann et al., 2016; Rosenberg and Spitzer, 2011). The spontaneous Ca^{2+} waves correlate the proliferation of radial glial cells in the cortical ventricular zone and sequentially regulate neuronal production (Owens et al., 2000; Owens and Kriegstein, 1998; Weissman et al., 2004). Endogenous activity is critical for neuronal migration and maturation in the developing neocortex (Bando et al., 2016, 2014; Cancedda et al., 2007; De Marco García et al., 2011; Hurni et al., 2017). Spontaneous Ca^{2+} transients control the migration speed and directionality of postnatally generated neuroblasts in the RMS (García-González et al., 2017; Platel et al., 2007). Moreover, the blockade of Ca^{2+} influx leads to the hindrance of cell migration (Komuro and Rakic, 1996; Komuro et al., 2015). Spontaneous Ca^{2+} transients act via multiple molecular mechanisms to regulate neurite extension and dendritic morphology development (Chen and Ghosh, 2005; Gu and Spitzer, 1995). During early neuronal development, the increase of

intracellular Ca^{2+} promotes the growth of dendrites and local Ca^{2+} signaling controls the branching or retraction of dendrites (Chevaleyre et al., 2002; Lohmann and Wong, 2005; Rajan and Cline, 1998).

Endogenous activity and spontaneous Ca^{2+} signaling are also present during all stages of adult neurogenesis in the SVZ-OB. Intercellular Ca^{2+} waves propagating bidirectionally via gap junctions between neural progenitor cells and neighboring astrocytes in the SVZ may play an active role in shaping the behavior of neural progenitor cells (Lacar et al., 2011). Migrating neuroblasts also exhibit spontaneous Ca^{2+} transients driven by voltage-gated L-type Ca^{2+} channels (Darcy and Isaacson, 2009) in the subependymal layer of OB. Interestingly, increasing endogenous activity facilitates, while decreasing endogenous activity compromises the survival rate of adult-born GCs in the OB (Lin et al., 2010). Our recent finding demonstrated that spontaneous Ca^{2+} transients are ubiquitously present in the immature adult-born JGCs *in vivo* (Maslyukov et al., 2018). This endogenous activity is tetrodotoxin (TTX)-sensitive, relatively insensitive to anesthesia and is robustly present in the awake state during the whole recording time period (approximately 5 weeks). The strength of endogenous activity in the adult-born JGCs exhibits a bell-shaped dependence on cell's age, peaking around 3 weeks after birth (Maslyukov et al., 2018). However, the role of this endogenous activity in the development of adult-born neurons is not explored yet.

1.2.2 Sensory-driven neuronal activity

Sensory-driven neuronal activity is a keystone in sculpting the coarse neural circuits in the postnatal brain. The development of adult-born neurons is also dependent on sensory-driven activity, however, to which extent the adult neurogenesis is regulated by sensory-driven activity still needs further

investigations. The generation of neuroblasts in the SVZ seems to be independent of sensory input (Kirschenbaum et al., 1999). The migration of neuroblasts in the adult RMS was not affected by deprivation of sensory input (Kirschenbaum et al., 1999; Petreanu and Alvarez-Buylla, 2002). Moreover, odor deprivation did not change the morphology of adult-born neurons (Dahlen et al., 2011; Mizrahi, 2007; Petreanu and Alvarez-Buylla, 2002). These data suggested that sensory input is not essential for early-phase development of adult-born neurons. Yet, several reports have demonstrated the important role of extrinsic signals, especially odorant-induced activity, on the fate determination and maintenance of the adult-born neurons in the OB (Bastien-Dionne et al., 2010; Fiske and Brunjes, 2001; Frazier-Cierpial and Brunjes, 1989). Manipulations that could reduce activity: naris occlusion (Corotto and Henegars, 1994; Cummings et al., 1997; Mandairon et al., 2006; Pothayee et al., 2017), naris cauterization and benzodiazepine treatment (Yamaguchi and Mori, 2014), deletion of sensory inputs from olfactory sensory neurons (Petreanu and Alvarez-Buylla, 2002), axotomy of olfactory receptor neurons (Mandairon et al., 2003), or chemical ablation of olfactory (Denizet et al., 2017) decreased survival and integration of adult-born neurons. Conversely, manipulations that could increase olfactory activity: odor enrichment (Bovetti et al., 2009; Rochefort et al., 2002), odor discrimination training (Alonso et al., 2006; Moreno et al., 2009), or olfactory associated tasks (Sultan et al., 2011) increased the survival and integration of adult-born neurons.

1.3 CREB signaling pathway in adult neurogenesis and neuronal development

The cAMP-responsive element binding protein (CREB) is a transcription factor regulating diverse processes as neuronal development, synaptic plasticity, and neuronal survival as well as learning and memory (Flavell and Greenberg, 2008;

Sakamoto et al., 2011; West and Greenberg, 2011). Mice with deletion of CREB died immediately after birth (Rudolph et al., 1998). CREB plays a critical role in the development of the central nervous system and is important for neuronal growth and survival (Lonze et al., 2002). CREB function as a Ca^{2+}-inducible transcription factor and subsequently facilitate the expression of various activity-dependent genes, for example, the expression of immediate early genes activated by neurotransmitters (for a review, see Shaywitz and Greenberg, 1999). This CREB mediated transcription requires its phosphorylation on Ser133 induced by various extracellular signals, for example, the Ca^{2+} influx into neurons (Kornhauser et al., 2002; Lonze and Ginty, 2002). The activated form of CREB, pCREB, promotes transcription of many target genes, e.g. insulin-like growth factor 1 (IGF-1), nerve growth factor (NGF), and brain-derived neurotrophic factor (BDNF) which are important for neuronal differentiation and survival (Dworkin and Mantamadiotis, 2010).

CREB signaling pathway plays critical roles in both perinatal and adult neurogenesis. In the brain development of zebrafish, pCREB has been shown to be present throughout the embryonic brain and concentrated in the neurogenic zones (Dworkin et al., 2007). This suggested the important function of pCREB in the neural system development. Previous reports provided evidence from rodents that CREB regulates differentiation, morphogenesis, and survival of adult-born neurons in the OB (Giachino, 2005; Herold et al., 2011) and hippocampus (Fujioka, 2004; Jagasia et al., 2009; Nakagawa et al., 2002). Moreover, inhibition of endogenous CREB activity blocked ischemia-induced survival of neural precursors in the dentate gyrus (Zhu et al., 2004). Conversely, the activation of CREB increased the number of survived hippocampal adult-born neurons (Zhu et al., 2004). In conclusion, CREB signaling pathway positively regulates the development and maturation of adult-born neurons.

1.4 Potassium channels in adult-born neurons of the OB

Numerous publications have reported various regulators of adult neurogenesis. However, less is known about the ion channels in the neuroblasts and immature neurons. Neural stem cells in the SVZ have a more negative resting membrane potential caused by abundant inward-rectifier potassium channels (Kir) and low input resistance caused by numerous leaking channels (Figure 3). Migrating neuroblasts in the RMS possess higher resting potential and input resistance than neural stem cells. This change might be a result of the down-regulation of Kir channels and gap junctions. Neuroblasts predominantly express Kv1 isoforms, a type of voltage-gated potassium channels, including Kv1.1, Kv1.2, and Kv1.6 (Wang, 2003). Adult neuroblasts exhibit no substantial voltage gated sodium current (Belluzzi et al., 2003; Carleton et al., 2003; Liu et al., 2009; Walker et al., 2007). To date, delayed rectifying K^+ currents are the only known voltage-gated channel currents found in the adult neuroblasts (Belluzzi et al., 2003; Yasuda and Adams, 2010). In the OB, the immature adult-born neurons quickly express a suite of ion channels which characterize interneuron properties and obtain the ability to fire first truncated and then full action potentials. Ion channel expression in maturing neurons is accompanied by a decrease of input resistance.

Kir2.1 is an inward rectifying potassium channel encoded by the *KCNJ2* gene. Kir2.1 has a substantial open probability at resting membrane potential. Kir2.1 overexpression was demonstrated to significantly decrease the resting membrane potential but not affecting the spiking pattern of the neuron and thus widely used as a tool to suppress neuronal excitability (Cancedda et al., 2007; De Marco García et al., 2011; Gu et al., 2003; Johns et al., 1999; Nitabach et al., 2002; Yu et al., 2004).
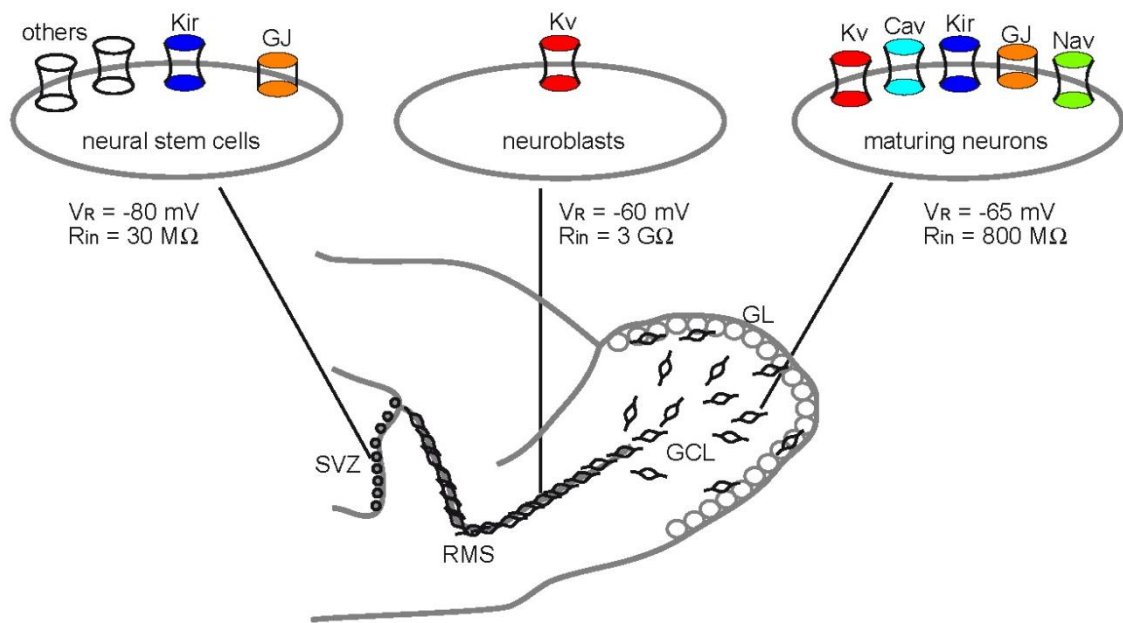
Figure 3. A graphic chart illustrating the changing of resting membrane properties and functional ion channel expression patterns of adult-born neurons during neuronal maturation in the mouse OB. Migrating neuroblasts and immature adult-born neurons have only very few ion channels and characterized by high input resistance. NSC, neural stem cell; Kv, voltage-gated potassium channels; Kir, inward rectifying potassium channels; GJ, gap junction; V_R, resting membrane potential; R_{in}, input resistance.

The voltage-gated potassium channel Kv1.2 encoded by the *KCNA2* gene belongs to the delayed rectifier class of potassium channels enabling efficient repolarization after an action potential. Genetic mutations of Kv1.2 lead to an alteration of endogenous neuronal activity and give rise to neurological disorders in humans, e.g. epilepsy (Syrbe et al., 2015). The overexpression of Kv1.2 is predicted to alter spike-timing-dependent plasticity which sequentially affects the connection strength between neurons (Gütig and Sompolinsky, 2006). Taken together, the characterized expression profiles of potassium channels enable the adult-born neurons to gain proper electrophysiological properties during certain time period and are important for electrical maturation. Any manipulation perturbing the potassium channel expression patterns may change the

electrophysiological properties of the adult-born neurons (Cameron et al., 1995; Lin et al., 2010; Parent et al., 1997).

1.5 Aim

The aim of the present study is, therefore, to investigate **the roles of endogenous and sensory-driven activity in regulating the development of adult-born neurons in the mouse olfactory bulb**. We will analyze which neuronal activity regulates i) the lateral migration, ii) the morphogenesis, and iii) the survival of adult-born JGCs and iv) which molecular signaling pathway is involved in the development of adult-born JGCs.

2. Materials and Methods

2.1 Construction of lentiviral vectors

All lentiviral vectors (Figure 4) are based on FUGW backbone (Lois et al., 2002) (plasmid #14883, Addgene). The EGFP in the original FUGW plasmid was replaced by a Ca^{2+} indicator Twitch-2B at BamHI and EcoRI restriction sites to generate FUW-Twitch-2B, which was used in the *in vivo* odor deprivation and immunostaining experiments. Afterward, Kv1.2wt-T2A or Kir2.1wt-T2A fragment was magnified by PCR (Phusion High-Fidelity PCR Kit, New England Biolabs) from plasmid pcDNA3-Kv1.2wt (a gift from Holger Lerche lab, Tübingen) and Mgi-Kir2.1wt (a gift from Carlos Lois lab, Caltech) and inserted into FUW-Twitch-2B between XbaI and BamHI restriction sites. In the forward primer of Kir2.1wt, a restriction site of NheI was used which has compatible cleavage end with XbaI.
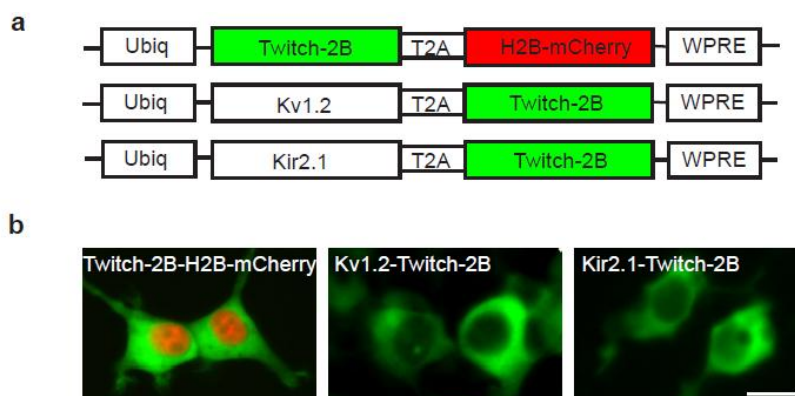
Figure 4. Schematic diagram illustrating the lentivirus-based bicistronic expression system of Twitch-2B and nuclear mCherry, Kv1.2, or Kir2.1. a, Schematics of the lentiviral constructs used in this study. **b,** Sample images showing the transient expression of the lentiviral vectors in HEK293 cells, which are clearly indicating the cytosol distribution of Twitch-2B and nuclear-located mCherry. Scale bar = 10 µm.

To construct Lenti-Twitch-2B-T2A-H2B-mCherry, which served as control: (i) the sequence of nuclear-located protein H2B (source plasmid H2B-strawberry,

plasmid #20970, Addgene) was subcloned into FUGW to generate Lenti-H2B-GFP with BamHI and AgeI restriction sites. (ii) GFP was replaced by mCherry with AgeI and EcoRI restriction sites. (iii) a T2A sequence was introduced after Twitch-2B by PCR and insertion between BglII and NotI in Rv-CAG-Twitch-2B plasmid. (iv) H2B-mCherry-WPRE was subcloned into Rv-CAG-Twitch-2B-T2A with NotI and XhoI to generate Rv-CAG-Twitch-2B-T2A-H2B-mCherry. (v) the whole cassette Twitch-2B-T2A-H2B-mCherry was subcloned to FUW-Twitch-2B at XbaI and XhoI sites to generate Lenti-Twitch-2B-T2A-H2B-mCherry.

Table 1. All primers used for the construction of lentiviral vectors.

Primer list	Sequence
Kv1.2wt-T2A forward	5'-GCTCTAGAGCCACCATGACAGTGGCCACCGG-3'
Kv1.2wt-T2A reverse	5'-CGGGATCCTGTGGGCCAGGATTCTCCTCGACGTCACCGCATGTTAGCAGACTTCCTCTGCCCTCTCCACTGCCTACCGGGACATCAGTTAACATTTTGGT-3'
Kir2.1wt-T2A forward	5'-CTAGCTAGCATGGGCAGTGTGAGAACCA-3'
Kir2.1wt-T2A reverse	5'-CGGGATCCTGTGGGCCAGGATTCTCCTCGACGTCACCGCATGTTAGCAGACTTCCTCTGCCCTCTCCACTGCCTACCGGTATCTCCGATTCTCGCCTTAA-3'
H2B forward	5'-CGCGGATCCGCCACCATGCCTGAACCCTCTAAGTCT-3'
H2B reverse	5'-CCACCGGTGCCACCTTAGAGCTAGTGTACTTGGTAACTGC-3'
mCherry forward	5'-CCACCGGTcGCCACCATGGTGAGCAAGGGC-3'
mCherry reverse	5'-CGGAATTCGCCACCTTACTTGTACAGCTCGTCCAT-3'
Twitch-2B-T2A forward	5'-GAAGATCTTCGGCGACTCCGACAC-3'
Twitch-2B-T2A reverse	5'-ATGCGGCCGCTGGGCCAGGATTCTCCTCGACGTCACCGCATGTTAGCAGACTTCCTCTGCCCTCTCCACTGCCTACCGGATCCTCAATGTTGTGACGGAT-3'
H2B-mCherry-WPRE forward	5'-GAATGCGGCCGCCGCCACCATGCCTGAACCCTCTAAGTCTG-3'
H2B-mCherry-WPRE reverse	5'-CCGCTCGAGGTCGACGGTATCGATGCG-3'

All DNA polymerases, restriction enzymes, T4 DNA ligases and chemically competent E. coli cells were purchased from New England Biolabs. All primers (Table 1) were synthesized by Invitrogen. T2A sequence was introduced by PCR. The sequence of T2A used in this study is 5'-TGGGCCAGGATTCTCCTCGACGTCACCGCATGTTAGCAGACTTCCTCTG CCCTCTCCACTGCCTACCGG-3', which is inserted in the corresponding reverse primers.

2.2 Lentivirus production

The second generation of virus packaging system was used in this study. Briefly, HEK-293T packaging cells were transiently transfected by plasmids encoding target genes (Lenti-Twitch-2B-T2A-H2B-mCherry, Lenti-Kv1.2-T2A-Twitch-2B, or Lenti-Kir2.1-T2A-Twitch-2B), plus viral packaging helper plasmids pMD2.G (plasmid #12259, Addgene) and psPAX2 (plasmid #12260, Addgene) as described previously (Liang et al., 2016). Lipofectamine 3000 reagent (Invitrogen) was used for transfection. The overexpression of K^+ channel was demonstrated to reduce the lentivirus-producing capacity of HEK293 cells (Okada et al., 2015). As Ba^{2+} ion has a similar radius to K^+ ion, the divalent Ba^{2+} ion is able to bind to the selective filter of several classes of potassium channels, especially Kir2.1. Thus, Ba^{2+} (0.3 mM) was added into culture medium to block potassium currents to keep HEK293 cells healthy and increase the virus titer. Approximately 48-72 hours after transfection, cell culture supernatant containing viral particles was collected and concentrated about 300 fold by centrifugation at 27,000 rpm at 4°C for 4 hours (Sorvall WX Ultracentrifuge, Thermo Scientific). Concentrated supernatants were titrated in 293T cells. Titers of about 8×10^9 virus particles per ml concentrated supernatant were used for the following experiments.

2.3 Animals

All experimental procedures were conducted according to German federal and state regulations and were approved by the state government of Baden-Württemberg. All animals were maintained in the animal facility of the University of Tübingen. 3-month-old C57BL/6J mice of both sexes obtained from Charles River Laboratories were used in this study. However, for testing the odor-evoked responsiveness (Chapter 2.6.4), only male mice were employed, as literature points out that odor detection in female rodents is markedly influenced by circulating levels of certain hormones and thus olfactory sensitivity varies according to hormonal status (Good et al., 1976; Pietras and Moulton, 1974).

2.4 Chronic cranial window installation

A chronic cranial window was made over the OB of 3-month-old male C57BL/6J mice as described earlier (Kovalchuk et al., 2015; Liang et al., 2016). Mice were anesthetized by intraperitoneal (i.p.) injection of ketamine/xylazine (80/4 µg/g body weight (BW). Anesthetic depth was monitored by toe pinches throughout the surgery and additional ketamine/xylazine (40/2 µg/g of BW) was injected when necessary. Dexamethasone (2 µg/g BW, Sigma-Aldrich, St. Louis, MO, USA) was administered intramuscularly (i.m.) before the surgery. Local anesthesia lidocaine (2%, AstraZeneca, Wedel, Germany) was applied subcutaneously 5 minutes before removing the scalp over the OB. Bepanthen™ (Bayer, Germany) was used to prevent dehydration of mouse's eyes. A circular cranial opening (3 mm in diameter) was made by repeated drilling over the two OB hemispheres with a microdrill. Small pieces of bone were removed with a sharp blade and tweezers. Extreme care was taken, not to damage any blood vessels on the surface of the OB. Standard extracellular solution (125 mM NaCl, 4.5 mM KCl, 26 mM NaHCO$_3$, 1.25 mM NaH$_2$PO$_4$, 2 mM CaCl$_2$, 1 mM MgCl$_2$ and

20 mM glucose, pH 7.4, bubbled continuously with 95% O_2 and 5% CO_2) was used to rinse the opening in the skull, which was then covered with a 3-mm-diameter glass coverslip (Warner Instruments, Hamden, CT, USA). The gap between the edge of the coverslip and the skull was filled with cyanoacrylate glue and then strengthened by dental cement. During the surgery, and until full recovery, the mouse was kept on a heated plate with temperature of 37 °C. Postoperative care included an analgesic dose of carprofen (5 µg/g BW, Pfizer, Berlin, Germany) for 3 days subcutaneously and the antibiotic Baytril (1:100 v/v, Bayer, Leverkusen, Germany) in drinking water for consecutive 10 days. Mice were allowed to recover for at least 3-4 weeks and were subsequently examined for window clarity and new bone growth. Mice that passed the quality control were injected with lentiviruses into the RMS.

2.5 Lentivirus injection into the RMS

Animals with a chronic cranial window over the OB were anesthetized with ketamine/xylazine as aforementioned and fixed to a stereotaxic device (Stoelting, Wood Dale, IL, USA) by ear bars. The eyes of anesthetized animals were covered with Bepanthen^{TM}. Then 2% lidocaine was applied subcutaneously to the skin overlying the left and the right injection sites. In case there was some dental cement covering the injection sites, it was removed by careful drilling. Lentiviruses were stereotactically injected into the RMS at the following coordinates: anterior-posterior +3.0 mm from bregma; medial-lateral ±0.83 from the middle line, and dorsal-ventral −2.95 ± 0.05 mm from the pial surface. Approximately, 0.8-1 µl of the lentivirus-containing solution was injected into the RMS of each hemisphere. Thereafter, a metal bar (see Figure 5a) required for head fixation during the subsequent imaging sessions, was fixed to the caudal part of the skull with dental cement. The other exposed parts of the skull were also covered with dental cement. The mice were returned to the home cage, and

carprofen as an analgesic for postoperative pain (5 µg/g BW) was injected subcutaneously for 3 days.

2.6 *In vivo* two-photon imaging

2.6.1 Set up

Mice with chronic cranial windows were anesthetized either with isofluorane or a 3-component-narcotics (Fentanyl 0.05 µg/g BW, Midazolam 5.0 µg/g BW, Medetomidine 0.5 µg/g BW) depending on the imaging purpose, see details in each section. Breathing rate and body temperature were monitored continuously using the anesthesia monitoring system (AD Instruments, Sydney, Australia). The head of the mouse was fixed with the metal bar to the *X-Y* table with a heating plate, ensuring consistent positioning through imaging sessions (Figure 5). *In vivo* two-photon imaging was performed using a customized microscope based on the Olympus FV1000 system (Olympus, Tokyo, Japan) and MaiTai Deep See Laser (Spectra-Physics, Mountain View, CA, USA), with a Zeiss x20 water-immersion objective lens.
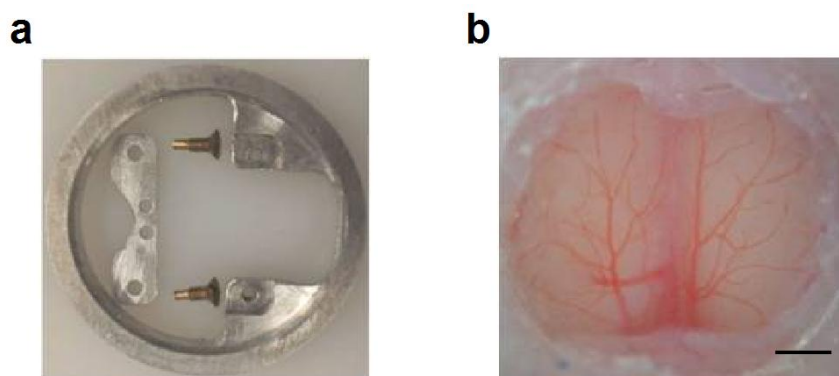

Figure 5. **The setup of mouse fixation and imaging**. **a**, Custom-made head fixation frame (top view). **b**, An example of cranial glass window over two hemispheres of the olfactory bulb. Scale bar = 0.5 mm.

2.6.2 Imaging migration of adult-born JGCs

Mice were anesthetized with isofluorane (2% for induction, 0.8-1.0% for maintenance) and then transferred into the imaging setup. The temperature was kept at 37°C and breathing rate was monitored during the whole imaging session and usually maintained at the level of 110-140 breaths per minute. To measure the migration speed, the adult-born neurons were imaged at 8 and 14 DPI according to the protocol established in our previous work (Liang et al., 2016). This approach combined two complementary techniques: single-cell tracking and blood vessel visualization. To create landmarks for single-cell tracking, we labeled blood vessels in the OB via i.p. injection of sulforhodamine B (0.1 ml/20g BW, 1 mM in PBS, Sigma-Aldrich, St. Louis, MO, USA). One single injection enabled visualization of blood vessels for around 2 h. All adult-born neurons were labeled by Twitch-2B and their positions were recorded every 15 minutes for continuous 4 hours together with blood vessel pattern. In practice, 3~5 minutes after injection of sulforhodamine B, each field of view (FOV) (635 × 635 μm, from dura to 200 μm depth) was sequentially scanned with 890 nm excitation wavelength and a 570nm dichroic mirror. The same FOVs were imaged again with exactly the same settings at 11, 25 and 45 DPI.

2.6.3 Imaging spontaneous Ca^{2+} transients of adult-born JGCs

Anesthesia is known to modify the activity of the olfactory bulb interneurons (Kato et al., 2012; Nicoll, 1972; Wachowiak et al., 2013) and was shown to suppress the ongoing spontaneous activity during early postnatal development (Adelsberger et al., 2005). In order to avoid any influence of anesthesia on spontaneous activity, the spontaneous Ca^{2+} transients were recorded in awake mice. To habituate the mice to get used to the fixation on the imaging setup, a 10-12 days training was given before experimental recording. Mice first got

accustomed to the experimenter by handling in the cage and then in the setup. This procedure was repeated (3-5 times) in the first one or two days of training. When the mice were familiar with the setup, they were held on the hand for 5 seconds and repeated 3-5 times during the day. The next day mice were fixed in the imaging setup for the first time with the implanted holder in a ring by screwing (Figure 5a). This ring was attached to an X-Y sliding table, which allows the animal to be positioned under the objective of the two-photon microscope. After fixing the head, the body of the animal rested comfortably on the base plate. The first head fixation lasted for 1 minute. In the following 10 days, the duration of the head fixation gradually increased to 2 hours. Each animal received its individual training program depending on the reaction of the animal. In this study, each mouse was fixed in the setup less than 2 hours. The well trained and cooperative mice were used for further experiments.

Spontaneous Ca^{2+} transients of adult-born JGCs were recorded at 12 DPI continuously for 2 minutes in awake mice with a frame rate of 7-10 Hz. Imaging was done using a customized two-photon microscope based on Olympus FV-1000 system (Olympus, Tokyo, Japan) and MaiTai Deep See Laser (Spectra Physics, Mountain View, CA). Briefly, Twitch-2B was excited at 890 nm and the emitted light was collected using Zeiss 20x water-immersion objective (NA 1.0) and split into 2 channels by a 515 nm long-pass dichroic mirror. In addition, the emission light originating from mCerulean3 was filtered with a 475/64 band-pass filter and the emission light originating from cpVenusCD was filtered with a 500 long-pass filter (Semrock, Rochester, NY).

2.6.4 Imaging odor-evoked Ca^{2+} transients of adult-born JGCs

Mice were anesthetized with 3-component-narcotics and then transferred into the imaging setup with a heating plate. The temperature was kept at 37°C and

breathing rate was around 140 breaths per minute during the whole imaging session. Odors were applied through a custom-made flow-dilution olfactometer, positioned in front of the snout of freely breathing mice as described previously (Homma et al., 2013; Kovalchuk et al., 2015). An individual trial consisted of a single pulse of mixed odors (2-hexanone (2-HA), isoamyl acetate (IAA) and ethyl tiglate (ET); 0.6% of saturated vapor each). The odor delivery was not timed relative to respiration. Odors were applied as a brief 4-second-long pulse with an inter-pulse interval of at least 2 minutes. Each cell was stimulated twice. All odors were purchased from Sigma-Aldrich and of highest commercially available purity. The same setup settings and Ca^{2+} imaging protocol were used as described in Chapter 2.6.3 with a frame rate of 8.4 Hz.

2.6.5 Imaging morphology of adult-born JGCs

Immediately after recording the odor-evoked Ca^{2+} transients, the morphology of adult-born JGCs was imaged under 890 nm excitation wavelength, with a 570 nm dichroic mirror and a 20x water-immersion objective. A zoom factor of 2x was used for control adult-born JGCs, and 4x for Kv1.2 and Kir2.1 overexpressing adult-born JGCs due to their tiny size. The adult-born JGCs without overlapping with others were selected for imaging and Sholl analysis.

2.7 Odor deprivation and two-photon imaging of odor-deprived mice

The nasal septum separates the left and right nasal cavities and olfactory sensory neurons project exclusively to the ipsilateral hemisphere of the OB. Therefore, unilateral naris closure blocks the sensory input to the ipsilateral hemisphere of the OB and leaves the contralateral hemisphere unaffected. To block the sensory input of the OB, unilateral naris closure was performed at 5 DPI according an established protocol (Cummings et al., 1997). Nose plugs

were constructed of 2-3 mm polyethylene tube (0.58 mm inner diameter, 0.96 mm outer diameter, Portex, UK) and suture thread (size 3-0, Ethicon, Germany) by the following protocol: (1) A length of suture thread was threaded through a piece of tube. (2) A piece of hair was tied around the thread. (3) The thread was tied into one or two knots around the hair. (4) The knot(s) was pulled into the lumen of the tube. (5) The ends of thread and hair were trimmed until only very short hair remained extending from the tubing. The perfect length of the plug for 4-5-month-old mice is 3-4. The opposite end of the tubing was beveled for ease of insertion. Mice were anesthetized by 3-component-narcotics as described above. The plug was quickly inserted into the naris. Then the mice were injected with antidote to reverse anesthesia and returned to their home cages. These mice were monitored carefully for their breathing and body weight in the first 3 days after naris occlusion.

Because the naris-occluded mice could not be anesthetized by isofluorane effectively, 3-component-narcotics was used for anesthesia, and antidote was given after each imaging session. At endpoints, mice were transcardially perfused to test the success of the odor deprivation (OD) model via immunohistochemistry as described below.

2.8 Immunohistochemistry

After decapitation, the mice were transcardially perfused with 4% PFA in phosphate buffer saline (PBS). The brains were removed and fixed with 4% PFA for 24 hours at 4°C, and then cryoprotected in 25% sucrose in PBS overnight at 4°C. Next, the brains were embedded in Tissue Tek (Sakura, Zoeterwoude, The Netherlands) and frozen at -80°C. The immunostaining procedure was performed on free-floating sagittal cryoslices (thickness 30 - 50 μm) at room temperature. The sections were incubated in a blocking buffer containing 5%

normal donkey serum (Jackson Immuno Research, Dianova) and 1% Triton-X 100 (Sigma, USA) in PBS for 1 hour to prevent nonspecific background staining. After blocking, the sections were incubated with the primary antibodies diluted in the blocking buffer. The primary antibodies were used in the following concentration: goat polyclonal antibody against GFP (Rockland 600-101-215, 1:1,000), mouse monoclonal antibody against Kv1.2 (NeuroMab K14/16, 1:200), rabbit monoclonal antibody against pCREB (Cell Signaling 9198S, 1:400), mouse monoclonal antibody against NeuN (Millipore MAB377, 1:1,000), rabbit polyclonal antibody against Kir2.1 (Alomone APC026, 1:100), and sheep polyclonal antibody against TH (Millipore AB1542, 1:2,000). After overnight incubation with primary antibodies, the sections were rinsed in PBS three times for 10 minutes each and then incubated with secondary antibodies (2% BSA in PBST) for 2 hours in the dark. The secondary antibodies were as follows: donkey-anti-mouse, anti-rabbit, or anti-sheep IgG-conjugated Alexa Fluor 488 (A21202, A21206, or A11015 1:1,000), donkey-anti-goat IgG-conjugated Alexa Fluor 594 (A11058, 1:1,000), donkey-anti-mouse IgG conjugated Alexa Fluor 680 (A10038, 1:1,000), all purchased from Invitrogen (Grand Island, NY). Afterward, the sections were washed three times in PBS for 10 minutes. Finally, the sections were transferred to Superfrost Plus charged glass slides (Langenbrink, Emmendingen, Germany) and mounted in Vectashield Mounting Medium (Vector Laboratories, USA) or ProLong gold antifade mountant (Invitrogen).

Immunostained slices were imaged using the Olympus Fluoview 300 laser scanning microscope coupled with a MaiTai mode-locked laser (Spectra Physics). Alexa Fluor 488 and 594 were excited simultaneously at 800 nm and their fluorescence was split with a 570 LP dichroic mirror. Alexa Fluor 680 was excited at 800 nm and the signal was collected in the second channel with a 670LP dichroic mirror.

2.9 Analyses

2.9.1 Analysis of Kv1.2 expression level

All brain slices were stained and imaged under same parameters concerning antibody concentration and incubation time, laser power, and photomultiplier (PMT) voltage. All images were analyzed offline by using ImageJ and the following protocol: (i) Generate substacks of Kv1.2 and Twitch-2B by splitting the 2 channels of the original stack; (ii) Measure the background noise value, caused by nonspecific binding of secondary antibody conjugated with Alexa Fluor 488 in 5 negative control slices, which were stained with secondary antibodies only (i.e. without primary antibodies); (iii) The median noise value was subtracted from Kv1.2 substack; (iv) A custom-written Matlab code was used to calculate the intensity of fluorescence in the soma and surrounding neuropil separately; (v) The relative Kv1.2 expression level was calculated as the ratio of the somatic fluorescence divided by the fluorescence of the surrounding neuropil. Besides, we also noted that in some cells the overexpression of Kv1.2 resulted in the pronounced cytosolic presence of the construct, giving a cell a donut-shape appearance. We thus quantified the fraction of cells with such donut-shaped Kv1.2 expression pattern.

2.9.2 Analysis of migration of adult-born JGCs

The analysis of migration speed of adult-born JGCs was the same as described in Liang et al., 2016. The 3D image stacks combining adult-born JGCs and blood vessels acquired during the consecutive imaging sessions were aligned offline using the blood vessel pattern as anatomic landmark. Each cell was annotated with an identification number. Cells from the consecutive time points were tracked every 15 minutes according to their location and morphology throughout the 17 time points from 0 minute to 4 hours to generate a series of annotated

stacks. Then, the history and trace of every single cell were sorted out according to those stacks. The center of cell's soma in each annotated stack was marked as a position point, and then the cell's trajectory was reconstructed based on these points. Next, the X-Y coordinates of each position point of a cell were read using the Fluoview 3.0 Viewer (Olympus). For Z axis coordinates, the depth of cells was the relative depth from the dura. With 3D coordinates for each track point, migration distance (D) between two points in space was calculated by the following formula:

$$D = \sqrt{(X1-X0)^2 + (Y1-Y0)^2 + (Z1-Z0)^2}$$,

where (X1, Y1, Z1) and (X0, Y0, Z0) were coordinates of the target cell's position measured at current and previous temporally consecutive stacks, respectively. Migration speed was defined as the translocation of cell's soma between the two consecutive sessions divided by the respective time period (μm per 15 minutes). Taking into account the 2 μm step size of the acquired stacks, a cell was considered moving if the translocation of cell's soma between the two consecutive sessions was >4 μm. Adult-born JGCs undergo salutatory migration pattern, thus, they may stay quiescent, or migrate once or several times during the 4-hours recording period. The highest value of all migrating steps was defined as the maximum migration speed and the median value of all migrating steps was defined as median migration speed.

2.9.3 Analysis of spontaneous Ca^{2+} transients

Data analysis was performed offline with ImageJ and custom-made routines in Matlab (The MathWorks, United States). Circular regions of interest (ROIs) were manually drawn and placed within soma of each cell. Fluorescence trace for each cell was obtained by averaging all pixels within the ROI. The signal used for background subtraction was obtained from the ROI of the comparable size devoid of any fluorescent processes and located near the cell of interest. The

image stack was separated into 2 substacks for mCerulean3 and cpVenus^{CD} channels, respectively. The fluorescence traces were measured separately for both substacks and filtered using low pass Butterworth infinite impulse response filter with a cut-off frequency of 0.6 Hz. Then the ratio of Twitch-2B fluorescence was calculated using the formula:

$$\text{Ratio} = \frac{F\,(cpVenus^{CD})_{Soma} - F\,(cpVenus^{CD})_{Background}}{F\,(mCerulean3)_{Soma} - F\,(mCerulean3)_{Background}}.$$

Thereafter, the traces were imported into the Matlab to analyze the following parameters: maximum ratio and the normalized area under the curve (AUC) above the threshold of 2.4, normalized to the total recording time (AUC/sec) (Figure 6). The values for maximum ratios were calculated as follows: the filtered traces were processed by sliding average algorithm with a window size of 1.5 seconds to determine the maximum ratio (maximal average value). The traces shown in all figures (Figure 9, 10, 14, 18 and 23) are non-processed.
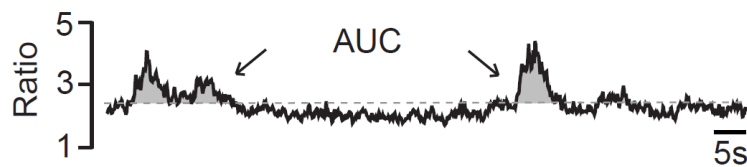

Figure 6. **A representative example of spontaneous Ca^{2+} transients recorded from a Twitch-2B labeled adult-born JGC at 12 DPI in awake mouse**. The dashed line indicates the cutting line of Ca^{2+} transients triggered by action potentials (Twitch-2B ratio of 2.4). The grey areas indicate the area under the curve (AUC) above 2.4.

In contrast to the majority of cortical neurons, which are predominantly silent under control conditions and fire only a few action potentials either spontaneously or in response to a sensory stimulus, the majority of juxtaglomerular neurons in the olfactory bulb have high baseline spiking frequencies, reaching up to 80 Hz (Homma et al., 2013). Because the decay time constants of Ca^{2+} indicators are in the range of 1-3 seconds (Thestrup et al., 2014), in juxtaglomerular cells Ca^{2+}

transients evoked by individual action potentials usually melt together resulting in a somewhat shaky but relatively flat baseline (see Figure 3D in Homma et al., 2013). Thus, using a single wavelengths indicator one cannot distinguish between a silent (Figure 3C in Homma et al., 2013) and a continuously spiking cell (Figure 3D in Homma et al., 2013). However, this is easily possible when using the ratiometric Ca^{2+} indicator (this study). In the latter case the silencing of a neuron reduces both the baseline and the maximum ratio of a cell to its resting level.

According to our recent work (Maslyukov et al., 2018), the Twitch-2B ratio of 2.4 is inferred as the threshold for spontaneous activity. Topical application of a blocker of voltage-gated Na^+ channels tetrodotoxin (TTX, 2 µM) in an acute experiment completely blocked the spontaneous Ca^{2+} transients, which indicated that the spontaneous Ca^{2+} transients were driven by activation of voltage-gated Na^+ channels. Under TTX there was no change in the baseline Twitch-2B ratio of adult-born cells. However, the maximum ratio was suppressed substantially by the TTX application. Because the highest observed Twitch-2B ratio in the presence of TTX was 1.92, we assumed that all cells with Twitch-2B ratios ≤1.92 were electrically silent (Maslyukov et al., 2018). To account for potential background-subtraction errors and in order to avoid false positive events, we introduced a substantial safety margin between 1.92 and 2.4 and considered a cell as spontaneously active only if its Twitch-2B ratio was above the value of 2.4. We categorized the adult-born immature JGCs into 3 groups based on their overall Twitch-2B ratios as: (i) continuously active cells: the Twitch-2B ratio was above 2.4 during the whole recording time; (ii) intermittently active cells: the Twitch-2B ratio was increasing above 2.4 and subsequently decreasing below this value; (iii) other cells: this group contained cells whose Twitch-2B ratio was below 2.4 during the whole recording time, thus combining electrically silent and uncertain cells (Maslyukov et al., 2018).

2.9.4 Analysis of odor-evoked responsiveness of adult-born JGCs

The odor-evoked Ca^{2+} transients were detected with a custom-made Igor Pro routine in individual neurons. First, background fluorescence, measured in neuropil surrounding the adult-born JGCs, was subtracted from all signals. Second, all signals were expressed as relative Twitch-2B ratio changes (ΔR/R). For automatic detection of responding cells, all ΔR/R traces were smoothed with a binomial filter (time window 0.3 s). Each smoothed trace was subtracted from the original ΔR/R trace, resulting in the "baseline noise" trace. Ca^{2+}transients were automatically detected with a template-matching algorithm, taking into account their sharp rise. They were accepted as signals if their amplitude was three times larger than the standard deviation of the corresponding baseline noise values (Homma et al., 2013). The amplitude and AUC were calculated to quantify the strength of the odor-evoked Ca^{2+} transients (Figure 7).
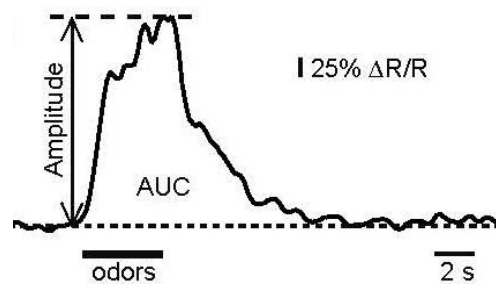

Figure 7. A representative example of an odor-evoked Ca^{2+} transient recorded from a Twitch-2B labeled adult-born JGC at 20 DPI under anesthesia. The change of the Twitch-2B ratio of adult-born JGC during odor stimulus is characterized by the amplitude and AUC of the corresponding Ca^{2+} transient.

2.9.5 Sholl analysis

The dendritic morphology of adult-born JGCs was analyzed both *in vivo* and *in situ*, the three-dimensional stacks were imported into Neuromantic software (https://www.reading.ac.uk/neuromantic/body_index.php) for 3D reconstruction.

Neuronal morphology was manually traced to have accurate reconstructions, and then digitally reconstructed neurons were imported into Image J (https://imagej.nih.gov/ij/) and analyzed with the Simple Neurite Tracer plugin. The following morphological parameters have been analyzed: the number of dendritic branches and the total dendritic branch length (TDBL). Sholl analysis was performed by counting the number of intersections between dendrites and centered on the soma concentric spheres with 10 μm radius increments (Sholl, 1953).

2.9.6 Analysis of survival rate

All FOVs including cells and blood vessels were imaged at 14, 25 and 45 DPI under the same settings. The size of each image stack was 635 μm x 635 μm x 200 μm (XYZ). By using blood vessels as a landmark, a cell was considered surviving if its soma sat exactly at the same position between the two time points (14 and 25 DPI, or 25 and 45 DPI). An error of 4 μm was tolerated due to the resolution of the microscope.

2.9.7 Analysis of pCREB expression level

All brain slices were stained and imaged under the same conditions, e.g. antibody concentration and incubation time, laser power, PMT level and so on. Each slice was stained with 3 antibodies simultaneously (Table 2).

Table 2. The setup for imaging pCREB immunostaining. Anti-GFP antibody was used to recognize Twitch-2B in the adult-born JGCs.

1st Antibody	2nd Antibody	Excitation wavelength	Dichroic Mirror	Filter
anti-pCREB	Alexa-488	800 nm	570 nm	568 ± 40 nm
anti-GFP	Alexa-594	800 nm	570 nm	536 nm LP
anti-NeuN	Alexa-680	800 nm	670 nm	no filter

All images were processed offline by using ImageJ and the following protocol: (i)

Generate 3 substacks for pCREB, GFP (Twitch-2B) and NeuN staining by splitting the original 3D stack. (ii) Draw ROIs of the adult-born JGCs in the GFP (Twitch-2B) stack at the central plane (Z-axis) on the single slice. (iii) Find the corresponding frame (same depth) in the NeuN stack, exactly in the same plane of the soma center. In order to avoid noise from the corresponding frame due to the non-specific binding of the secondary antibody, a median of 5 ROIs of the darkest area in the FOV was used to quantify the background noise. (iv) Subtract the median background noise value from the NeuN stack to generate images which theoretically only contain signals from NeuN proteins by using the plug-in in ImageJ. (v) Adjust the threshold of the image to highlight all NeuN positive regions and draw ROIs for NeuN positive cells in the whole field of view. (vi) Measure the intensity of NeuN positive mature neurons and GFP (Twitch-2B) positive adult-born JGCs in the stack of pCREB. (vii) The relative pCREB expression level is calculated as the intensity of pCREB fluorescence of each GFP positive adult-born JGC divided by the median intensity of all NeuN positive mature neurons located in the same field of view.

2.10 Statistics

Statistical analyses were performed using the GraphPad Prism 7 software. Shapiro-Wilk test was used to check the normality of the distribution of the data points within the data sets. For normally distributed data, Student's t-test was used for comparison of the two groups (e.g. Control and Odor-deprived) and one way ANOVA was used for comparison of the 3 groups (e.g. Control, Kv1.2, and Kir2.1) followed by the Tukey's multiple comparison test. For nonparametric (not normally distributed) data sets, Mann-Whitney test was used for comparison between the two groups (e.g. Control and Odor-deprived) and Kruskal-Wallis test for comparison of three groups (e.g. Control, Kv1.2, and Kir2.1) followed by the Dunn's multiple comparison test. Chi-square test was used for comparing the

fractions of continuously active, intermittently active, and other cells between different datasets. Kolmogorov-Smirnov test was used for comparing the cumulative distributions of data. All comparisons between two samples were two-sided. $P < 0.05$ was considered as statistically significant. Box plots were used to present 5 parameters of the dataset: minimum, 1st percentile, median, 3rd percentile, and maximum. In the text the data are given as mean ± SEM without special indicating. In order to avoid variability caused by various mouse behaviors or the environment, we compared the median value for all cells acquired in each mouse (median per mouse) among groups.

3. Results

3.1 Overexpression of Kv1.2 or Kir2.1 decreases endogenous neuronal activity

3.1.1 The bicistronic lentiviral vectors enabling simultaneous overexpression of Kv1.2/Kir2.1 and Twitch-2B

Because the control virus contains a red fluorescence protein mCherry located in the nucleus (Figure 4a), it is very easy to distinguish Kv1.2 and Kir2.1 overexpressing cells from control cells. The transduction efficiency of viruses was initially tested in HEK293 cell cultures (Figure 4b) and then in mice. In both cases transducted cells showed bright Twitch-2B fluorescence. In order to test the overexpression level of Kv1.2 or Kir2.1 in the adult-born JGCs, we quantified the relative expression levels of Kv1.2 or Kir2.1 at 10 DPI by means of immunohistochemistry. The anti-Kv1.2 antibody often showed a clear donut-shaped labeling on the cell membrane of Kv1.2 overexpressing adult-born JGCs (Figure 8a, lower panel). However, the endogenous expression of Kv1.2 was very low and often difficult to be seen by eye (Figure 8a, upper panel). To quantify the relative expression level of Kv1.2 in the adult-born JGCs, we calculated the ratio of the intensity of Kv1.2 staining of the cell soma divided by the intensity of the surrounding neuropil, which does not contain any structures overexpressing Kv1.2 and therefore should be similar for all slices (see Chapter 2.10.1). About 40% of control adult-born JGCs showed extremely low or no expression of Kv1.2 (40 out of 96 cells from 6 mice). However, this fraction was only about 6% in Kv1.2-overexpressing adult-born JGCs (9 out of 155 cells from 6 mice) (Figure 8b). The median normalized Kv1.2 fluorescence was 1.51 ± 2.08 (median ± interquartile range (IQR)) in control, but increased to 2.1 ± 1.05 (median ± IQR) in Kv1.2-overexpressing adult-born JGCs. Thus, the somatic Kv1.2 expression level was higher in Kv1.2-overexpressing adult-born JGCs

than control cells (Figure 8b). Furthermore, we also found that approximately 22% of Kv1.2-overexpressing adult-born JGCs (median per mouse, n = 6 mice) displayed a donut-shaped expression pattern of Kv1.2 in cell somata (Figure 8a, c). In contrast, no such pattern was observed in control adult-born JGCs. Taken together, these results demonstrated the efficiency of bicistronic lentiviral-mediated *in vivo* gene delivery and the up-regulated expression and disturbed distribution pattern of Kv1.2 channel.
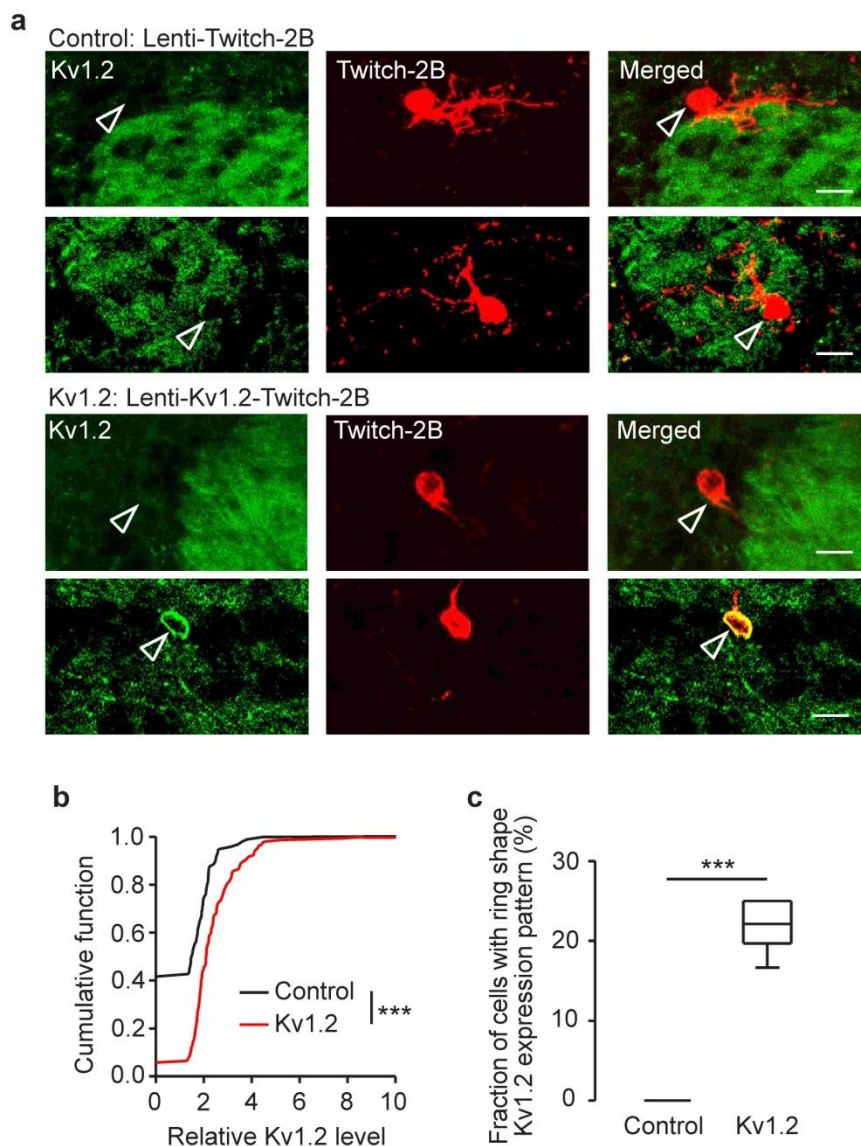

Figure 8. Bicistronic lentiviral vectors induced simultaneous overexpression of Kv1.2 and Twitch-2B. a, Sample images showing the expression of Kv1.2 in control (upper panel) and Kv1.2-overexpressing (lower panel) adult-born JGCs at 10 DPI. Scale bar = 10 μm. **b,**

Cumulative distributions of the relative Kv1.2 expression levels in control and Kv1.2 overexpressing adult-born JGCs. Kolmogorov–Smirnov test, $P = 1\times10^{-8}$, $D = 0.398$. **c,** Box plot showing the median (per mouse) fraction of adult-born JGCs with donut-shaped Kv1.2 expression pattern. Unpaired t test with Welch's correction: $t_5 = 17.13$, $P = 1.2\times10^{-5}$. Control: n = 96 cells, 6 mice; Kv1.2: n = 155 cells, 6 mice.

Besides, we had also attempted immunostaining of Kir2.1, however, the commercially available anti-Kir2.1 antibodies showed insufficient labeling in the olfactory bulb tissue. Nevertheless, due to the similarity of the Kv1.2 and Kir2.1 viral constructs, we expect a similar expression level of Kir2.1. Because Kir2.1 or Kv1.2 is located inside the same transcription cassette with Twitch-2B, the bicistronic system enables the transcription of Kir2.1 and Twitch-2B as a single mRNA that is cleaved later, before translation. Since we had observed clear Twitch-2B fluorescence in the adult-born JGCs both *in vivo* and *in vitro*, the Kir2.1 gene should have been transcribed simultaneously.

3.1.2 The perturbed endogenous activity in Kv1.2- and Kir2.1-overexpressing adult-born JGCs

Next, we tested whether the endogenous activity was perturbed by the overexpression of Kv1.2 or Kir2.1. The spontaneous Ca^{2+} transients were studied in the control, Kv1.2- and Kir2.1-overexpressing adult-born JGCs at 12 DPI in awake mice. The results showed a robust presence of spontaneous Ca^{2+} transients in control adult-born JGCs, and, surprisingly, also in Kv1.2- and Kir2.1-overexpressing adult-born JGCs (Figure 9).
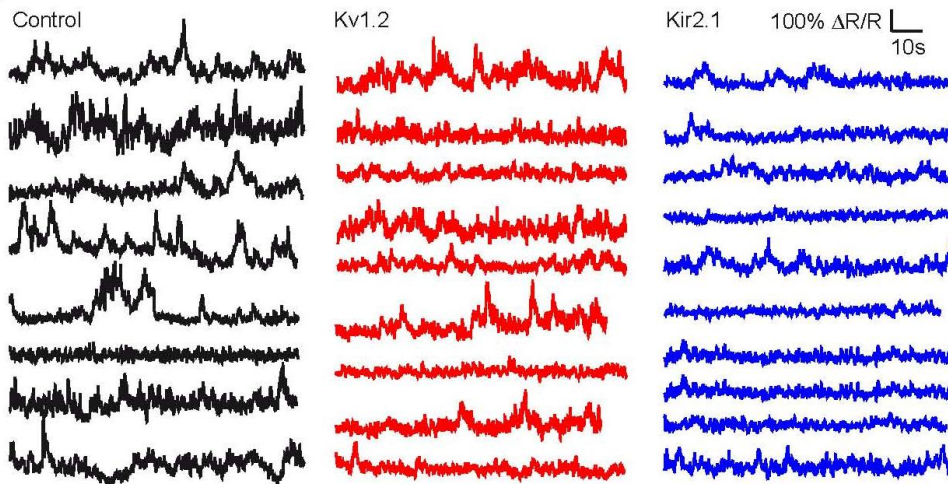
Figure 9. Sample traces representing spontaneous Ca^{2+} transients in control (black), Kv1.2 (red) and Kir2.1 overexpressing (blue) adult-born JGCs at 12 DPI. All traces were recorded in awake mice.

In order to quantify the impact of the overexpression of Kv1.2 and Kir2.1 on the spontaneous Ca^{2+} transients, several parameters of the recorded traces were analyzed. Using the Twitch-2B ratio of 2.4 as a threshold of being electrically active or silent (see Chapter 2.10.3) adult-born JGCs were categorized into 3 groups as continuously active cells (Twitch-2B ratio is > 2.4 during the entire recording period), intermittently active cells (Twitch-2B ratio is sometimes > 2.4) and other cells (Twitch-2B ratio is always < 2.4) (Figure 10a). Although not significant, there was a trend towards fewer continuously active cells in Kv1.2 and Kir2.1 group (Control 12%, Kv1.2 5.9% and Kir2.1 4.5%; Figure 10b). This data suggested that the overexpression of Kv1.2 or Kir2.1 specifically suppressed the activity of continuously spiking adult-born JGCs. We used the maximum Twitch-2B ratio during the recording period and the AUC/sec (Figure 6, 10a) as measures of the strength of spontaneous activity in each individual neuron. Interestingly, the cumulative distribution of the maximum Twitch-2B ratio shifted leftward with Kv1.2- and Kir2.1-overexpressing adult-born JGCs (Figure 10c). Further comparisons of the subpopulations with high maximum Twitch-2B ratios (above the 75th percentile) showed a significant reduction of the maximum

Twitch-2B ratio of Kv1.2- and Kir2.1-overexpressing adult-born JGCs (Control: 6.13 ± 1.52; Kv1.2: 5.03 ± 1.09; Kir2.1: 4.33 ± 1.04; Figure 10d). The same was true for AUC/sec (Figure 10e, f), showing a significant reduction in strongly active Kv1.2- or Kir2.1-overexpressing adult-born JGCs (Control: 2.2 ± 1.26; Kv1.2: 1.03 ± 0.82; Kir2.1: 0.8 ± 0.56).
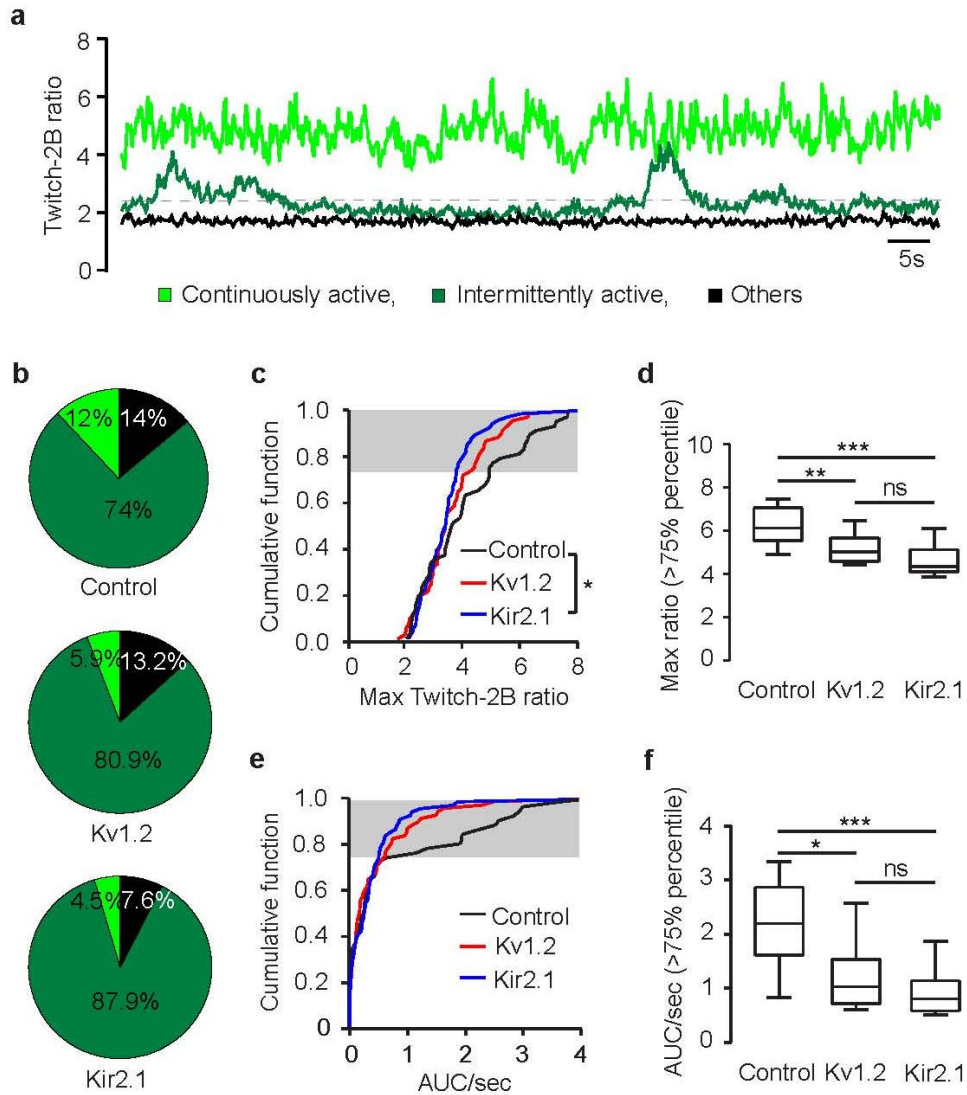

Figure 10. Overexpression of Kv1.2 or Kir2.1 perturbs endogenous activity of adult-born JGCs at 12 DPI. a, Traces showing the Ca^{2+} dynamics of adult-born JGCs with different spiking patterns. **b**, Pie charts illustrating the fractions of continuously active, intermittently active and other adult-born JGCs. Chi-square test, $P = 0.4$. **c**, Cumulative distributions of maximum Twitch-2B ratios in control, Kv1.2- and Kir2.1-overexpressing adult-born JGCs. Kolmogorov-Smirnov test: Control *vs.* Kv1.2: $P = 0.32$, $D = 0.172$; Control *vs.* Kir2.1: $P = 0.042$, $D = 0.254$; Kv1.2 *vs.* Kir2.1: $P = 0.47$, $D = 0.144$. **d**, Box plot comparing the subpopulations of

adult-born JGCs with maximum Twitch-2B ratios above the 75th percentile (gray area in (**c**)). One-way ANOVA: F$_{2, 45}$ = 12.89, P = 3.8×10^{-5}, *post hoc* Tukey's multiple comparisons: Control *vs.* Kv1.2: P = 8.7×10^{-3}; Control *vs.* Kir2.1: P = 2×10^{-5}; Kv1.2 *vs.* Kir2.1: P = 0.09. **e**, Cumulative function for the distribution of AUC/sec in control, Kv1.2- and Kir2.1-overexpressing adult-born JGCs. Kolmogorov-Smirnov test: P > 0.05 for all comparisons. **f**, Box plot comparing the subpopulations of adult-born JGCs with AUC/sec above the 75th percentile (gray area in (**e**)). Kruskal-Wallis test: P = 2×10^{-4}, *post hoc* Dunn's multiple comparisons: Control *vs.* Kv1.2: P = 0.024; Control *vs.* Kir2.1: P = 1×10^{-4}; Kv1.2 *vs.* Kir2.1: P = 0.34. **b, c, e**: Control: n = 50 cells, 7 mice; Kv1.2: n = 68 cells, 7 mice; and Kir2.1: n = 66 cells, 5 mice. **d, f**, Control: n = 15 cells, 7 mice; Kv1.2: n = 18 cells, 7 mice; and Kir2.1: n = 17 cells, 5 mice. *P < 0.05, **P < 0.01, ***P < 0.001, ns = not significant.

Taken together, these data suggested that the overexpression of Kv1.2 or Kir2.1 selectively changed the spiking behavior of frequently or even continuously active cells by decreasing their fraction as well as their area under the curve and the maximum Twitch-2B ratio.

3.2 Overexpression of Kv1.2 or Kir2.1 inhibits the migration of adult-born JGCs

3.2.1 The impaired migration of Kv1.2- and Kir2.1-overexpressing adult-born JGCs

Because of the critical role of endogenous activity in regulating the neuronal migration during perinatal development (Bando et al., 2016, 2014; De Marco García et al., 2011; Hurni et al., 2017), we examined whether the migration of Kv1.2- and Kir2.1-overexpressing adult-born JGCs was affected. The migration speed of adult-born JGCs was first measured at 8 DPI via continuous monitoring of cell's position during a 4-hours-long imaging session. Kv1.2- and Kir2.1-overexpressing adult-born JGCs both showed impaired motility (Figure 11a). Specifically, the cells had a significantly lower maximum and median migration speed as well as shorter net translocation distance (Figure 11b-d; Table 3). Moreover, at 8 DPI the fraction of Kv1.2- or Kir2.1-overexpressing

adult-born JGCs, which migrated during the 4 hours time period was also smaller compared to that of control JGCs (Figure 11e; Table 3). These data suggested that the overexpression of Kv1.2 or Kir2.1 impaired the migration of adult-born JGCs.
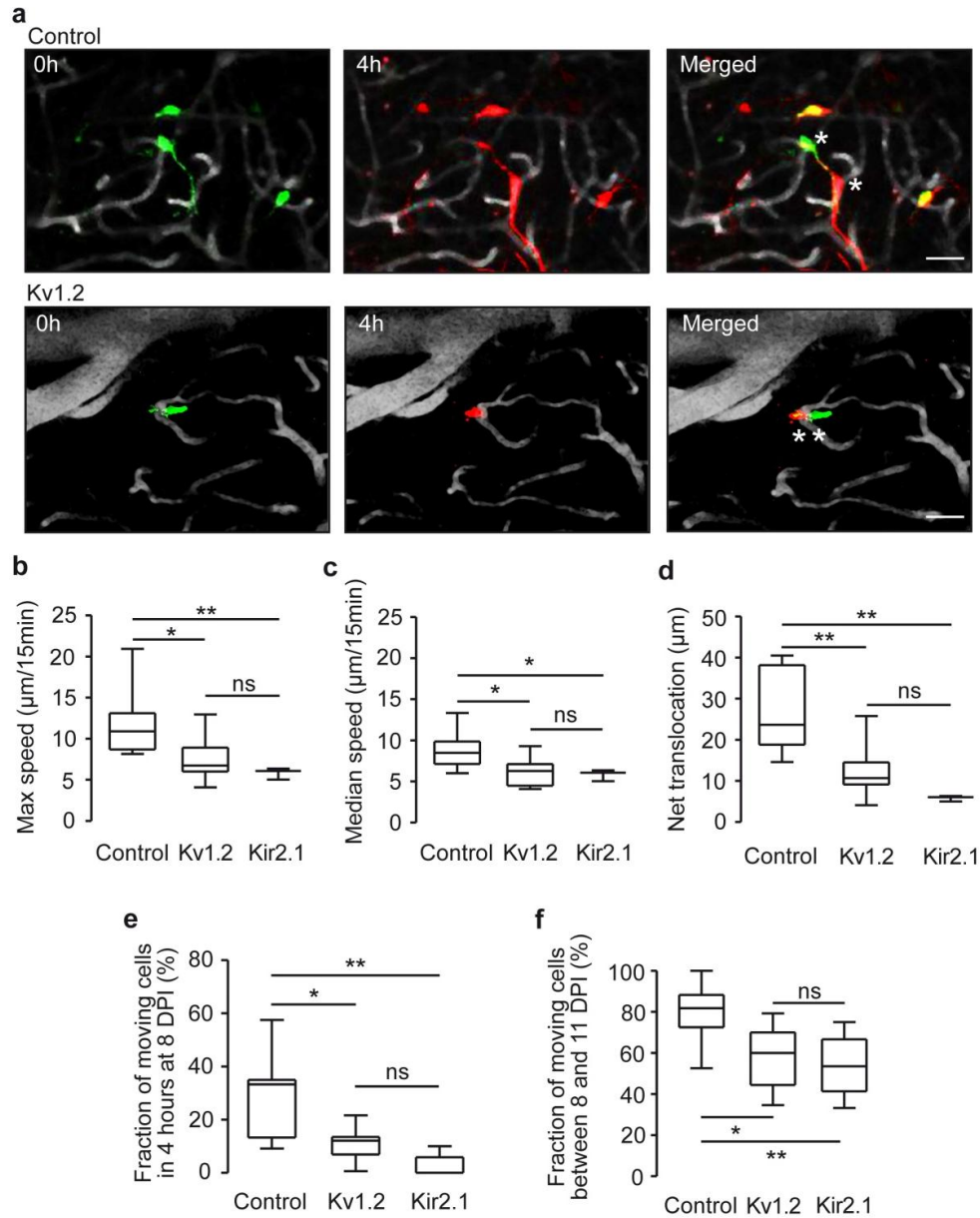

Figure 11. Overexpression of Kv1.2 or Kir2.1 impaired the migration of adult-born JGCs. a, Pseudocolor images showing the positions (0h in green, 4h in red) of control (upper panel) and Kv1.2-overexpressing (lower panel) adult-born JGCs and blood vessels (in gray) during 4-hour-long recordings (see timestamps, relative time) at 8 DPI. Asterisks mark the cell positions at 0h and 4h. Scale bar = 20 µm. **b-d**, Box plots showing the median (per mouse) maximum migration speed (**b**), median migration speed (**c**) and the net translocation distance (**d**) in 4 hours

of control, Kv1.2- and Kir2.1-overexpressing adult-born JGCs. **b**, Kruskal-Wallis test: $P = 1.8\times10^{-3}$, *post hoc* Dunn's multiple comparisons: Control *vs.* Kv1.2: $P = 0.022$; Control *vs.* Kir2.1: $P = 8\times10^{-3}$; Kv1.2 *vs.* Kir2.1: $P = 0.77$. **c**, One-way ANOVA: $F_{2, 22} = 5.949$, $P = 8.6\times10^{-3}$, *post hoc* Tukey's multiple comparisons: Control *vs.* Kv1.2: $P = 0.015$; Control *vs.* Kir2.1: $P = 0.044$; Kv1.2 *vs.* Kir2.1: $P = 0.97$. **d**, Kruskal-Wallis test: $P = 5\times10^{-4}$, *post hoc* Dunn's multiple comparisons: Control *vs.* Kv1.2: $P = 9.2\times10^{-3}$; Control *vs.* Kir2.1: $P = 3.7\times10^{-3}$; Kv1.2 *vs.* Kir2.1: $P = 0.72$. **b-d**, Control: n = 13 mice; Kv1.2: n = 9 mice; Kir2.1: n = 3 mice (another 3 mice showed no migrating cells). **e**, Box plot of the fraction of control, Kv1.2- and Kir2.1-overexpressing adult-born JGCs, which migrated during 4 hours. Kruskal-Wallis test: $P = 2\times10^{-4}$, *post hoc* Dunn's multiple comparisons: Control *vs.* Kv1.2: $P = 0.037$; Control *vs.* Kir2.1: $P = 2\times10^{-4}$; Kv1.2 *vs.* Kir2.1: $P = 0.22$. Control: n = 11 mice; Kv1.2: n = 10 mice; Kir2.1: n = 6 mice. **f**, Box plot of the fraction of control, Kv1.2- and Kir2.1-overexpressing adult-born JGCs, which migrated between 8-11 DPI. One-way ANOVA: $F_{2, 19} = 7.982$, $P = 3\times10^{-3}$, *post hoc* Tukey's multiple comparisons: Control *vs.* Kv1.2: $P = 0.011$; Control *vs.* Kir2.1: $P = 6.6\times10^{-3}$; Kv1.2 *vs.* Kir2.1: $P = 0.59$. Control: n = 9 mice; Kv1.2: n = 11mice; Kir2.1: n = 8 mice. *$P < 0.05$, **$P < 0.01$, ***$P < 0.001$, ns = not significant.

Table 3. Summary of the migration parameters of adult-born JGCs at 8 DPI. § Data are presented as median ± IQR.

	Control	Kv1.2	Kir2.1
Maximum speed at 8 dpi (µm/15min)	10.44 ± 0.48	7.46 ± 0.85*	5.82 ± 0.40*
Median speed at 8 dpi (µm/15min)	8.59 ± 0.58	6.11 ± 0.56*	5.82 ± 0.40*
Net translocation (µm)	25.14 ± 2.68	12.25 ± 2.00*	5.82 ± 0.40*
Fraction of moving cells§ in 4 hours at 8 dpi %	33.33 ± 21.67	12.13 ± 6.62*	0 + 5.91*
Fraction of moving cells between 8 and 11dpi %	79.20 ± 4.68	59.51 ± 4.23*	51.97 ± 4.54*

Because adult-born JGCs have saltatory migration pattern (Liang et al., 2016), some of them might not move during the 4-hour-long recording period. Therefore, a longer imaging interval of 3 days was introduced to evaluate the overall motility of the populations of adult born cells. The same FOVs were imaged at 8 and 11 DPI under the same conditions. We defined the cells which changed their position between 8 and 11 DPI as migrating cells. Kv1.2- and Kir2.1-overexpressing adult-born JGCs exhibited smaller fractions of migrating cells between 8-11 DPI (Figure 11f; Table 3). To test whether this impairment of migration is chronic, we further studied the migration behaviors of control, Kv1.2-

and Kir2.1-overexpressing adult-born JGCs at 14 DPI. The migration of control cells is known to slow down at 14 compared to 8 DPI (REF). Consistently, at this age we did not find any significant difference between control and Kv1.2-overexpressing adult-born JGCs in regard to the maximum and median migration speed, net translocation distance, and fraction of migrating cells during 4 hours (Figure 12a-c; Table 4). Unexpectedly, at 14 DPI Kir2.1-overexpressing adult-born JGC did not migrate at all (0 out of 60 cells from 4 mice, Figure 12d). This data suggested that Kir2.1 overexpression had stronger inhibition on the migration of adult-born JGCs compared to Kv1.2 overexpression.
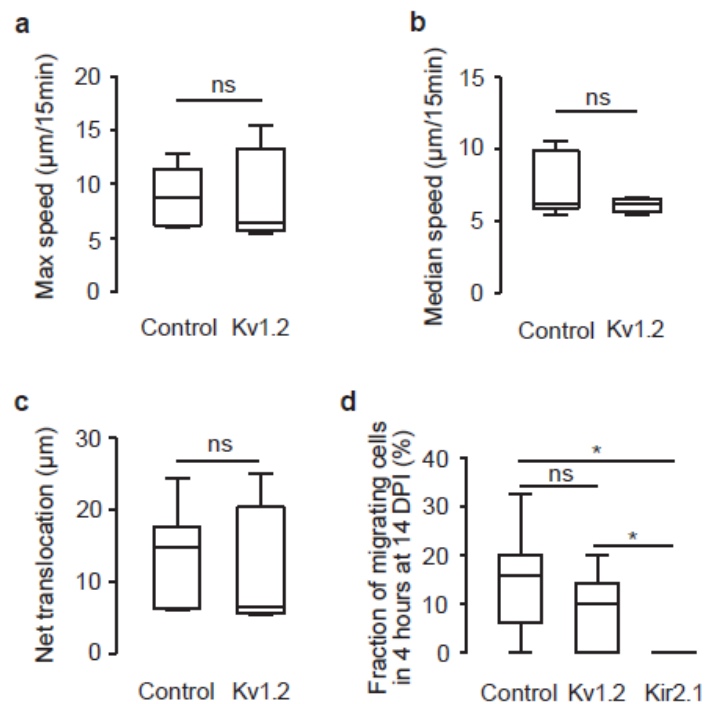

Figure 12. Overexpression of Kv1.2 or Kir2.1 inhibits the migration of adult-born JGCs at 14 DPI. a-c, Box plots showing the median (per mouse) maximum migrating speed (**a**), median migrating speed (**b**) and the net translocation distance in 4 hours (**c**) of control and Kv1.2-overexpressing adult-born JGCs. Mann-Whitney test: **a**, $P = 0.68$; **b**, $P = 0.82$; **c**, $P = 0.69$. Control: n = 10 mice, Kv1.2: n = 7 mice. **d**, Box plot showing the fraction of migrating control, Kv1.2- and Kir2.1-overexpressing adult-born JGCs in 4 hours at 14 DPI. One-way ANOVA: $F_{2,18} = 4.013$, $P = 0.036$, *post hoc* Welch's t test: Control *vs.* Kv1.2: $P = 0.17$; Control *vs.* Kir2.1: $P = 1.9 \times 10^{-3}$; Kv1.2 *vs.* Kir2.1: $P = 0.041$. Control: n = 10 mice, Kv1.2: n = 7 mice, Kir2.1: n = 4 mice. *$P < 0.05$, ns = not significant.

Table 4. Summary of the migration parameters of adult-born JGCs at 14 DPI. § Data are presented as median ± IQR.

	Control	Kv1.2	Kir2.1
Maximum speed at 14 dpi (µm/15min)	8.86 ± 1.02	8.46 ± 2.36	-
Median speed at 14 dpi § (µm/15min)	6.21 ± 3.97	7.11 ± 3.88	-
Net translocation (µm)	13.0 ± 2.65	12.56 ± 3.81	-
Fraction of moving cells in 4 hours at 14 dpi %	14.42 ± 3.39	7.91 ± 3.04*	0*

3.2.2 The arrival of Kv1.2- and Kir2.1-overexpressing adult-born JGCs in GL

In addition we observed similar densities of adult-born JGCs. This argues against a dramatic impairment of their tangential and radial migration. Their densities were calculated by the number of adult-born JGCs divided by the volume of the corresponding 3D image stack. The results showed similar densities of control, Kv1.2- and Kir2.1-overexpressing adult-born JGCs at both 8 DPI and 14 DPI (Figure 13; Table 5), suggesting that the arrival of adult-born neurons in the GL was not affected by the overexpression of Kv1.2 or Kir2.1.
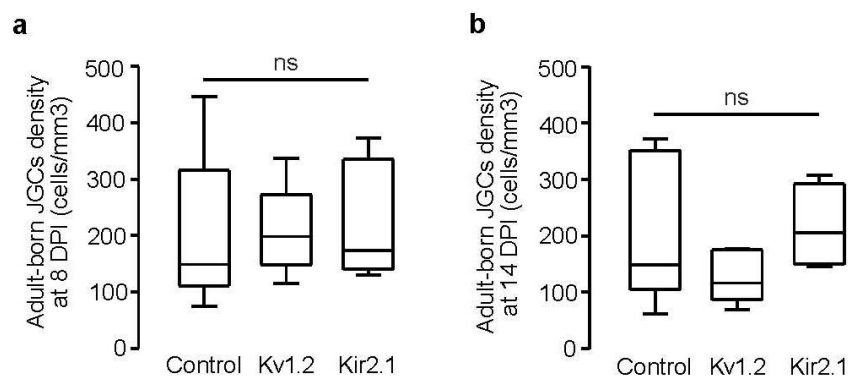

Figure 13. Overexpression of Kv1.2 or Kir2.1 does not influence the density of adult-born JGCs in the GL. a, b, Box plots showing the cell density of adult-born JGCs in the GL at 8 DPI (**a**) and 14 DPI (**b**) of control, Kv1.2 and Kir2.1 groups. One-way ANOVA: (**a**) $F_{2, 17} = 0.048$, $P = 0.95$; (**b**) $F_{2, 13} = 2.18$, $P = 0.15$. $P > 0.05$ for all *post hoc* Tukey's multiple comparisons. **a,** Control: n = 5 mice; Kv1.2: n = 9 mice; Kir2.1: n = 6 mice; **b,** Control: n = 5 mice; Kv1.2: n = 7 mice; and Kir2.1: n = 4 mice. ns = not significant.

Table 5. The density of adult-born JGCs at 8 and 14 DPI in the GL of OB.

cells per mm^3	Control	Kv1.2	Kir2.1
adult born JGCs density at 8 dpi	200.7 ± 64.03	207.0 ± 24.27	219.2 ± 42.24
adult born JGCs density at 14 dpi	212.5 ± 59.24	122.9 ± 15.44	215.9 ± 37.97

In summary, the overexpression of Kv1.2 or Kir2.1 impaired the lateral migration of adult-born JGCs without affecting the pace of their arrival in the GL. Furthermore, Kir2.1 overexpression showed stronger inhibition effect on the migration of adult-born JGCs than Kv1.2 overexpression.

3.3 Odor deprivation does not affect the migration of adult-born JGCs

Having discovered the impaired lateral migration in adult-born JGCs overexpressing Kv1.2 or Kir2.1, we next tested whether migration parameters are also sensitive to changes in the sensory input. To this end, we employed unilateral naris occlusion at 5 DPI and compared the migration parameters of adult-born JGCs (as above) in the odor-deprived (OD) side with that of the non-OD side.

3.3.1 Naris occlusion blocks sensory input

Due to the specific anatomy of the nasal cavity (see Chapter 2.7), naris occlusion prevented odors from reaching the ipsilateral nasal olfactory epithelium, whereas the contralateral olfactory epithelium received normal amount of odors. To verify the efficiency and reliability of naris occlusion method, odor responsiveness of adult-born JGCs was checked at 20 DPI. When applying odor stimuli broadly activating the dorsal OB, majority (70.89% ± 11.23%) of adult-born JGCs in control bulb showed strong responsiveness to odors,

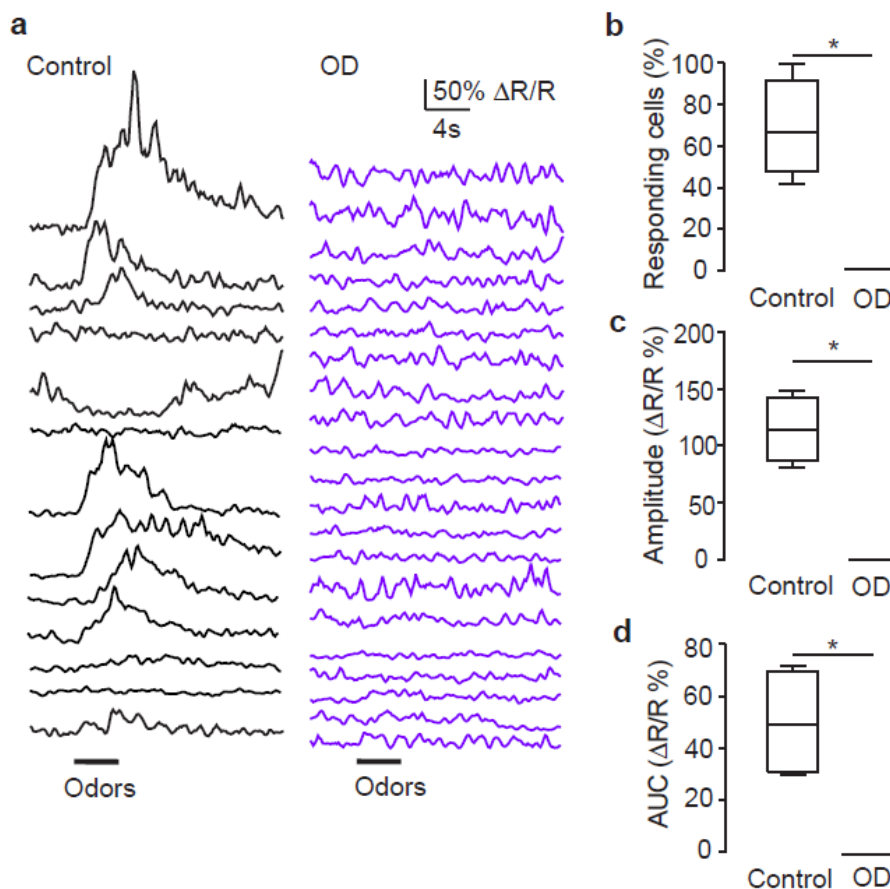however, none of the adult-born JGCs in the OD bulb responded (Figure 14).

Figure 14. Naris closure blocked odor-evoked responsiveness of adult-born JGCs. a, Sample traces showing the odor-evoked Ca^{2+} transients of control and odor-deprived (OD) adult-born JGCs. Odors are a mixture of 2-HA, IAA and ET (see Chapter 2.6.4). **b-d**, Box plots illustrating the median (per mouse) fractions of responding cells (**b**), the amplitude (**c**) and the AUC (**d**) of odor-evoked Ca^{2+} transients in control and OD adult-born JGCs. **b-d**, Unpaired t test with Welch's correction: **b**, $t_3 = 6.314$, $P = 0.008$. **c**, $t_3 = 7.708$, $P = 4.5 \times 10^{-3}$. **d**, $t_3 = 4.87$, $P = 0.017$. n = 4 mice for each group. *$P < 0.05$, **$P < 0.01$, ns = not significant.

Dopaminergic neurons of the olfactory bulb are reliably identified by the expression of tyrosine hydroxylase (TH), the first enzyme in the dopamine biosynthetic pathway (Baker et al., 1993; Cave and Baker, 2009; Cummings et al., 1997). As odor-modulated afferent activity is required for expression of TH, the expression level of TH is widely used to verify the efficiency of odor deprivation models (Baker et al., 1993, Cummings et al., 1997). After ~2 weeks

(5-20 DPI) of naris occlusion, immunohistochemical analysis showed a significant decrease in TH expression without affecting the size of the bulb (Figure 15). These data showed that unilateral naris occlusion successfully blocked odor perception in adult-born JGCs and also in the whole neural network of the OD hemisphere.
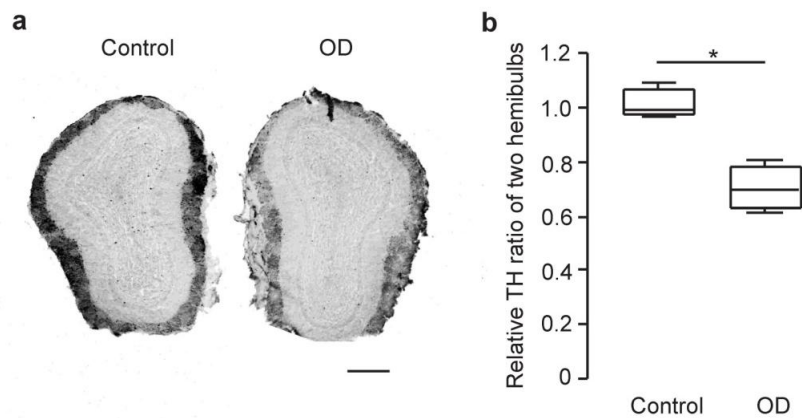

Figure 15. The influence of 2-week-long naris occlusion on the TH expression in the OB. a, Sample coronal sections of the OB from unilaterally odor-deprived mice. **b**, Box plot showing the ratio of mean immunofluorescence intensity in the GL of control and odor-deprived (OD) OB. Mann-Whitney test, $P = 7.9 \times 10^{-3}$. Control: n=5 mice; OD: n=4 mice. This data were published in Liang et al., 2016.

3.3.2 Odor deprivation does not affect the migration of adult-born JGCs

Next, we tested the migration behaviors of adult-born JGCs under OD condition using experimental procedures and analysis described above (Chapter 3.2.1, Figure 11). Surprisingly, control and odor-deprived adult-born JGCs showed similar migration parameters as control (Figure 16). At the same time, migration behavior of adult-born JGCs from the contralateral (control) hemisphere of the OD mice (Figure16) was similar to that of control mice (Figure 11).
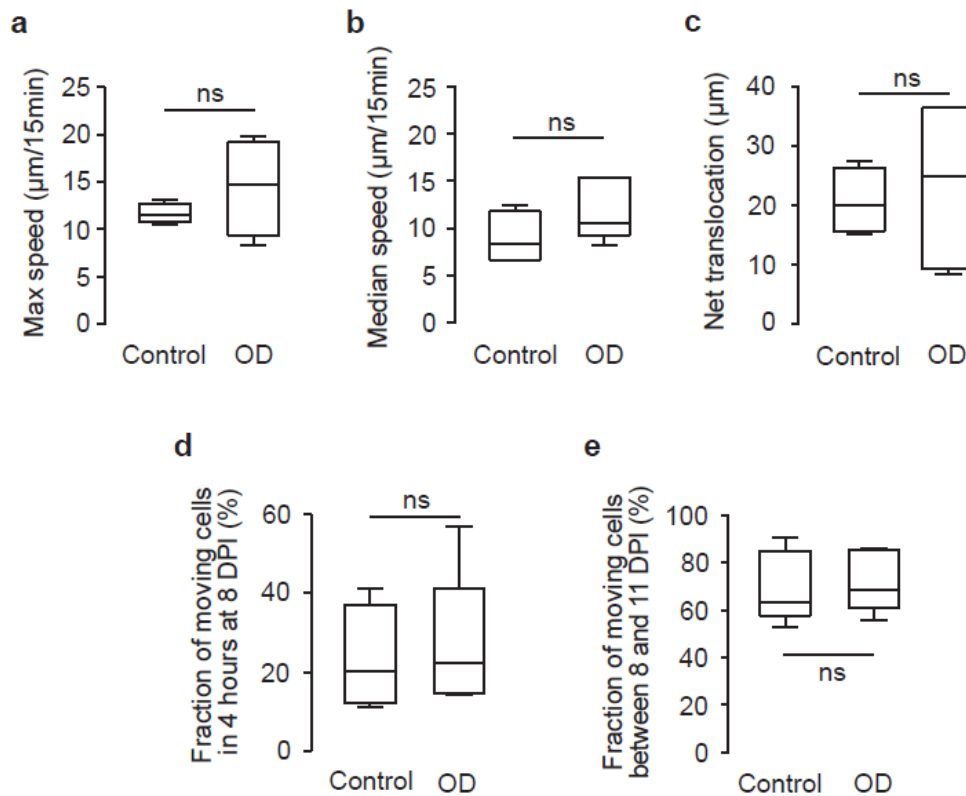
Figure 16. Odor deprivation does not affect the migration of adult-born JGCs. a-e, Box plots comparing the median (per mouse) maximum migration speed (**a**), median migration speed (**b**) and the net translocation (**c**) during 4 hours, the fraction of migrating cells in 4 hours at 8 DPI (**d**), and the fraction of migrating cells between 8-11 DPI (**e**) of control and odor-deprived adult-born JGCs. **a-c,** and **e**, Unpaired test: $P > 0.05$ for all comparisons. **d**, Mann-Whitney test: $P = 0.96$. n = 5 mice for each group. ns = not significant.

We further extended the recording period to nearly 10 days with 12-hours intervals. The positions of individual adult-born JGC and blood vessel pattern were recorded every 12 hours from 6.5 DPI to 14.5 DPI. The net translocation distance per 12 hours exhibited no difference between control and odor-deprived adult-born JGCs (Figure 17a). Considering that approximately 60% of adult-born JGCs undergo multidirectional migration (Liang et al., 2016), we calculated both the net translocation distance and the cumulative translocation distance between 6.5 and 14.5 DPI. Control and odor-deprived adult-born JGCs showed similar net and cumulative translocation distances (Figure 17b).
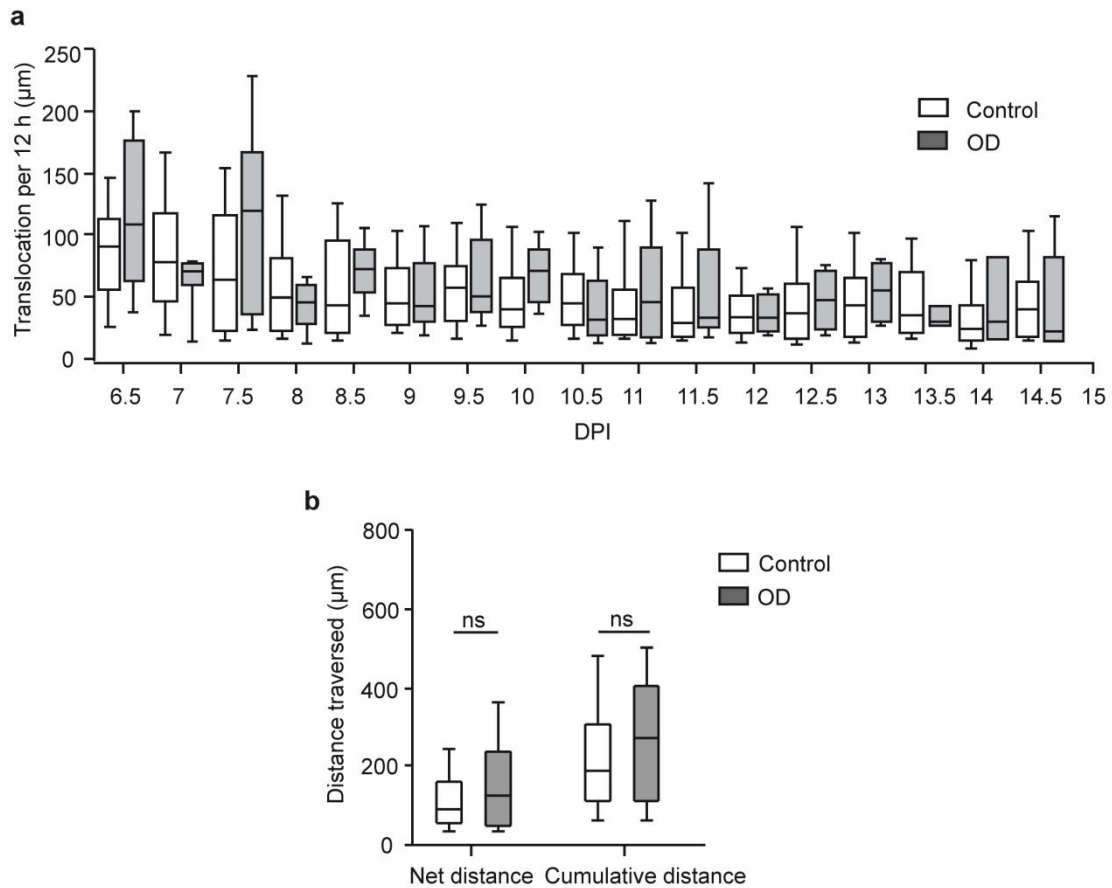
Figure 17. The effect of naris closure on the global migration properties of adult-born JGCs. a, Box plot showing migration speed (translocation per 12 hours) of adult-born JGCs on different days in GL. Man-Whitney test, $P > 0.05$ for comparisons of all time points. Control: n = 206 cells, 8 mice; OD: n= 35 cells, 4 mice. **b**, Comparison of the net or cumulative migration distances of adult-born JGCs. Mann-Whitney test, $P > 0.05$. ns = not significant. Control: n = 234 cells, 8 mice; OD: n= 25 cells, 4 mice. This data were published in Liang et al., 2016.

Taken together, sensory input had no influence on the properties of lateral migration of adult-born JGCs.

3.3.3 Odor deprivation does not affect the endogenous neuronal activity of adult-born JGCs

Because the impaired endogenous neuronal activity of Kv1.2 or Kir2.1 overexpressing adult-born JGCs inhibited their migration (see above), we tested whether the endogenous activity of adult-born JGCs was influenced in

odor-deprived mice. To this end, the same imaging and analysis protocols as above (Chapter 3.1.3, Figure 10) were used. Surprisingly, control and odor-deprived adult-born JGCs displayed nearly the same pattern of spontaneous Ca^{2+} transients (Figure 18a). Further analyses indicated that the maximum Twitch-2B ratio (Figure 18b) and AUC/sec (Figure 18c) were similar between the two groups. This data showed that odor deprivation did not influence endogenous activity of adult-born JGCs.
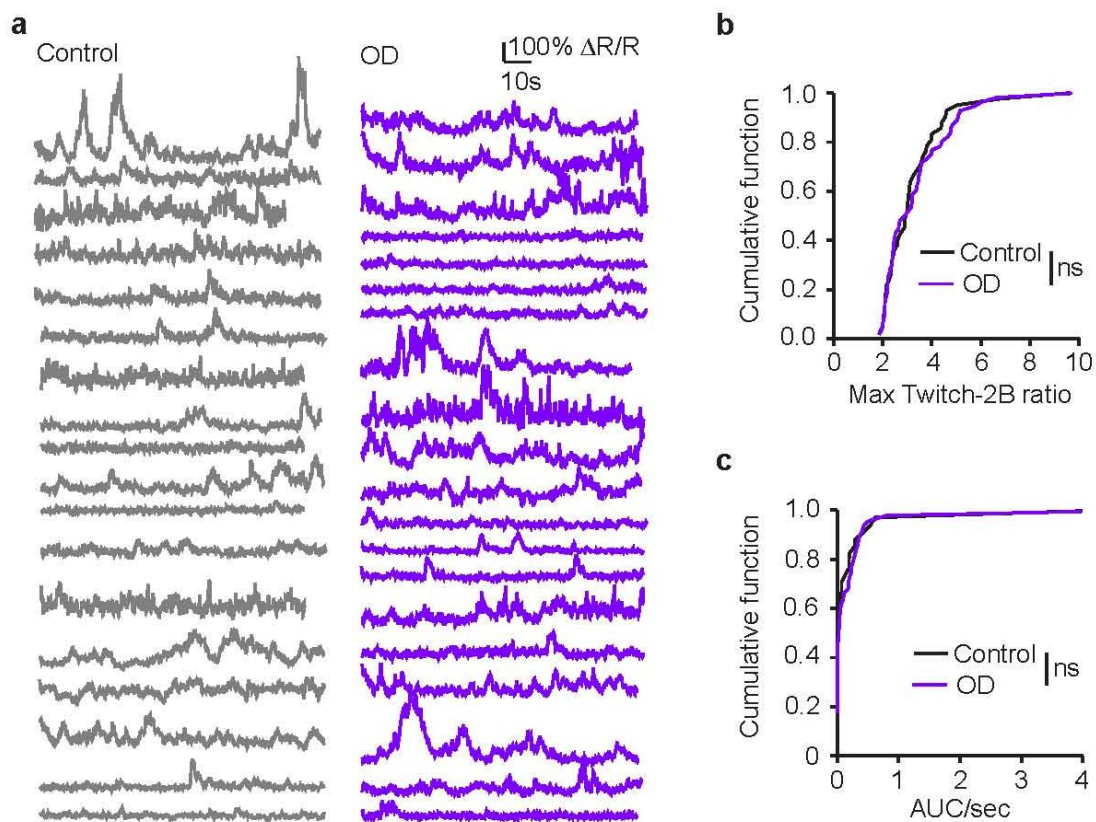

Figure 18. Odor deprivation does not alter endogenous activity of adult-born JGCs. a, Sample traces showing spontaneous Ca^{2+} transients of control and odor-deprived (OD) adult-born JGCs at 12 DPI in awake mice. **b, c,** Cumulative distributions of maximum Twitch-2B ratio (**b**) and AUC/sec (**c**) in control and OD adult-born JGCs. Kolmogorov-Smirnov test: (**c**) $P = 0.62$; (**d**) $P = 0.45$. Control: n = 34 cells, 4 mice; OD: n = 47 cells, 4 mice. ns = not significant.

In conclusion, the overexpression of Kv1.2 or Kir2.1 impaired the endogenous neuronal activity and inhibited the lateral migration of adult-born JGCs. Although

the odor deprivation blocked the odor-evoked activity, it did not change the endogenous activity of adult-born JGCs. The functional integrity of endogenous activity in odor-deprived adult-born JGCs enabled them to migrate normally (Figure 19).
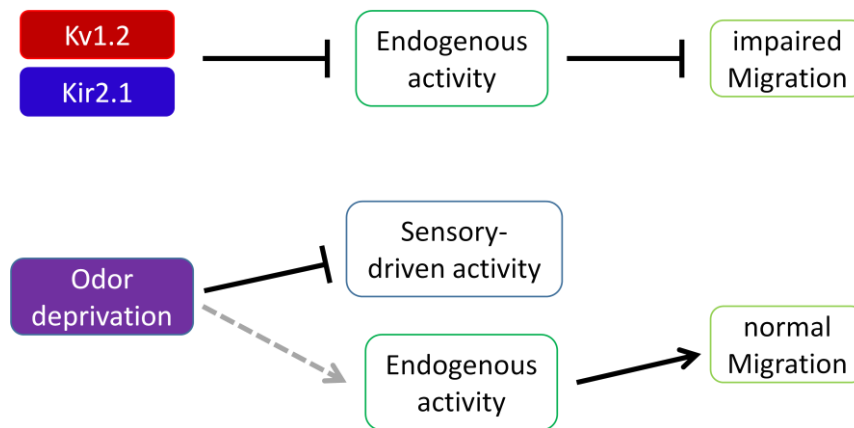

Figure 19. Diagram illustrating the mechanism underlying the lateral migration of adult-born JGCs. Spontaneous activity seems to play a key role in the lateral migration of adult-born JGCs in the GL of the OB.

3.4 Overexpression of Kv1.2 or Kir2.1 impairs the morphogenesis of adult-born JGCs

3.4.1 Retarded morphogenesis of Kv1.2- and Kir2.1-overexpressing adult-born JGCs

The immature adult-born cells in the RMS maintain a spindle shape morphology to enable the fast migration. Upon arrival in the GCL and GL, they obtain dendritic tree quickly (Carleton et al., 2003; Petreanu and Alvarez-Buylla, 2002). Under control conditions migrating adult-born JGCs quickly acquired rather complex morphology shortly after reaching the GL, i.e. at 9-11 DPI (Figure 2a in Kovalchuk et al., 2015). However, Kv1.2- and Kir2.1-overexpressing adult-born JGCs displayed remarkably retarded morphology even at 20 DPI (Figure 20a). These cells had shorter total dendritic branch length (TDBL) and fewer dendritic

branches compared to control adult-born JGCs (Figure 20b, c; Table 6). By measuring the number of intersections between dendrites and soma concentric spheres with 10 μm radius increments (inset of Figure 20d), Sholl analysis also demonstrated that overexpression of Kv1.2 or Kir2.1 significantly decreased the morphological complexity of the adult-born JGCs (Figure 20d).

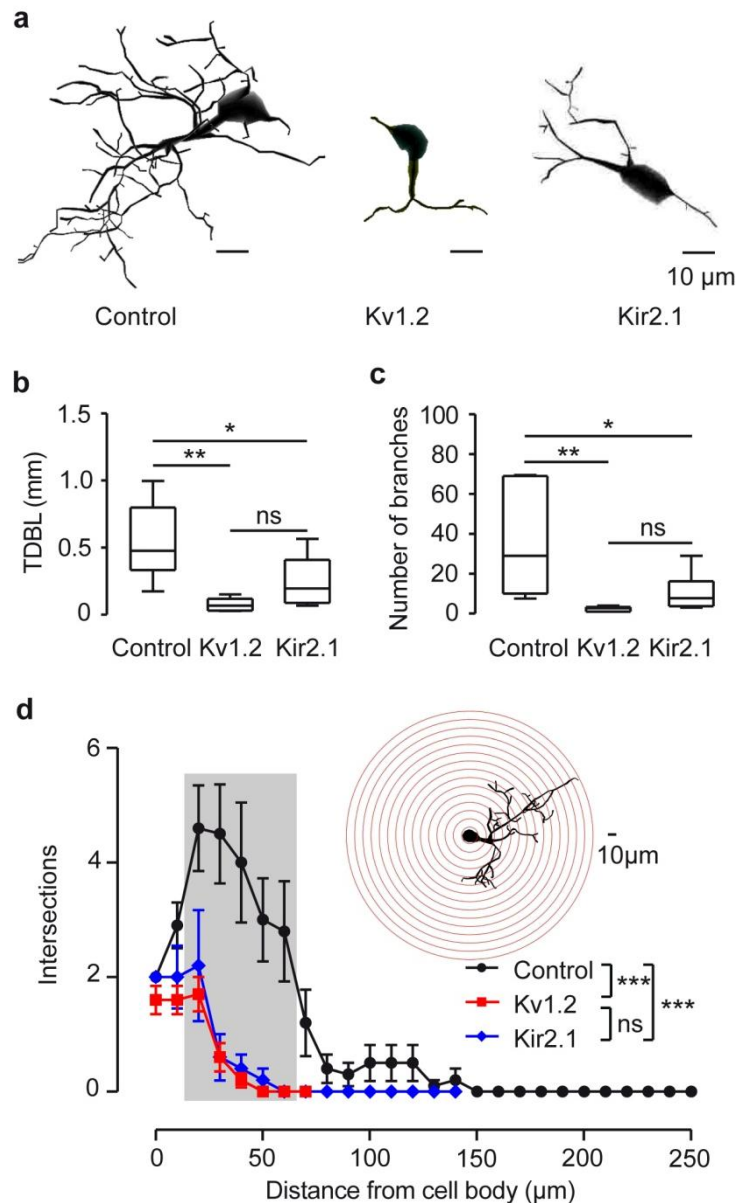**Figure 20. Overexpression of Kv1.2 or Kir2.1 impairs the morphogenesis of adult-born JGCs. a**, Examples of reconstructed adult-born JGCs at 20 DPI from *in vivo* two-photon imaging. Both Kv1.2- and Kir2.1-overexpressing cells displayed retarded morphology. Scale bar = 10μm. **b-c,** Box plots showing the median (per mouse) total dendritic branch length (TDBL) (**b**) and

number of dendritic branches (**c**) of control, Kv1.2- and Kir2.1-overexpressing adult-born JGCs imaged *in vivo* at 20 DPI. **b**, One-way ANOVA: $F_{2, 16}$ = 9.53, P = 1.9×10^{-3}, *post hoc* Tukey's multiple comparisons: Control *vs.* Kv1.2: P = 1.6×10^{-3}; Control *vs.* Kir2.1: P = 0.033; Kv1.2 *vs.* Kir2.1: P = 0.352. **c**, One-way ANOVA, $F_{2, 16}$ = 7.389, P = 5.3×10^{-3}, *post hoc* Tukey's multiple comparisons: Control *vs.* Kv1.2: P = 5.8×10^{-3}; Control *vs.* Kir2.1: P = 0.035; Kv1.2 *vs.* Kir2.1: P = 0.678. **b, c,** Control: n = 7 mice; Kv1.2: n = 6 mice; and Kir2.1: n = 6 mice. Results are median ± IQR. **d,** Sholl analysis showing the complexity of control, Kv1.2- and Kir2.1-overexpressing adult-born JGCs. The inset diagram showing a sample cell overlaid with Sholl spheres with a step size of 10 μm. Two-way ANOVA: $F_{2, 312}$ = 68.54, P = 1×10^{-9}, *post hoc* Tukey's multiple comparisons: ***P < 0.001 for intersections between 10-70 μm from cell body (gray area). ns = not significant. n = 5 mice per group. Results are mean ± SEM.

Table 6. Summary of the TDBL and the number of dendritic branches of control, Kv1.2- and Kir2.1-overexpressing adult-born JGCs imaged *in vivo* at 20 DPI. The same data set as in Figure 20 b, c.

	Control	Kv1.2	Kir2.1
Total dendritic length (μm)	568.2 ± 108.8	75.9 ± 20.41**	246.6 ± 77.02*
Dendritic branch numbers	36.14 ± 9.71	2.42 ± 0.49**	10.58 ± 3.91*

Because a relatively low laser power was used for *in vivo* imaging of Twitch-2B to avoid photobleaching and phototoxicity, some fine dendritic structures might have being overlooked. For better visualization of fine structures, the OBs of control as well as Kv1.2- and Kir2.1-overexpressing mice were fixed and the Twitch-2B fluorescence was enhanced by means of immunohistochemistry. Also under these conditions the immunostained Kv1.2- and Kir2.1-overexpressing adult-born JGCs showed significantly shorter TDBL, fewer dendrite branches and poorer complexity than control cells (Figure 21; Table 7). Note the shorter TDBL of adult-born JGCs in slices (Figure 21b, d) compared with *in vivo* cells (Figure 20b, d). This was most likely caused by the sectioning of brain tissue. In this case, some long dendrites of control adult-born JGCs were truncated. Nevertheless, the slice data confirmed the significantly retarded morphology of Kv1.2- and Kir2.1-overexpressing adult-born JGCs.
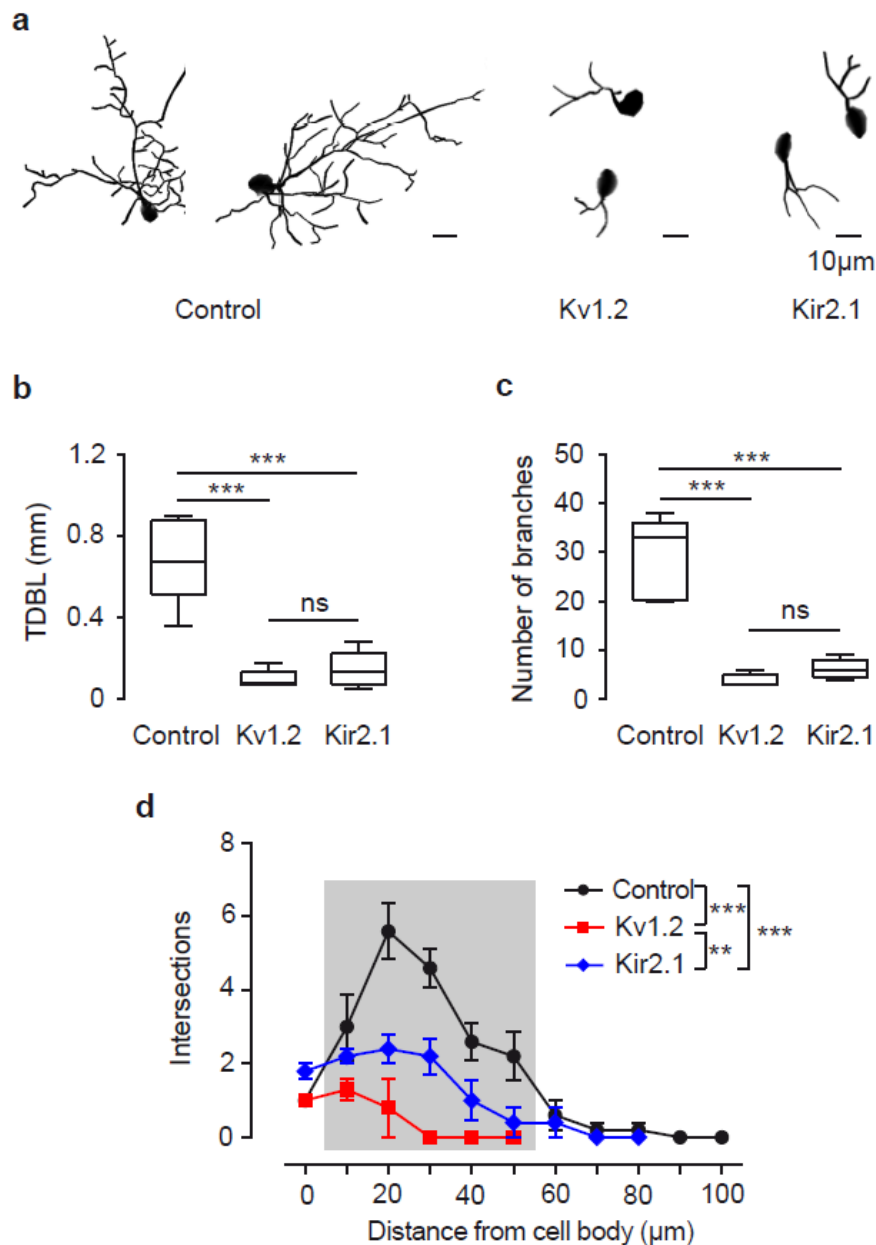
Figure 21. Immunohistochemistry confirms the retarded morphology of Kv1.2- and Kir2.1-overexpressing adult-born JGCs. a, Examples of reconstructed control, Kv1.2- and Kir2.1-overexpressing adult-born JGCs at 20 DPI after immunohistochemical enhancement of cell staining. Scale bar = 10µm. **b, c**, Box plots describing the median (per mouse) TDBL (**b**) and dendritic branch numbers (**c**) of adult-born JGCs. **b**, Kruskal-Wallis test: $P = 1.2 \times 10^{-3}$, *post hoc* Mann-Whitney tests: Control *vs.* Kv1.2: $P = 7.9 \times 10^{-3}$; Control *vs.* Kir2.1: $P = 7.9 \times 10^{-3}$; Kv1.2 *vs.* Kir2.1: $P = 0.42$. **c**, One-way ANOVA: $F_{2, 12} = 39.43$, *post hoc* Tukey's multiple comparisons: Control *vs.* Kv1.2: $P = 1 \times 10^{-5}$; Control *vs.* Kir2.1: $P = 2.7 \times 10^{-5}$; Kv1.2 *vs.* Kir2.1: $P = 0.73$. **d**, Sholl analysis illustrating the complexity of adult-born JGCs morphologies in brain slices at 20 DPI. Two-way ANOVA: $F_{2, 132} = 49.1$, $P = 1 \times 10^{-10}$, *post hoc* Tukey's multiple comparisons: ***$P < 0.001$ for intersections of 10-50 µm from cell body (gray area), n = 5 mice per group. Results are mean

± SEM. ns = not significant.

Table 7. Summary of TDBL and number of dendritic branches of control, Kv1.2- and Kir2.1-overexpressing adult-born JGCs at 20 DPI from immunohistochemistry. The same data set as in Figure 21 b, c, presented as median ± IQR.

	Control	Kv1.2	Kir2.1
Total dendritic length (μm)	670.1 ± 361.3	82.59 ± 62.67**	133.9 ± 149.56**
Dendritic branch numbers	33 ± 15.75	3 ± 2***	6 ± 3.5***

3.4.2 Odor deprivation does not affect the morphogenesis of adult-born JGCs

Next we tested whether the absence of sensory input influences the morphological development of adult-born JGCs. Sholl analysis of *in vivo* imaged cells showed that at 20 DPI odor-deprived adult-born JGCs had morphology comparable with that of control cells (Figure 22). This data suggests that early morphological development of adult-born JGCs does not require sensory input. Interestingly, the morphology of control adult-born JGCs from the group in the OD mice (Figure22) was similar with the control adult-born JGCs in the non-OD mice (Figure 20, Mann-Whitney test, $P > 0.05$ for comparisons of TDBL and number of dendritic branches; Two-way ANOVA, $P > 0.05$ for comparison of intersections). These consistent results suggested that our OD method did not affect the overall health condition of the OB or the mice.

In summary, the overexpression of Kv1.2 or Kir2.1 strongly impaired the morphogenesis of adult-born JGCs whereas odor deprivation had no effect. These data suggested that endogenous but not sensory-driven activity regulated the morphogenesis of adult-born JGCs during early development.
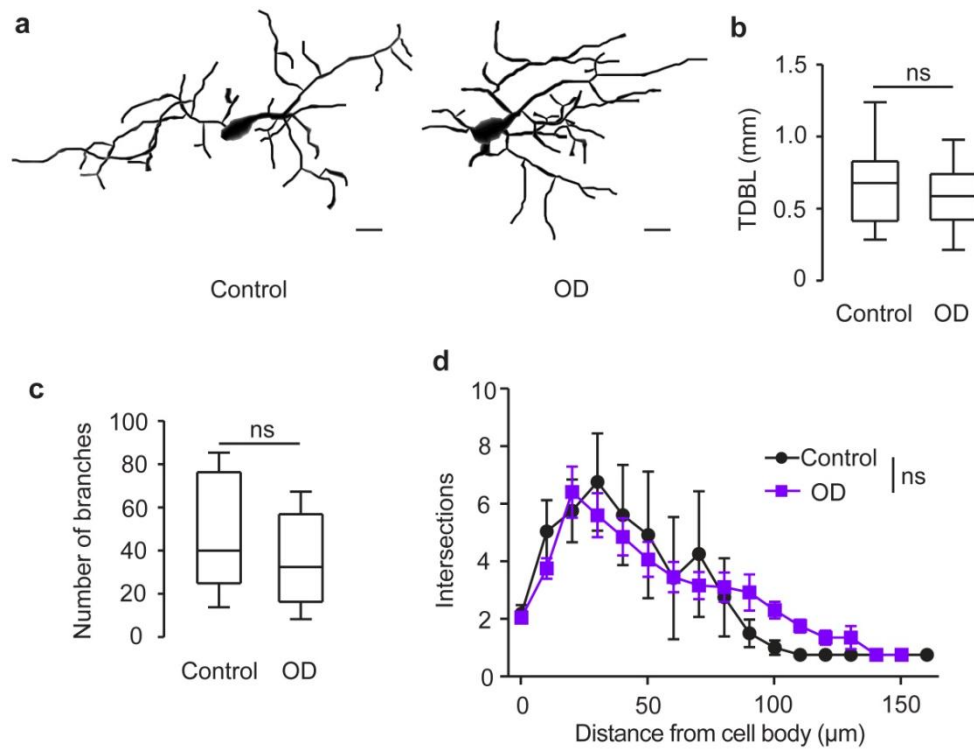
Figure 22. Odor deprivation does not impair the morphology of adult-born JGCs. a,
Examples of reconstructed *in vivo* recorded control and odor-deprived adult-born JGCs at 20 DPI.
Scale bar = 10μm. **b, c**, Box plots illustrating the median (per mouse) TDBL (**b**) and the median
(per mouse) number of dendritic branches (**c**) of adult-born JGCs. Unpaired two-tailed *t* test, *P* >
0.05 for both comparisons. **d**, Sholl analysis showing the similar complexity of adult-born JGCs
morphologies between control and odor-deprived adult-born JGCs. Two-way ANOVA: $F_{1, 425}$ =
0.011, *P* = 0.92. Results are mean ± SEM. n = 4 mice for each group. ns = not significant.

3.5 Overexpression of Kv1.2 or Kir2.1 suppresses odor-evoked activity of adult-born JGCs

Since the Kv1.2- and Kir2.1-overexpressing adult-born JGCs displayed inhibited
migration and retarded morphology, could they still integrate into the neural
circuits? In order to test the *in vivo* functional integrity of Kv1.2- and
Kir2.1-overexpressing adult-born JGCs, we tested their odor responsiveness.
The odor responsiveness of adult-born JGCs was tested at 20 DPI, when these
cells are highly responsive to odors (Kovalchuk et al., 2015; Livneh et al., 2014).
Interestingly, Kv1.2- and Kir2.1-overexpressing adult-born JGCs showed

suppressed responsiveness to odors (Figure 23a). Whereas around 61.5% ± 8.6% (52 out of 78 cells, 6 mice) of control adult-born JGCs responded to odor mixture (2-HA, IAA and ET), this fraction reached 51% ± 6.1% (31 out of 59 cells, 7 mice) for Kv1.2- and only 24.8% ± 6% (16 out of 63 cells, 6 mice) for Kir2.1-overexpressing adult-born JGCs (Figure 23b; Table 8). These data suggest that Kir2.1 overexpression strongly inhibited odorant responsiveness of adult-born JGCs. Furthermore, even though some Kv1.2- and Kir2.1-overexpressing adult-born JGCs responded to odorants, the strength of these responses was much smaller compared to that of control cells (e.g. smaller amplitude and AUC of the odor-evoked Ca^{2+} transients, Figure 23c, d; Table 8).
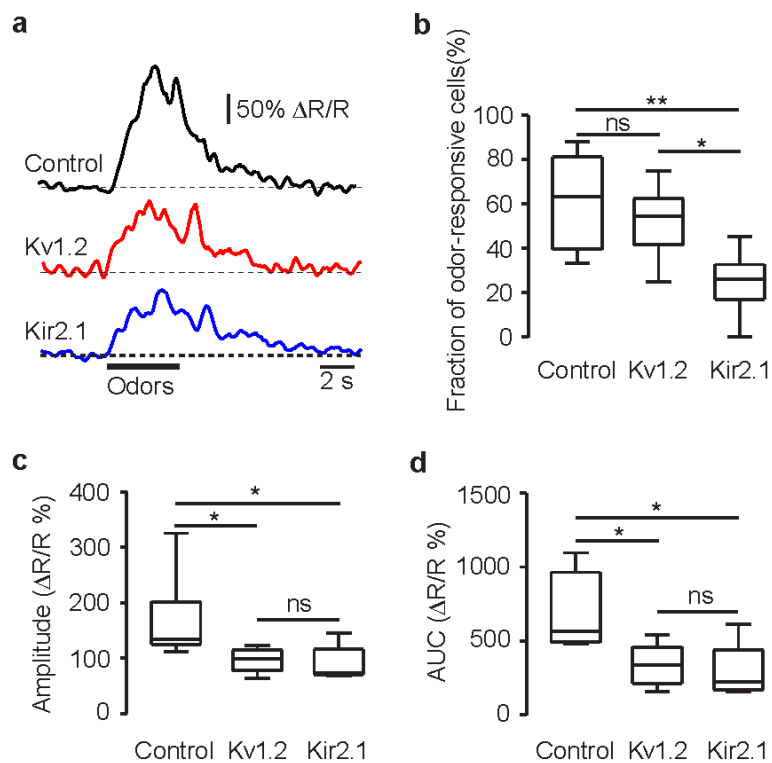
Figure 23. Overexpression of Kv1.2 or Kir2.1 suppresses odor-evoked Ca^{2+} transients in adult-born JGCs. a, Sample traces showing odor-evoked Ca^{2+} transients of control, Kv1.2- and Kir2.1-overexpressing adult-born JGCs at 20 DPI. **b**, Box plot showing median (per mouse) fractions of odor-responding cells in control, Kv1.2- and Kir2.1-overexpressing adult-born JGCs. One way ANOVA: $F_{2,16} = 7.061$, $P = 6.3×10^{-3}$, *post hoc* Tukey's multiple comparisons: Control *vs.* Kv1.2: $P = 0.542$; Control *vs.* Kir2.1: $P = 5.9×10^{-3}$; Kv1.2 *vs.* Kir2.1: $P = 0.04$. Control: n = 6 mice;

Kv1.2: n = 7 mice; Kir2.1: n = 6 mice. **c, d**, Box plots summarizing the median (per mouse) amplitude (**c**) and AUC (**d**) of odor-evoked Ca^{2+} transients. **c,** Kruskal-Wallis test: $P = 1.5 \times 10^{-3}$, *post hoc* Dunn's multiple comparisons: Control *vs.* Kv1.2: $P = 0.016$; Control *vs.* Kir2.1: $P = 0.016$; Kv1.2 *vs.* Kir2.1: $P = 0.99$. **d,** Kruskal-Wallis test, $P = 4.8 \times 10^{-3}$, *post hoc* Dunn's multiple comparisons: Control *vs.* Kv1.2: $P = 0.027$; Control *vs.* Kir2.1: $P = 0.032$; Kv1.2 *vs.* Kir2.1: $P = 0.99$. Control: n = 7 mice, Kv1.2: n = 7 mice, Kir2.1: n = 5 mice. *$P < 0.05$, **$P < 0.01$, ns = not significant. Results are median ± IQR.

Table 8. Summary of the parameters of odor-evoked Ca^{2+} transients in control, Kv1.2- and Kir2.1-overexpressing adult-born JGCs. Fractions of responsive adult-born JGCs in the respective cohort are shown as mean ± SEM. Amplitude and AUC of odor-evoked responses are presented as median ± IQR. The same data set as in Figure 23.

	Control	Kv1.2	Kir2.1
Fraction of odor responsive adult born JGCs %	61.47 ± 8.63	51.02 ± 6.12	24.84 ± 5.96*
Amplitude (ΔR/R %)	134.5 ± 76.2	98.89 ± 36.24*	73.75 ± 45.83*
Area under the curve (ΔR/R %)	563.6 ± 471.8	336.2 ± 247.6*	223.1 ± 266.5*

In summary, notwithstanding that the odor-evoked activity occurred in some Kv1.2- and Kir2.1-overexpressing adult-born JGCs, the strength of odor-evoked Ca^{2+} transients was reduced. Besides, the overexpression of Kir2.1 decreased the response probability of adult-born JGCs.

3.6 Overexpression of Kv1.2 or Kir2.1 decreases the survival rate of adult-born JGCs

Considering the severely impaired migration, morphogenesis and odor responsiveness of Kv1.2- and Kir2.1-overexpressing adult-born JGCs, we continued by exploring the fate of these cells. To this end, all adult-born JGCs were monitored over a time period of a month from 14 to 45 DPI. The adult-born JGCs which stayed at the same position and possessed similar morphology during the recording time period were considered as surviving cells (for details see Chapter 2.10.6). Interestingly, fewer surviving cells were found in Kv1.2- and

Kir2.1-overexpressing adult-born JGCs (Figure 24). The mean (per mouse) survival rates between 14-25 DPI were: Control: 65.86% ± 5.64%; Kv1.2: 39.45% ± 6.45%; Kir2.1: 32% ± 5.79% (Figure 24c). Thus, the overexpression of Kv1.2 or Kir2.1 diminished the survival rate of the adult-born JGCs from 14 to 25 DPI. The median (per mouse) survival rates between 25-45 DPI, the time period when adult-born JGCs in control mice are stationary, were: Control: 80% ± 20.76%; Kv1.2: 80% ± 24.17%; Kir2.1 43.93% ± 27.81% (Figure 24d). Unexpectedly, in this case Kv1.2-overexpressing adult-born JGCs exhibited survival rate similar to that of control cells, whereas Kir2.1 overexpression continued decreasing cell survival. The survival rate of control adult-born JGCs was estimated to be 52.68% (65.86% (14-25 DPI) x 80% (25-45 DPI) = 52.68%) between 14-45 DPI. This number is consistent with the published data (Mandairon et al., 2006; Petreanu and Alvarez-Buylla, 2002; Winner et al., 2002).

Thus, overexpression of Kv1.2 significantly decreased the survival rate of adult-born JGCs during the early phase of survival (14-25 DPI). Kir2.1 overexpression decreased the survival rate of adult-born JGCs both during the early (14-25 DPI) and the late phase (25-45 DPI).
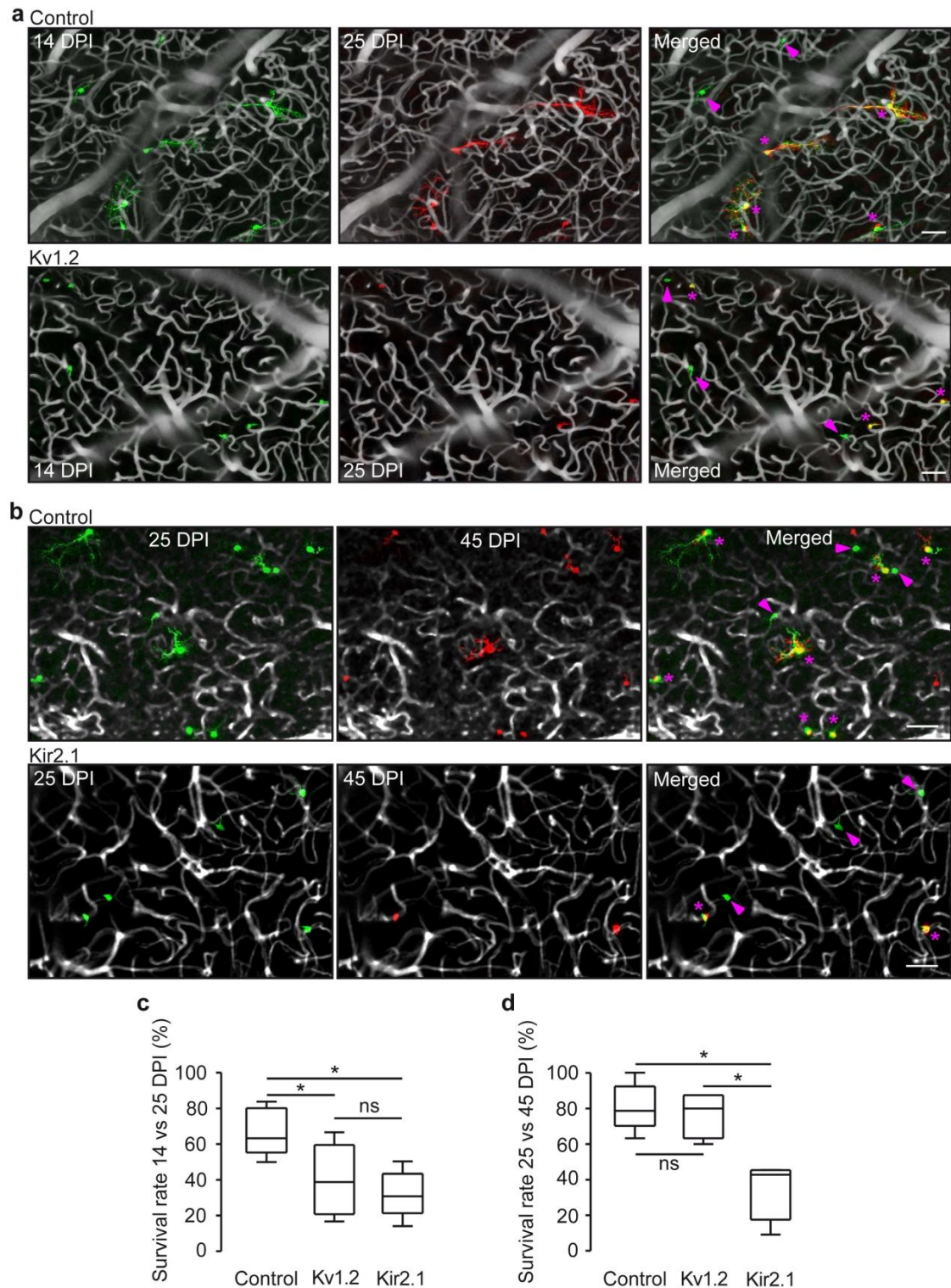
Figure 24. Overexpression of Kv1.2 or Kir2.1 decreases the survival rate of adult-born JGCs. a, b, Sample maximum projection images (MPIs) showing the median (per mouse) fractions of control, Kv1.2- and Kir2.1-overexpressing adult-born JGCs surviving between 14-25 DPI (**a**), and between 25-45 DPI (**b**). **a,** Control: MPI of 40-80 μm below the dura; Kv1.2: MPI of 20-50 μm below the dura; **b**, Control: MPI of 13-80 μm below the dura; Kir2.1: MPI of 33-65 μm

below the dura. Asterisks indicate cells, which have survived till 25 or 45 DPI. Arrowheads indicate cells, which disappeared during the recording period. All images are cropped and none of the cells shown here was in reality close to the border of the imaging stack. Scale bar = 50 µm. **c, d,** Box plot showing median (per mouse) fractions of cells among control, Kv1.2- and Kir2.1-overexpressing adult-born JGCs surviving between 14-25 DPI (**c**) and 25-45 DPI (**d**). **c**, One-way ANOVA: $F_{2, 15}$ = 6.947, *P* = 8.1×10^{-3}, *post hoc* Tukey's multiple comparisons: Control vs. Kv1.2: *P* = 0.024; Control vs. Kir2.1: *P* = 9.6×10^{-3}; Kv1.2 vs. Kir2.1: *P* = 0.69. Control: n = 5 mice; Kv1.2: n = 8 mice; Kir2.1: n = 5 mice. **d**, Kruskal-Wallis test: *P* = 8.5×10^{-3}, *post hoc* Dunn's multiple comparisons: Control vs. Kv1.2: *P* = 0.99; Control vs. Kir2.1: *P* = 0.03; Kv1.2 vs. Kir2.1: *P* = 0.046. Control: n = 5 mice, Kv1.2: n = 5 mice, Kir2.1: n = 4 mice. **P* < 0.05, ***P* < 0.01, ns = not significant*.

3.7 CREB signaling in Kv1.2- or Kir2.1-overexpressing adult-born JGCs

Previous reports demonstrated that CREB signaling pathway is involved in the differentiation and survival of adult-born neurons in the OB (Giachino, 2005; Herold et al., 2011). Those studies encouraged us to further investigate whether the CREB signaling pathway is inhibited in Kv1.2- and Kir2.1-overexpressing adult-born JGCs. Immunohistochemical analysis showed that at 10 DPI the expression of pCREB was high in control adult-born JGCs but decreased remarkably in Kv1.2- and Kir2.1-overexpressing adult-born JGCs (Figure 25a). The pCREB expression is typically abundant in developing neurons and low in mature neurons (Giachino, 2005; Herold et al., 2011; Jagasia et al., 2009). To quantify the relative level of CREB in adult-born JGCs, we normalized the pCREB fluorescence of adult-born JGCs to that of the surrounding NeuN positive resident neurons. At 10 DPI the median (per mouse) relative pCREB levels were: Control: 19.74 ± 1.73; Kv1.2: 5.61 ± 0.73; Kir2.1: 5.79 ± 0.77 (Figure 25b) and at 28 DPI these values reached: Control: 4.56 ± 0.55; Kv1.2: 1.52 ± 0.16; Kir2.1: 1.37 ± 0.15 (Figure 25c). Thus, the pCREB levels in Kv1.2- and Kir2.1-overexpressing adult-born JGCs were clearly lower compared to control cells.
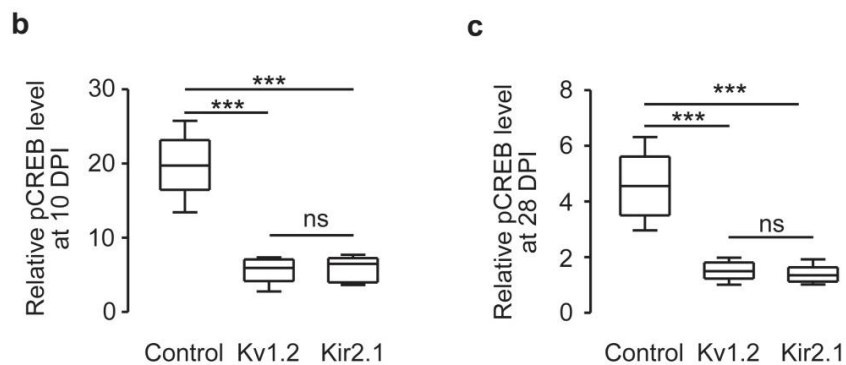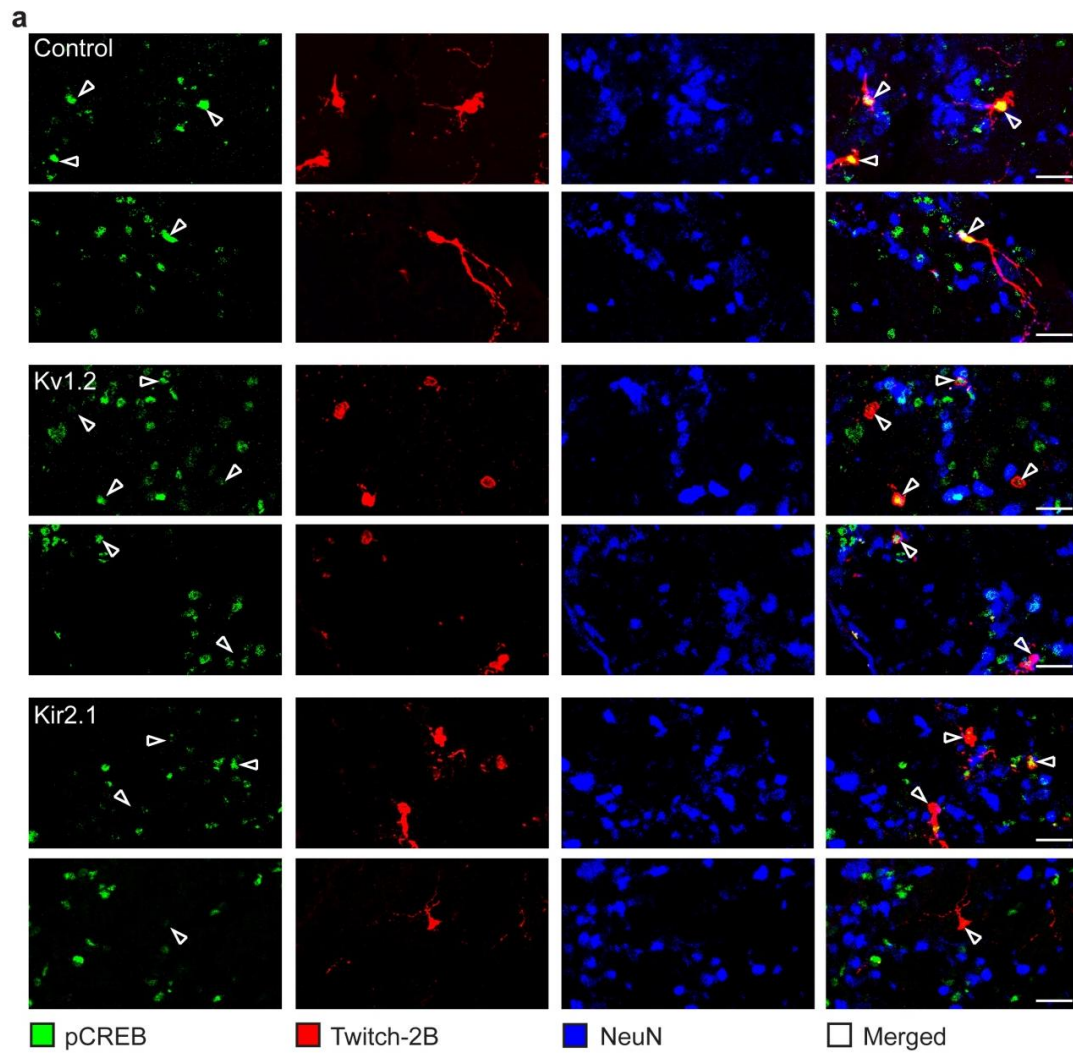
Figure 25. Overexpression of Kv1.2 or Kir2.1 down-regulates pCREB signaling pathway. a, Sample maximum projection images (20 μm thickness for all) showing pCREB expression in control, Kv1.2- and Kir2.1-overexpressing adult-born JGCs at 10 DPI. Anti-GFP antibodies were used to visualize Twitch-2B-positive adult-born JGCs and anti-NeuN antibodies helped to visualize mature neurons in the GL. Scale bar = 20 μm. **b, c**, Box plots showing the median (per mouse) relative pCREB expression levels of control, Kv1.2- and Kir2.1-overexpressing

adult-born JGCs at 10 DPI (**b**) and 28 DPI (**c**). **b**, One-way ANOVA: $F_{2, 14}$ = 45.73, P = 7.3×10^{-7}, *post hoc* Tukey's multiple comparisons: Control *vs.* Kv1.2: P = 2×10^{-6}; Control *vs.* Kir2.1: P = 4×10^{-6}; Kv1.2 *vs.* Kir2.1: P = 0.99. Control: n = 6 mice, Kv1.2: n = 6 mice, Kir2.1: n = 5 mice. **c**, One-way ANOVA: $F_{2, 12}$ = 27.88, P = 3×10^{-5}, *post hoc* Tukey's multiple comparisons: Control *vs.* Kv1.2: P = 1×10^{-4}; Control *vs.* Kir2.1: P = 7×10^{-5}; Kv1.2 *vs.* Kir2.1: P = 0.95. n = 5 mice each group. ***P < 0.001, ns = not significant. Results are median ± IQR.

Interestingly, the pCREB expression in control adult-born JGCs dropped down sharply from 10 to 28 DPI (10 DPI: 19.74 ± 1.73; 28DPI: 4.56 ± 0.55. Unpaired t test with Welch's correction, P = 1.59×10^{-4}), which suggested that the pCREB regulated genetic transcription (see Chapter 1.3) was more active at earlier age. This corresponded to the fast migration and morphogenesis during early development when a large amount of cytoskeleton proteins were needed to enable motility and form dendritic structures.

Evidently, these data showed that pCREB signaling pathway was down-regulated in Kv1.2- and Kir2.1-overexpressing adult-born JGCs.

4. Discussion

To our knowledge, this is the first study demonstrating that endogenous activity regulates the migration, morphogenesis, and early-phase survival (14-25 DPI) of adult-born JGCs, whereas sensory-driven activity does not affect migration or morphogenesis but influences late-phase survival (25-45 DPI) of adult-born JGCs. Particularly, the early development of adult-born JGCs is very sensitive to the proper level of endogenous activity. Even moderate alteration of endogenous activity via overexpression of Kv1.2 or Kir2.1 leads to dramatic impairment of neuronal migration, morphogenesis, and survival. However, adult-born JGCs migrate and grow dendritic processes normally in the absence of sensory-driven activity. Moreover, the CREB signaling pathway is down-regulated in Kv1.2- and Kir2.1-overexpressing adult-born JGCs. Based on these findings, we propose endogenous activity coupling with CREB signaling pathway regulates the early development of adult-born neurons in the mouse olfactory bulb.

4.1 Endogenous activity regulates the migration of adult-born neurons

We report here for the first time that endogenous activity but not sensory-driven activity regulates the migration of adult-born neurons in the GL of the mouse OB (Figure 19). During adult neurogenesis adult-born cells undergo migration, differentiation and integration which take place in the fully mature and constantly wiring neural circuits. So far, the mechanisms regulating the migration of adult-born cells remain unclear. Unlike adult-born GCs which stop migration and integrate into the circuits at the same position, many adult-born JGCs may stop for long time periods (from 12 h to a few days) before resuming the movement and can even traverse several glomeruli before integration (Liang et al., 2016). Therefore we questioned what are the mechanisms underlying this unique

migrating pattern, sensory input or intrinsic factors? From our recent work, we found a ubiquitous presence of spontaneous Ca^{2+} transients in immature adult-born JGCs *in vivo*. This endogenous activity is robustly present in awake state during the whole recording time period (from 8 DPI until 44 DPI, approximately 5 weeks). The strength of this activity showed a bell-shaped dependence on cell's age, peaking around 3 weeks after birth (Maslyukov et al., 2018). Interestingly, during the arising phase of the endogenous activity, the migration speed and overall cell motility of adult-born JGCs decreased by age, for example from 8 to 14 DPI (Figure 11 and 12). Furthermore, at the time of peak strength of endogenous activity (~3 weeks of age), about 80% of adult-born JGCs were stable (see Fig. 7C from Liang et al., 2016). These findings suggest that the increasing strength of endogenous activity is a stop signal for migration of adult-born JGCs, in agreement with the role of endogenous activity in the migration of cortical neurons during perinatal development (Bando et al., 2014; Bando et al., 2016; Hurni et al., 2017). Increasing (Bando et al., 2014; Hurni et al., 2017) or decreasing (De Marco Garcia et al., 2011) endogenous activity impaired the migration and laminar positioning of postnatally generated cortical neurons. These indirect evidence and our data implied a role of endogenous activity in the migration of adult-born cells. To test our hypothesis, we genetically overexpressed Kv1.2 or Kir2.1 in the adult-born neurons to selectively change the spiking behavior of frequently or even continuously active cells by decreasing their fraction as well as their area under the curve and the maximum Twitch-2B ratio. Our *in vivo* data demonstrated that this moderate alteration of endogenous activity severely inhibited lateral migration of adult-born JGCs. Moreover, Kir2.1 overexpression led to stronger inhibition on neuronal migration at 14 DPI than Kv1.2, which might due to its role in decreasing neuronal excitability.

Contrastively, the blockade of sensory-driven activity in an odor deprivation

model did not affect either fine single-step migration (every 15 minutes in 4 hours at 8 DPI) or global migration (every 12 hours from 5.5–14.5 DPI) of adult-born JGCs. This finding is accordant with previous reports showing that neuroblasts still migrate in the RMS and OB without sensory input (Kirschenbaum et al., 1999; Petreanu and Alvarez-Buylla, 2002). We further investigated the reason of this normal migration under odor deprivation condition and found the endogenous activity was well preserved in these odor-deprived adult-born JGCs. This functional integrity of endogenous activity probably maintained the migration ability of the adult-born neurons in the absence of sensory input. Putting all together, endogenous but not sensory-driven activity regulates the lateral migration of adult-born neurons in the GL of mouse OB.

4.2 Endogenous activity regulates the morphogenesis of adult-born neurons

Our results demonstrated that the moderate alteration of endogenous activity significantly withheld the morphogenesis of adult-born JGCs *in vivo*. Furthermore, adult-born JGCs developed normal morphology in the absence of sensory-driven activity. This is in accordance with previous data which showed the morphological development of adult-born JGCs at 10-13 DPI (Mizrahi 2007) and adult-born GCs (Petreanu et al., 2002; Dahlen et al., 2011) is not dependent on sensory input.

In the perinatal brain, impaired endogenous neuronal activity inhibits morphogenesis (Cancedda et al., 2007; De Marco García et al., 2011) and increasing endogenous activity alters the pattern of morphogenesis (Bando et al., 2016). Before our study, the role of endogenous activity in the morphogenesis of adult-born neurons was not clear yet. The genetically modified endogenous activity via overexpression of ESKir2.1 (a gain-of-function mutation form of

inward rectifying potassium channel, which is supposed to decrease neuronal excitability) or NaChBac (bacterial voltage-gated sodium channel, which is supposed to increase neuronal firing) showed no significant effect on the morphogenesis of adult-born GCs in the OB (Lin et al., 2010). Another study showed the knockdown of voltage-gated sodium channels (Na$_V$1.1-1.3) decreased morphological complexity of postnatally generated GCs (Dahlen et al., 2011). The different results might due to different modifications of neuronal activity by those channels and different brain development stages (adult or postnatal). Here we show the *in vivo* morphogenesis of adult-born JGCs is regulated by endogenous but not sensory-driven activity.

4.3 Endogenous and sensory-driven activity regulate the survival of adult-born neurons

Our results provided *in vivo* evidence that endogenous and sensory-driven activity regulate survival of adult-born neurons in a chronological pattern. Endogenous activity regulates neuronal survival in the early phase (14-25 DPI) and sensory-driven activity takes over the stage in the late phase (25-45 DPI).

It has been reported that ~50% of adult-born neurons die shortly after arriving the OB (Petreanu and Alvarez-Buylla, 2002; Winner et al., 2002). The reason for this born-to-die phenomenon is not elucidated yet. In the present study, we monitored the positions and morphology of adult-born JGCs *in vivo* at single-cell level from 14 to 45 DPI. Our results showed that impaired endogenous activity clearly decreased neuronal survival rate in Kv1.2- and Kir2.1-overexpressing adult-born JGCs during the early phase (14-25 DPI) (Figure 24c). The finding that Kv1.2-overexpressing adult-born JGCs showed similar survival rate during the late phase (25-45 DPI) as control cells suggested that the inhibition effect of Kv1.2 overexpression on neuronal survival vanished away after 25 DPI. This

finding suggested that endogenous activity only influenced the early-phase survival of adult-born neurons. In addition, Kir2.1 overexpression further decreased the survival rate of adult-born JGCs during the late phase (Figure 24d). Combining the strong inhibition effect of Kir2.1 overexpression on odor-evoked activity of adult-born JGCs (Figure 23b), we inferred that the lower survival rate of Kir2.1-overexpressing adult-born JGCs was caused by the impairment of odor-evoked activity. From the comparison between Kv1.2- and Kir2.1-overexpressing adult-born JGCs, we concluded that endogenous activity regulates the survival in an early phase (14-25 DPI) and sensory-driven activity dominantly regulates survival in the late phase (25-45 DPI). This data is consistent with an *in situ* study which showed increasing of cell-intrinsic excitability enhanced survival of adult-born GCs while decreasing of cell-intrinsic excitability compromised survival of adult-born GCs (Lin et al., 2010). Because of the role of neuronal activity in triggering various transcription programs (Flavell and Greenberg, 2008), Kv1.2 and Kir2.1-overexpressing adult-born neurons with improper level of endogenous activity might fail to launch adequate gene transcriptions (for example BDNF, cytoskeleton proteins) which are crutial for growth and survival of neurons.

It is demonstrated that deprivation of sensory-driven activity decreases the survival rate of adult-born neurons (Mandairon et al., 2006, 2003; Petreanu and Alvarez-Buylla, 2002; Saghatelyan et al., 2005; Yamaguchi and Mori, 2005), while enhancement of sensory-driven activity increases the survival rate of adult-born neurons (Bovetti et al., 2009; Rochefort et al., 2002; Rochefort and Lledo, 2005). These studies suggested a critical period of death after odor deprivation during 14-28 DPI for adult-born GCs and 15-30 DPI for adult-born JGCs. However, our results inferred that sensory-driven activity dominantly regulates survival in the late phase from 25 to 45 DPI. This likely comes for two reasons. First, the previous studies used long-lasting and extreme deprivation

model, e.g. anosmic transgenic mice lacking all electrical activity in the olfactory epithelium and electrical input into the OB; naris occlusion or naris cauterization method which totally blocked any sensory input to the whole olfactory bulb. In these odor-deprived olfactory bulbs, the neuronal activity of not only adult-born neurons but also any other types of neurons as well as the whole network was blocked. The mechanisms of generating spontaneous (endogenous) activity of adult-born neurons are related to the neural network, including depolarizing of GABA, transient synaptic connections, extrasynaptic transmission, gap junctions coupling and pacemaker neurons (Blankenship and Feller, 2010). Previous study showed that after 3 weeks of odor deprivation in rat pups the spontaneous (endogenous) activity was inhibited significantly due to the robust changes in olfactory bulb anatomy and neurochemistry (Guthrie et al., 1999). Thus, in these long-lasting and extreme odor-deprived bulbs, the odor-evoked activity and endogenous activity were probably both suppressed. The previous reported high death rate of adult-born neurons during the first 15-30 days might be caused by superimposed inhibition effects on both endogenous and sensory-driven activity. In the present work, we used Kv1.2 overexpression to solely inhibit endogenous activity and Kir2.1 overexpression to inhibit both endogenous and sensory-driven activity of adult-born neurons while keeping the activity of neural network intact. Since Kir2.1-overexpressing adult-born JGCs showed similar survival rate as Kv1.2-overexpressing cells during 14-25 DPI yet much lower survival rate during 25-45 DPI, we propose that sensory-driven activity dominantly regulates the survival of adult-born neurons from 25 DPI onward.

4.4 Coordinated endogenous activity and genetic programs during the early development of adult-born neurons

Our data revealed an important role of endogenous activity in activating CREB signaling pathway to trigger a wide spectrum of activity-dependent transcription

programs to promote the neuronal migration, morphogenesis, and survival of immature adult-born neurons. The impaired migration, morphogenesis and survival of Kv1.2- and Kir2.1-overexpressing adult-born JGCs prompted us to further investigate in which mechanisms endogenous activity regulates the early development of adult-born JGCs. As a primary link between electrical activity and biochemical events, intracellular Ca^{2+} acts as a second messenger to mediate a wide spectrum of cellular functions and rapidly transduces neuronal activity to gene expression (for review, see Flavell and Greenberg, 2008; Zheng and Poo, 2007). Recent studies have revealed that Ca^{2+}-dependent signaling pathways are deployed in neuronal development for regulating cytoskeletal dynamics associated with neuronal migration, axon and dendrite development and regeneration, and synaptic plasticity (Zheng and Poo, 2007). Among these activity regulated factors, CREB is one of the most important transcription factors regulating the expression of c-fos, BDNF, tyrosine hydroxylase, and numerous neuropeptides. BDNF supports the survival of existing neurons and facilitates the growth and differentiation of new neurons and synapses.

In this study, we report that immature adult-born neurons need a proper level of endogenous activity to activate pCREB related transcriptions to promote dendritic growth and maintain neuronal survival. Inhibition of endogenous activity in the adult-born neurons down-regulates pCREB signaling pathway and also likely the expression of skeleton proteins and neurotrophins, which finally leads to impaired migration, retarded morphology and decreased survival of adult-born neurons. Future studies investigating which genes and proteins are involved in the regulating neuronal morphogenesis and survival will highlight the potency to reprogram neural stem cells for clinical therapies.

4.5 The interplay between endogenous and sensory-driven activity in adult-born neurons

To the best of our knowledge, we for the first time report the interplay between endogenous and sensory-driven activity during the development of immature adult-born neurons. Our data demonstrate the robust presence of endogenous activity in immature adult-born neurons, which is well maintained even in the absence of sensory input. However, endogenous activity may directly or indirectly interfere with the sensory-driven activity in adult-born neurons.

By using *in vivo* two-photon Ca^{2+} imaging in awake mice, we found that the endogenous activity of adult-born neurons was not affected by odor-deprivation. The odor-deprived immature adult-born JGCs at 12 DPI exhibited similar properties of spontaneous Ca^{2+} transients as control cells (Figure 18). In other words, the absence of sensory-driven activity did not affect the overall strength of endogenous activity. This finding confirmed the robustness of endogenous activity in adult-born neurons as shown in other embryonic and postnatal studies showing that endogenous (spontaneous) activity relies on different co-existing and maybe also cooperating mechanisms to maintain its presence (Blankenship and Feller, 2010; Kirkby et al., 2013; Luhmann et al., 2016). As discussed above, long-lasting (30 days) odor deprivation changed the global network activity of olfactory bulb including endogenous (spontaneous) activity (Guthrie et al., 1999). Another study showed only by 12 days of deprivation, the bulb starts to display smaller size (Brunjes et al., 1985). Here in our study, the adult-born JGCs were deprived for 1 week (from 5 DPI to 12 DPI) at which time odor deprivation has not changed the OB size (Figure 15) and adult-born JGCs displayed robust endogenous activity (Fgiure18). This suggests that the olfactory bulb has several redundant mechanisms to maintain the endogenous activity without sensory input.

We further investigated whether endogenous activity influences sensory-driven

activity in these immature neurons. Altered endogenous activity in Kv1.2- and Kir2.1-overexpressing adult-born JGCs (Figure 10) suppressed the odor-evoked activity (Figure 23), suggesting an interference of endogenous activity in sensory-driven activity. This interference might function directly or indirectly. For instance, dysfunction of endogenous activity may isolate the adult-born neuron from the synchronized neural network, thus directly affect their responses to sensory input. Or, impaired endogenous activity inhibits the morphogenesis of adult-born neurons and reduces the synaptic connections between adult-born neurons and neighboring neurons. In this case, adult-born neurons cannot receive strong enough afferent input to evoke responsiveness. Our finding highlights the interplay between endogenous and sensory-driven activity in adult-born neurons and confirms the seminal work of Arieli et al. which demonstrated that the variability of evoked cortical responses is regulated by ongoing spontaneous activity in the cat visual cortex (Arieli et al., 1996; Ferezou and Deneux, 2017).

4.6 The mechanisms underlying the early development of adult-born neurons

Based on the results of the present study, we propose a mechanism to account for the early development of adult-born neurons. We found that endogenous neuronal activity regulates the migration, morphogenesis, and survival of adult-born neurons in the mouse OB by coupling with CREB signaling pathway mediated transcription programs (Figure 26). Endogenous and sensory-driven activity regulates survival of adult-born neurons in a chronological pattern. Endogenous activity determines the early development of adult-born neurons (e.g. until 25 DPI), whereas sensory-driven activity regulates survival of adult-born neurons from 25 DPI onward. Both types of neuronal activity are

important for the final integration of adult-born neurons into the adult olfactory bulb network.
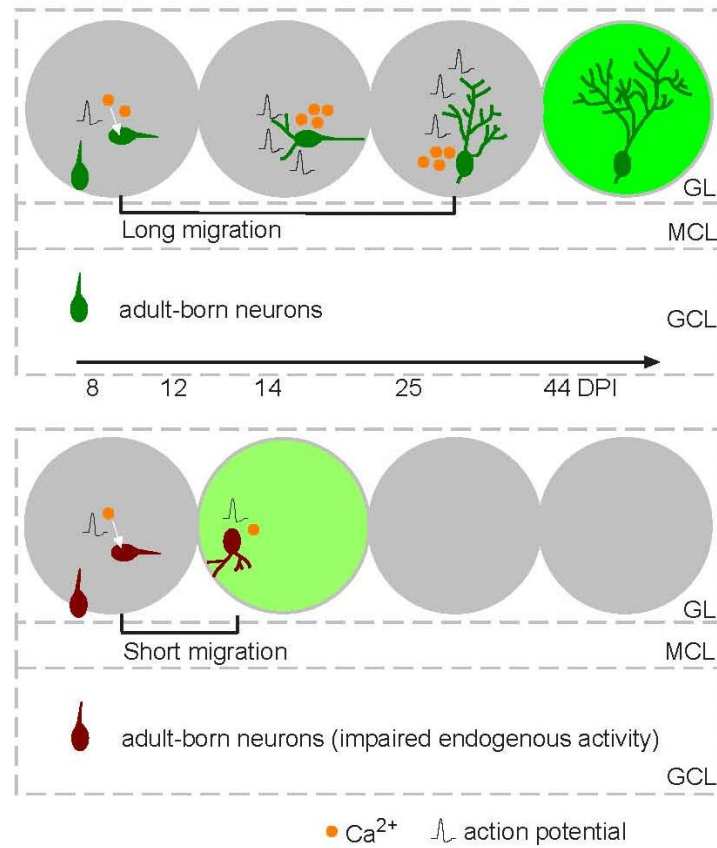

Figure 26. Roles of endogenous activity during early development of adult-born neurons. Adult-born neurons arrive in the GL and traverse one or several glomeruli to integrate into the neural circuits. Endogenous activity plays key roles in the migration, morphogenesis and survival of adult-born neurons. Adult-born neurons with a proper level of endogenous activity successfully integrate into the glomerulus (dark green), whereas cells with impaired endogenous activity cannot integrate into the glomerulus (light green) and probably die later. GL, glomerular layer; MCL, mitral cell layer; GCL, granule cell layer.

Summary

Thousands of adult-born neurons are added to the mouse olfactory bulb on a daily basis. The mechanisms underlying the migration, morphogenesis and survival of adult-born neurons are not well understood. In the present work, we studied the roles of endogenous and sensory-driven neuronal activity in the *in vivo* development of adult-born neurons in the mouse olfactory bulb. We utilized the overexpression of potassium channel, Kv1.2 or Kir2.1, to genetically modify the endogenous activity of adult-born neurons. By using *in vivo* two-photon Ca^{2+} imaging in awake mice, we found a ubiquitous presence of spontaneous Ca^{2+} transients in control and even Kv1.2- and Kir2.1-overexpressing adult-born neurons. The overexpression of Kv1.2 or Kir2.1 selectively changed the spiking behavior of frequently or even continuously active cells by decreasing their fraction as well as their area under the curve and the maximum Twitch-2B ratio. We further monitored the *in vivo* development of these Kv1.2- and Kir2.1-overexpressing adult-born neurons and discovered that their migration, morphogenesis, odor-evoked responsiveness, and early-phase (14-25 DPI) survival rate were remarkably impaired. Furthermore, whereas Kv1.2-overexpressing adult-born neurons showed similar survival rate as control cells during the late-phase (25-45 DPI) survival, the Kir2.1-overexpressing cells showed significantly lower survival rate. It is probably because, unlike Kv1.2 overexpression which solely altered endogenous activity, Kir2.1 overexpression impaired both endogenous and sensory-driven activity. These data suggest that the survival of adult-born neurons was predominantly regulated by endogenous activity in the early phase and by sensory-driven activity in the late phase.

Furthermore, we tested the role of sensory-driven activity in the development of adult-born neurons. The odor-deprived adult-born neurons displayed normal migration and morphology, thus suggesting that sensory-driven activity did not affect the early development of adult-born neurons. Further analysis revealed

that the odor-deprived adult-born neurons maintained a normal level of endogenous activity.

We also explored the interplay between endogenous and sensory-driven activity. Using *in vivo* Ca^{2+} imaging of individual cells, we found that impaired endogenous activity was paralleled by suppressed sensory-driven activity. However, odor deprivation did not change the properties of spontaneous activity in adult-born neurons. This data suggest that endogenous activity is robust in immature adult-born neurons.

Finally, we explored which signaling pathway is involved in the development of adult-born neurons. Our results demonstrated that pCREB expression was down-regulated in Kv1.2- and Kir2.1-overexpressing adult-born neurons. We propose that impaired endogenous neuronal activity inhibits Ca^{2+}-pCREB signaling pathway as well as the expression of pCREB-dependent genes.

In conclusion, our data demonstrate that endogenous but not sensory-driven activity plays a key role in regulating migration, morphogenesis and early-phase survival of adult-born neurons in the mouse olfactory bulb, and identify an important role of Kv1.2/Kir2.1 in the developmental processes mentioned above. Furthermore, our work also identifies CREB signaling pathway as a mediator of the early development of adult-born neurons. Moreover, sensory-driven activity predominantly regulates neuronal survival in the late phase.

References

Adelsberger, H., Garaschuk, O., Konnerth, A., 2005. Cortical calcium waves in resting newborn mice. Nat. Neurosci. 8, 988–990. doi:10.1038/nn1502

Aimone, J.B., Li, Y., Lee, S.W., Clemenson, G.D., Deng, W., Gage, F.H., 2014. Regulation and function of adult neurogenesis: From Genes to Cognition. Physiol. Rev. 94, 991–1026. doi:10.1152/physrev.00004.2014

Alonso, M., Viollet, C., Gabellec, M.-M., Meas-Yedid, V., Olivo-Marin, J.-C., Lledo, P.-M., 2006. Olfactory discrimination learning increases the survival of adult-born neurons in the olfactory bulb. J. Neurosci. 26, 10508–10513. doi:10.1523/JNEUROSCI.2633-06.2006

Altman, J., 1969. Autoradiographic and histological studies of postnatal neurogenesis. J. Comp. Neurol. 137, 433–457. doi:10.1002/cne.901370404

Altman, J., Das, G.D., 1965. Autoradiographic and histoloaical evidence of postnatal hippocampal neurogenesis in rats. J. Comp. Neurol. 124, 319–336. doi:10.1002/cne.901240303

Arieli, A., Sterkin, A., Grinvald, A., Aertsen, A., 1996. Dynamics of ongoing activity: explanation of the large variability in evoked cortical responses. Science 273, 1868–1871. doi:10.1126/science.273.5283.1868

Bagley, J., LaRocca, G., Jimenez, D.A., Urban, N.N., 2007. Adult neurogenesis and specific replacement of interneuron subtypes in the mouse main olfactory bulb. BMC Neurosci. 8, 92. doi:10.1186/1471-2202-8-92

Baker, H., Morel, K., Stone, D.M., Maruniak, J.A., 1993. Adult naris closure profoundly reduces tyrosine hydroxylase expression in mouse olfactory bulb. Brain Res. 614, 109–116. doi:10.1016/0006-8993(93)91023-L

Bando, Y., Hirano, T., Tagawa, Y., 2014. Dysfunction of KCNK potassium channels impairs neuronal migration in the developing mouse cerebral cortex. Cereb. Cortex 24, 1017–1029. doi:10.1093/cercor/bhs387

Bando, Y., Irie, K., Shimomura, T., Umeshima, H., Kushida, Y., Kengaku, M., Fujiyoshi, Y., Hirano, T., Tagawa, Y., 2016. Control of spontaneous Ca^{2+} transients is critical for neuronal maturation in the developing neocortex. Cereb. Cortex 26, 106–117. doi:10.1093/cercor/bhu180

Bastien-Dionne, P.O., David, L.S., Parent, A., Saghatelyan, A., 2010. Role of sensory activity on chemospecific populations of interneurons in the adult olfactory bulb. J. Comp. Neurol. 518, 1847–1861. doi:10.1002/cne.22307

Belluzzi, O., Benedusi, M., Ackman, J., LoTurco, J.J., 2003. Electrophysiological differentiation of new neurons in the olfactory bulb. J. Neurosci. 23, 10411–10418. doi:10.1371/journal.pone.0037742

Blankenship, A.G., Feller, M.B., 2010. Mechanisms underlying spontaneous patterned activity in developing neural circuits. Nat. Rev. Neurosci. 11, 18–29. doi:10.1038/nrn2759

Boldrini, M., Fulmore, C.A., Tartt, A.N., Simeon, L.R., Pavlova, I., Poposka, V., Rosoklija, G.B., Stankov, A., Arango, V., Dwork, A.J., Hen, R., Mann, J.J., 2018. Human hippocampal neurogenesis persists throughout aging. Cell Stem Cell 22, 589–599.

doi:10.1016/j.stem.2018.03.015

Bond, A.M., Ming, G., Song, H., 2015. Review Adult mammalian neural stem cells and neurogenesis : five decades later. Stem Cell 17, 385–395. doi:10.1016/j.stem.2015.09.003

Bovetti, S., Veyrac, A., Peretto, P., Fasolo, A., de Marchis, S., 2009. Olfactory enrichment influences adult neurogenesis modulating GAD67 and plasticity-related molecules expression in newborn cells of the olfactory bulb. PLoS One 4, e6395. doi:10.1371/journal.pone.0006359

Brunjes, P.C., Smith-Crafts, L.K., McCarty, R., 1985. Unilateral odor deprivation: Effects on the development of olfactory bulb catecholamines and behavior. Dev. Brain Res. 22, 1–6. doi:10.1016/0165-3806(85)90063-X

Cameron, A., Mcewen, S., Gould E, 1995. Regulation of adult neurogenesis by excitatory input and NMDA receptor activation in the dentate gyrus. J. Neurosci. 75, 4687–4692.

Cancedda, L., Fiumelli, H., Chen, K., Poo, M. -m., 2007. Excitatory GABA action is essential for morphological maturation of cortical neurons *in vivo*. J. Neurosci. 27, 5224–5235. doi:10.1523/JNEUROSCI.5169-06.2007

Carleton, A., Petreanu, L.T., Lansford, R., Alvarez-Buylla, A., Lledo, P.-M., 2003. Becoming a new neuron in the adult olfactory bulb. Nat. Neurosci. 507–518. doi:10.1038/nn1048

Cave, J.W., Baker, H., 2009. Dopamine systems in the forebrain. Adv. Exp. Med. Biol. 651, 15–35. doi:10.1007/978-1-4419-0322-8_2

Chen, Y., Ghosh, A., 2005. Regulation of dendritic development by neuronal activity. J. Neurobiol. 64, 4–10. doi:10.1002/neu.20150

Chevaleyre, V., Moos, F.C., Desarménien, M.G., 2002. Interplay between presynaptic and postsynaptic activities is required for dendritic plasticity and synaptogenesis in the supraoptic nucleus. J. Neurosci. 22, 265–73. doi:22/1/265 [pii]

Corotto, F.S., Henegars, J.R., 1994. Odor deprivation leads to reduced neurogenesis and reduced neuronal survival in the olfactory bulb of the adult mouse. Neuroscience 61, 739–744. https://doi.org/10.1016/0306-4522(94)90397-2.

Cummings, D.M., Henning, H.E., Brunjes, P.C., 1997. Olfactory bulb recovery after early sensory deprivation. J. Neurosci. 17, 7433–7440. doi:177433-08

Dahlen, J.E., Jimenez, D.A., Gerkin, R.C., Urban, N.N., 2011. Morphological analysis of activity-reduced adult-born neurons in the mouse olfactory bulb. Front. Neurosci. 5, 1–8. doi:10.3389/fnins.2011.00066

Darcy, D.P., Isaacson, J.S., 2009. L-Type calcium channels govern calcium signaling in migrating newborn neurons in the postnatal olfactory bulb. J. Neurosci. 29, 2510–2518. doi:10.1523/JNEUROSCI.5333-08.2009

De Marco García, N. V, Karayannis, T., Fishell, G., 2011. Neuronal activity is required for the development of specific cortical interneuron subtypes. Nature 472, 351–355. doi:10.1038/nature09865

Denizet, M., Cotter, L., Lledo, P.M., Lazarini, F., 2017. Sensory deprivation increases phagocytosis of adult-born neurons by activated microglia in the olfactory bulb. Brain. Behav. Immun. 60, 38–43. doi:10.1016/j.bbi.2016.09.015

Dennis, C. V., Suh, L.S., Rodriguez, M.L., Kril, J.J., Sutherland, G.T., 2016. Human adult neurogenesis across the ages: An immunohistochemical study. Neuropathol. Appl.

Neurobiol. 42, 621–638. doi:10.1111/nan.12337

Dworkin, S., Heath, J.K., deJong-Curtain, T.A., Hogan, B.M., Lieschke, G.J., Malaterre, J., Ramsay, R.G., Mantamadiotis, T., 2007. CREB activity modulates neural cell proliferation, midbrain-hindbrain organization and patterning in zebrafish. Dev. Biol. 307, 127–141. doi:10.1016/j.ydbio.2007.04.026

Dworkin, S., Mantamadiotis, T., 2010. Targeting CREB signalling in neurogenesis. Expert Opin. Ther. Targets 14, 869–879. doi:10.1517/14728222.2010.501332

Eriksson, P.S., Perfilieva, E., Bjork-Eriksson, T., Alborn, A.M., Nordborg, C., Peterson, D.A., Gage, F.H., 1998. Neurogenesis in the adult human hippocampus. Nat Med 4, 1313–1317. doi:10.1038/3305

Ferezou, I., Deneux, T., 2017. Review: How do spontaneous and sensory-evoked activities interact? Neurophotonics 4, 031221. doi:10.1117/1.NPh.4.3.031221

Fiske, B.K., Brunjes, P.C., 2001. Cell death in the developing and sensory-deprived rat olfactory bulb. J. Comp. Neurol. 431, 311–319.

Flavell, S.W., Greenberg, M.E., 2008. Signaling mechanisms linking neuronal activity to gene expression and plasticity of the nervous system. Annu. Rev. Neurosci. 31, 563–590. doi:10.1146/annurev.neuro.31.060407.125631

Frazier-Cierpial, L., Brunjes, P.C., 1989. Early postnatal cellular proliferation and survival in the olfactory bulb and rostral migratory stream of normal and unilaterally odor-deprived rats. 289, 481–492. doi:10.1002/cne.902890312

Fujioka, T., 2004. Activation of cAMP signaling facilitates the morphological maturation of newborn neurons in adult hippocampus. J. Neurosci. 24, 319–328. doi:10.1523/JNEUROSCI.1065.03.2004

García-González, D., Khodosevich, K., Watanabe, Y., Rollenhagen, A., Lübke, J.H.R., Monyer, H., 2017. Serotonergic projections govern postnatal neuroblast migration. Neuron 94, 534–549. doi:10.1016/j.neuron.2017.04.013

Giachino, C., 2005. cAMP response element-binding protein regulates differentiation and survival of newborn neurons in the olfactory bulb. J. Neurosci. 25, 10105–10118. doi:10.1523/JNEUROSCI.3512-05.2005

Goldman, S.A., Nottebohm, F., 1983. Neuronal production, migration, and differentiation in a vocal control nucleus of the adult female canary brain. Proc. Natl. Acad. Sci. 80, 2390–2394. doi:10.1073/pnas.80.8.2390

Good, P.R., Geary, N., Engen, T., 1976. The effect of estrogen on odor detection. Chem. Senses 2, 45–50. doi:10.1093/chemse/2.1.45

Gould, E., Tanapat, P., McEwen, B.S., Flugge, G., Fuchs, E., 1998. Proliferation of granule cell precursors in the dentate gyrus of adult monkeys is diminished by stress. Proc. Natl. Acad. Sci. 95, 3168–3171. doi:10.1073/pnas.95.6.3168

Gu, C., Jan, Y., Jan, L.Y., 2003. A Conserved Domain in Axonal Targeting of Kv1 (Shaker) Voltage-Gated Potassium Channels. Science 80, 646–649. doi:10.1126/science.1086998

Gu, X., Spitzer, N.C., 1995. Distinct aspects of neuronal differentiation encoded by frequency of calcium transients. Nature 375, 784–787.

Guthrie, K.M.; Wilson, D.A.; Leon, M., 1999. Early unilateral deprivation modifies olfactory bulb function. J. Neurosci. 10, 3402–3412.

doi:https://doi.org/10.1523/JNEUROSCI.10-10-03402.1990

Gütig, R., Sompolinsky, H., 2006. The tempotron: a neuron that learns spike timing–based decisions. Nat. Neurosci. 9, 420–428. doi:10.1038/nn1643

Hanganu-Opatz, I.L., 2010. Between molecules and experience: Role of early patterns of coordinated activity for the development of cortical maps and sensory abilities. Brain Res. Rev. 64, 160–176. doi:10.1016/j.brainresrev.2010.03.005

Herold, S., Jagasia, R., Merz, K., Wassmer, K., Lie, D.C., 2011. CREB signalling regulates early survival, neuronal gene expression and morphological development in adult subventricular zone neurogenesis. Mol. Cell. Neurosci. 46, 79–88. doi:10.1016/j.mcn.2010.08.008

Homma, R., Kovalchuk, Y., Konnerth, A., Cohen, L.B., Garaschuk, O., 2013. *In vivo* functional properties of juxtaglomerular neurons in the mouse olfactory bulb. Front. Neural Circuits 7, 1–23. doi:10.3389/fncir.2013.00023

Hurni, N., Kolodziejczak, M., Tomasello, U., Badia, J., Jacobshagen, M., Prados, J., Dayer, A., 2017. Transient cell-intrinsic activity regulates the migration and laminar positioning of cortical projection neurons. Cereb. Cortex 27, 3052–3063. doi:10.1093/cercor/bhx059

Jagasia, R., Steib, K., Englberger, E., Herold, S., Faus-Kessler, T., Saxe, M., Gage, F.H., Song, H., Lie, D.C., 2009. GABA-cAMP response element-binding protein signaling regulates maturation and survival of newly generated neurons in the adult hippocampus. J. Neurosci. 29, 7966–7977. doi:10.1523/JNEUROSCI.1054-09.2009

Johns, D.C., Marx, R., Mains, R.E., O'Rourke, B., Marbán, E., 1999. Inducible genetic suppression of neuronal excitability. J. Neurosci. 19, 1691–7.

Kaplan, M.S., McNelly, N. a, Hinds, J.W., 1985. Population dynamics of adult-formed granule neurons of the rat olfactory bulb. J. Comp. Neurol. 239, 117–25. doi:10.1002/cne.902390110

Kato, H.K., Chu, M.W., Isaacson, J.S., Komiyama, T., 2012. Dynamic sensory representations in the olfactory bulb: modulation by wakefulness and experience. Neuron 76, 962–975. doi:10.1016/j.neuron.2012.09.037

Kirkby, L.A., Sack, G.S., Firl, A., Feller, M.B., 2013. A role for correlated spontaneous activity in the assembly of neural circuits. Neuron 80, 1129–1144. doi:10.1016/j.neuron.2013.10.030

Kirschenbaum, B., Doetsch, F., Lois, C., Alvarez-buylla, A., 1999. Adult subventricular zone neuronal precursors continue to proliferate and migrate in the absence of the olfactory bulb J. Neurosci. 19, 2171–2180. https://doi.org/10.1523/JNEUROSCI.19-06-02171.1999

Komuro, H., Rakic, P., 1996. Intracellular Ca^{2+} fluctuations modulate the rate of neuronal migration. Neuron 17, 275–285. https://doi.org/10.1016/S0896-6273(00)80159-2

Komuro, Y., Galas, L., Lebon, A., Raoult, E., Fahrion, J.K., Tilot, A., Kumada, T., Ohno, N., Vaudry, D., Komuro, H., 2015. The role of calcium and cyclic nucleotide signaling in cerebellar granule cell migration under normal and pathological conditions. Dev. Neurobiol. 75, 369–387. doi:10.1002/dneu.22219

Kornhauser, J.M., Cowan, C.W., Shaywitz, A.J., Dolmetsch, R.E., Griffith, E.C., Hu, L.S., Haddad, C., Xia, Z., Greenberg, M.E., 2002. CREB transcriptional activity in neurons is regulated by multiple, calcium-specific phosphorylation events. Neuron 34, 221–233. doi:10.1016/S0896-6273(02)00655-4

Kovalchuk, Y., Homma, R., Liang, Y., Maslyukov, A., Hermes, M., Thestrup, T., Griesbeck, O.,

Ninkovic, J., Cohen, L.B., Garaschuk, O., 2015. *In vivo* odourant response properties of migrating adult-born neurons in the mouse olfactory bulb. Nat. Commun. 6, 6349. doi:10.1038/ncomms7349

Lacar, B., Young, S.Z., Platel, J.C., Bordey, A., 2011. Gap junction-mediated calcium waves define communication networks among murine postnatal neural progenitor cells. Eur. J. Neurosci. 34, 1895–1905. doi:10.1111/j.1460-9568.2011.07901.x

Liang, Y., Li, K., Riecken, K., Maslyukov, A., Gomez-Nicola, D., Kovalchuk, Y., Fehse, B., Garaschuk, O., 2016. Long-term *in vivo* single-cell tracking reveals the switch of migration patterns in adult-born juxtaglomerular cells of the mouse olfactory bulb. Cell Res. 26, 1–17. doi:10.1038/cr.2016.55

Lin, C.W., Sim, S., Ainsworth, A., Okada, M., Kelsch, W., Lois, C., 2010. Genetically increased cell-intrinsic excitability enhances neuronal integration into adult brain circuits. Neuron 65, 32–39. doi:10.1016/j.neuron.2009.12.001

Liu, X.S., Chopp, M., Zhang, X.G., Zhang, R.L., Buller, B., Hozeska-Solgot, A., Gregg, S.R., Zhang, Z.G., 2009. Gene profiles and electrophysiology of doublecortin-expressing cells in the subventricular zone after ischemic stroke. J. Cereb. Blood Flow Metab. 29, 297–307. doi:10.1038/jcbfm.2008.119

Livneh, Y., Adam, Y., Mizrahi, A., 2014. Odor processing by adult-born neurons. Neuron 81, 1097–110. doi:10.1016/j.neuron.2014.01.007

Livneh, Y., Mizrahi, A., 2011. Long-term changes in the morphology and synaptic distributions of adult-born neurons. J. Comp. Neurol. 519, 2212–24. doi:10.1002/cne.22625

Lledo, P.-M., Alonso, M., Grubb, M.S., 2006. Adult neurogenesis and functional plasticity in neuronal circuits. Nat. Rev. Neurosci. 7, 179–93. doi:10.1038/nrn1867

Lledo, P.-M., Saghatelyan, A., Lemasson, M., 2004. Inhibitory Interneurons in the Olfactory Bulb: From Development to Function. Neurosci. 10, 292–303. doi:10.1177/1073858404263460

Lledo, P.M., Merkle, F.T., Alvarez-Buylla, A., 2008. Origin and function of olfactory bulb interneuron diversity. Trends Neurosci. 31, 392–400. doi:10.1016/j.tins.2008.05.006

Lohmann, C., Wong, R.O.L., 2005. Regulation of dendritic growth and plasticity by local and global calcium dynamics 37, 403–409. doi:10.1016/j.ceca.2005.01.008

Lois, C., Alvarez-Buylla, A., 1994. Long-distance neuronal migration in the adult mammalian brain. Science 264, 1145–1148. doi:10.1126/science.8178174

Lois, C., Hong, E.J., Pease, S., Brown, E.J., Baltimore, D., 2002. Germline transmission and tissue-specific expression of transgenes delivered by lentiviral vectors. Science 295, 868–72. doi:10.1126/science.1067081

Lonze, B.E., Ginty, D.D., 2002. Function and regulation of CREB family transcription factors in the nervous system. Neuron 35, 605–623. doi:10.1016/S0896-6273(02)00828-0

Lonze, B.E., Riccio, A., Cohen, S., Ginty, D.D., 2002. Apoptosis, axonal growth defects, and degeneration of peripheral neurons in mice lacking CREB. Neuron 34, 371–385. doi:10.1016/S0896-6273(02)00686-4

Luhmann, H.J., Sinning, A., Yang, J.-W., Reyes-Puerta, V., Stüttgen, M.C., Kirischuk, S., Kilb, W., 2016. Spontaneous neuronal activity in developing neocortical networks: from single cells to large-scale interactions. Front. Neural Circuits 10, 1–14. doi:10.3389/fncir.2016.00040

Luskin, M.B., 1993. Restricted proliferation and migration of postnatally generated neurons

derived from the forebrain subventricular zone. Neuron 11, 173–189. doi:10.1016/0896-6273(93)90281-U

Mandairon, N., Jourdan, F., Didier, A., 2003. Deprivation of sensory inputs to the olfactory bulb up-regulates cell death and proliferation in the subventricular zone of adult mice. Neuroscience 119, 507–516. doi:10.1016/S0306-4522(03)00172-6

Mandairon, N., Sacquet, J., Jourdan, F., Didier, A., 2006. Long-term fate and distribution of newborn cells in the adult mouse olfactory bulb: Influences of olfactory deprivation. Neuroscience 141, 443–51. doi:10.1016/j.neuroscience.2006.03.066

Maslyukov, A., Li, K., Su, X., Kovalchuk, Y., Garaschuk, O., 2018. Spontaneous calcium transients in the immature adult-born neurons of the olfactory bulb. Cell Calcium. doi:10.1016/j.ceca.2018.06.001

Ming, G., Song, H., 2011. Review adult neurogenesis in the mammalian brain : significant answers and significant questions. Neuron 70, 687–702. doi:10.1016/j.neuron.2011.05.001

Mizrahi, A., 2007. Dendritic development and plasticity of adult-born neurons in the mouse olfactory bulb. Nat. Neurosci. 10, 444–452. doi:10.1038/nn1875

Moreno, M.M., Linster, C., Escanilla, O., Sacquet, J., Didier, A., Mandairon, N., 2009. Olfactory perceptual learning requires adult neurogenesis. Proc. Natl. Acad. Sci. 106, 17980–17985. doi:10.1073/pnas.0907063106

Nakagawa, S., Kim, J.-E., Lee, R., Malberg, J.E., Chen, J., Steffen, C., Zhang, Y.-J., Nestler, E.J., Duman, R.S., 2002. Regulation of neurogenesis in adult mouse hippocampus by cAMP and the cAMP response element-binding protein. J. Neurosci. 22, 3673–3682. doi:20026301

Nicoll, R.A., 1972. The effects of anaesthetics on synaptic excitation and inhibition in the olfactory bulb. J. Physiol. 223, 803–814. doi:10.1113/jphysiol.1972.sp009875

Nitabach, M.N., Blau, J., Holmes, T.C., 2002. Electrical Silencing of Drosophila Pacemaker Neurons Stops the Free-Running Circadian Clock. Cell 109, 485–495.

Okada, M., Andharia, N., Matsuda, H., 2015. Increase in the titer of lentiviral vectors expressing potassium channels by current blockade during viral vector production. BMC Neurosci. 16, 30. doi:10.1186/s12868-015-0159-1

Owens, D.F., Flint, a C., Dammerman, R.S., Kriegstein, a R., 2000. Calcium dynamics of neocortical ventricular zone cells. Dev. Neurosci. 22, 25–33. doi:10.1159/000017424

Owens, D.F., Kriegstein, a R., 1998. Patterns of intracellular calcium fluctuation in precursor cells of the neocortical ventricular zone. J. Neurosci. 18, 5374–5388.

Parent, J.M., Yu, T.W., Leibowitz, R.T., Geschwind, D.H., Sloviter, R.S., Lowenstein, D.H., 1997. Dentate granule cell neurogenesis is increased by seizures and contributes to aberrant network reorganization in the adult rat hippocampus. J. Neurosci. 17, 3727–3738.

Penn, A.A., Shatz, C.J., 1999. Brain waves and brain wiring: the role of endogenous and sensory-driven neural activity in development. Pediatr. Res. 45, 447–458. doi:10.1203/00006450-199904010-00001

Petreanu, L., Alvarez-Buylla, A., 2002. Maturation and death of adult-born olfactory bulb granule neurons: role of olfaction. J. Neurosci. 22, 6106–6113. doi:20026588\r22/14/6106 [pii]

Pietras, R.J., Moulton, D.G., 1974. Hormonal influences on odor detection in rats: Changes associated with the estrous cycle, pseudopregnancy, ovariectomy, and administration of testosterone propionate. Physiol. Behav. 12, 475–491. doi:10.1016/0031-9384(74)90125-5

Platel, J.C., Lacar, B., Bordey, A., 2007. GABA and glutamate signaling: Homeostatic control of adult forebrain neurogenesis. J. Mol. Histol. 38, 303–311. doi:10.1007/s10735-007-9103-8

Pothayee, N., Cummings, D.M., Schoenfeld, T.J., Dodd, S., Cameron, H.A., Belluscio, L., Koretsky, A.P., 2017. Magnetic resonance imaging of odorant activity-dependent migration of neural precursor cells and olfactory bulb growth. Neuroimage 158, 232–241. doi:10.1016/j.neuroimage.2017.06.060

Rajan, I., Cline, H.T., 1998. Glutamate receptor activity is required for normal development of tectal cell dendrites *in vivo*. J. Neurosci. 18, 7836–7846.

Rochefort, C., Gheusi, G., Vincent, J.-D., Lledo, P.-M., 2002. Enriched odor exposure increases the number of newborn neurons in the adult olfactory bulb and improves odor memory. J. Neurosci. 22, 2679–2689. doi:20026260

Rochefort, C., Lledo, P.M., 2005. Short-term survival of newborn neurons in the adult olfactory bulb after exposure to a complex odor environment. Eur. J. Neurosci. 22, 2863–2870. doi:10.1111/j.1460-9568.2005.04486.x

Rosenberg, S.S., Spitzer, N.C., 2011. Calcium signaling in neuronal development. Cold Spring Harb. Perspect. Biol. 3, a004259–a004259. doi:10.1101/cshperspect.a004259

Rudolph, D., Tafuri, A., Gass, P., Hämmerling, G.J., Arnold, B., Schütz, G., 1998. Impaired fetal T cell development and perinatal lethality in mice lacking the cAMP response element binding protein. Proc. Natl. Acad. Sci. U. S. A. 95, 4481–6. doi:10.1073/pnas.95.8.4481

Saghatelyan, A., Roux, P., Migliore, M., Rochefort, C., Desmaisons, D., Charneau, P., Shepherd, G.M., Lledo, P.M., 2005. Activity-dependent adjustments of the inhibitory network in the olfactory bulb following early postnatal deprivation. Neuron 46, 103–116. doi:10.1016/j.neuron.2005.02.016

Sailor, K.A., Valley, M.T., Wiechert, M.T., Riecke, H., Sun, G.J., Adams, W., Dennis, J.C., Sharafi, S., Ming, G. li, Song, H., Lledo, P.M., 2016. Persistent structural plasticity optimizes sensory information processing in the olfactory bulb. Neuron 91, 384–396. doi:10.1016/j.neuron.2016.06.004

Sakamoto, K., Karelina, K., Obrietan, K., 2011. CREB: A multifaceted regulator of neuronal plasticity and protection. J. Neurochem. 116, 1–9. doi:10.1111/j.1471-4159.2010.07080.x

Shaywitz, A.J., Greenberg, M.E., 1999. CREB: A stimulus-induced transcription factor activated by a Diverse array of extracellular signals. Annu. Rev. Biochem. 68, 821–861. doi:10.1146/annurev.biochem.68.1.821

Sorrells, S.F., et al., 2018. Human hippocampal neurogenesis drops sharply in children to undetectable levels in adults. Nature. doi:10.1038/nature25975

Spalding, K.L., et al., 2013. Dynamics of hippocampal neurogenesis in adult humans. Cell 153, 1219–1227. doi:10.1016/j.cell.2013.05.002

Sultan, S., Lefort, J.M., Sacquet, J., Mandairon, N., Didier, A., 2011. Acquisition of an olfactory associative task triggers a regionalized down-regulation of adult born neuron cell death. Front. Neurosci. 5, 1–9. doi:10.3389/fnins.2011.00052

Syrbe, S., et al., 2015. De novo loss- or gain-of-function mutations in KCNA2 cause epileptic encephalopathy. Nat. Genet. 47, 393–399. doi:10.1038/ng.3239

Thestrup, T.,et al., 2014. Optimized ratiometric calcium sensors for functional *in vivo* imaging of neurons and T lymphocytes. Nat. Methods 11, 175–82. doi:10.1038/nmeth.2773

Wachowiak, M., Economo, M.N., Díaz-Quesada, M., Brunert, D., Wesson, D.W., White, J.A., Rothermel, M., 2013. Optical dissection of odor information processing *in vivo* using GCaMPs expressed in specified cell types of the olfactory bulb. Ann. Intern. Med. 158, 5285–8300. doi:10.1523/JNEUROSCI.4824-12.2013

Walker, T.L., Yasuda, T., Adams, D.J., Bartlett, P.F., 2007. The doublecortin-expressing population in the developing and adult brain contains multipotential precursors in addition to neuronal-lineage cells. J. Neurosci. 27, 3734–3742. doi:10.1523/JNEUROSCI.5060-06.2007

Wang, D.D., 2003. Biophysical properties and ionic signature of neuronal progenitors of the postnatal subventricular zone *in situ*. J. Neurophysiol. 90, 2291–2302. doi:10.1152/jn.01116.2002

Weissman, T.A., Riquelme, P.A., Ivic, L., Flint, A.C., Kriegstein, A.R., 2004. Calcium waves propagate through radial glial cells and modulate proliferation in the developing neocortex. Neuron 43, 647–661. doi:10.1016/j.neuron.2004.08.015

West, A.E., Greenberg, M.E., 2011. Neuronal activity – regulated gene transcription in synapse development and cognitive function. Cold Spring Harb Perspect Biol 1–21. doi:10.1101/cshperspect.a005744

Winner, B., Cooper-Kuhn, C.M., Aigner, R., Winkler, J., Kuhn, H.G., 2002. Long-term survival and cell death of newly generated neurons in the adult rat olfactory bulb. Eur. J. Neurosci. 16, 1681–1689. doi:10.1046/j.1460-9568.2002.02238.x

Yamaguchi, M., Mori, K., 2014. Critical periods in adult neurogenesis and possible clinical utilization of new neurons. Front. Neurosci. 8, 2013–2015. doi:10.3389/fnins.2014.00177

Yamaguchi, M., Mori, K., 2005. Critical period for sensory experience-dependent survival of newly generated granule cells in the adult mouse olfactory bulb. Proc. Natl. Acad. Sci. U. S. A. 102, 9697–9702. doi:10.1073/pnas.0406082102

Yasuda, T., Adams, D.J., 2010. Physiological roles of ion channels in adult neural stem cells and their progeny. J. Neurochem. 114, 946–959. doi:10.1111/j.1471-4159.2010.06822.x

Yu, C.R., Power, J., Barnea, G., O'Donnell, S., Brown, H.E.V., Osborne, J., Axel, R., Gogos, J.A., 2004. Spontaneous neural activity is required for the establishment and maintenance of the olfactory sensory map. Neuron 42, 553–566. doi:10.1016/S0896-6273(04)00224-7

Zhao, C., Deng, W., Gage, F.H., 2008. Mechanisms and Functional Implications of Adult Neurogenesis. Cell 132, 645–660. doi:10.1016/j.cell.2008.01.033

Zheng, J.Q., Poo, M., 2007. Calcium Signaling in Neuronal Motility. Annu. Rev. Cell Dev. Biol. 23, 375–404. doi:10.1146/annurev.cellbio.23.090506.123221

Zhu, D.Y., Lau, L., Liu, S.H., Wei, J.S., Lu, Y.M., 2004. Activation of cAMP-response-element-binding protein (CREB) after focal cerebral ischemia stimulates neurogenesis in the adult dentate gyrus. Proc. Natl. Acad. Sci. U. S. A. 101, 9453–7. doi:10.1073/pnas.0401063101

Zusammenfassung

Täglich wandern Tausende neue adult-geborene Neurone in den Riechkolben der Maus ein. Die Mechanismen, die der Migration, der Morphogenese und dem Überleben adult-geborener Neurone zugrunde liegen, sind jedoch weitgehend unbekannt. In der vorliegenden Arbeit untersuchten wir *in vivo* den Einfluss endogener und sensorisch-evozierter neuronaler Aktivität auf die Entwicklung adult-geborener Neurone im Riechkolben der Maus. Um die endogene Aktivität adult-geborener Neurone genetisch zu verändern induzierten wir eine Überexpression des Kaliumkanals Kv1.2 oder Kir2.1. Mittels *in vivo* Zwei-Photonen-Ca^{2+}-Mikroskopie in wachen Mäusen konnten wir sowohl in Kontrollzellen, als auch in den Kv1.2- und Kir2.1-überexprimierenden adult-geborenen Neuronen spontane Ca^{2+}-Transienten nachweisen. Die Überexpression von Kv1.2 bzw. Kir2.1 veränderte hierbei selektiv das „Spiking-Verhalten" stark aktiver und kontinuierlich aktiver Neurone. Der Anteil der stark aktiven Zellen, sowie die Fläche unter der Kurve des Ca^{2+}-Signals und das maximale Twitch-2B-Verhältnis, welches das intrazelluläre Ca^{2+}-Level wiederspiegelt, waren erniedrigt. Bei weiterer Untersuchung dieser Kv1.2- und Kir2.1-überexprimierenden Neuronen fanden wir heraus, dass ihre Migration, Morphogenese, ihr Duftstoff-evoziertes Antwortverhalten und ihre Überlebensrate in der frühen Phase (14-25 DPI) deutlich beeinträchtigt waren. Während Kv1.2-überexprimierende adult-geborene Neurone in der späten Phase (25-45 DPI), eine ähnliche Überlebensrate zeigten wie die Kontrollzellen, zeigten die Kir2.1-überexprimierenden Zellen eine signifikant niedrigere Überlebensrate. Dies ist vermutlich darauf zurückzuführen, dass, anders als bei der Kv1.2-Überexpression, bei welcher lediglich die endogene Aktivität verändert war, bei der Kir2.1-Überexpression sowohl die endogene als auch die sensorisch-evozierte Aktivität beeinträchtigt war. Diese Daten deuten darauf hin, dass das Überleben adult-geborener Neurone in der frühen Phase durch die endogene Aktivität und in der späten Phase durch die sensorisch-evozierte Aktivität bestimmt wird.

Darüber hinaus haben wir den Einfluss sensorisch-evozierter Aktivität auf die Entwicklung adult-geborener Neurone untersucht. Überraschenderweise zeigten adult-geborene Neurone unter „Geruchsdeprivation" eine normale Migrationsgeschwindigkeit und Morphologie, was darauf hindeutet, dass die sensorisch-evozierte Aktivität die Entwicklung der adult-geborenen Neuronen nicht beeinflusst. Weitere Analysen ergaben, dass adult-geborene Neurone trotz „Geruchsdeprivation" eine normale endogene Aktivität zeigten.

Wir untersuchten auch das Zusammenspiel zwischen endogener und sensorisch-evozierter Aktivität. Mit Hilfe von *in vivo* Ca^{2+}-Messungen einzelner Zellen konnten wir nachweisen, dass eine beeinträchtigte endogene Aktivität mit einer unterdrückten sensorischen Aktivität einherging. Allerdings, änderte die "Geruchsdeprivation" nicht die Eigenschaften der endogenen Aktivität adult-geborener Neurone. Dies deutet darauf hin, dass die endogene Aktivität in unreifen adult-geborenen Neuronen robust ist.

Schließlich untersuchten wir, welcher Signalweg an der Entwicklung adult-geborener Neurone beteiligt ist. Unsere Ergebnisse zeigten, dass die pCREB-Expression in Kv1.2- und Kir2.1-überexprimierenden adult-geborenen Neuronen herunterreguliert wurde. Wir vermuten, dass eine beeinträchtigte endogene Aktivität den Ca^{2+}-pCREB-Signalweg und Expression von pCREB-abhängigen Genen hemmt.

Zusammengefasst zeigen unsere Daten, dass die endogene neuronale Aktivitätskopplung mit dem CREB-Signalweg im Riechkolben der Maus, die Migration, Morphogenese und das Überleben in der frühen Phase reguliert. unsere Daten identifizieren eine wichtige Rolle von Kv1.2/Kir2.1 in den oben genannten Entwicklungsprozessen. Darüber hinaus identifiziert unsere Arbeit auch den CREB-Signalweg als Vermittler für die frühe Entwicklung von erwachsenen Neuronen. Die sensorisch-evozierte Aktivität hingegen reguliert das Überleben adult-geborener Neurone in der späten Phase.

Publications

Parts of the results presented in this thesis were published in the papers:

Maslyukov, A.*, **Li, K.***, Su, X., Kovalchuk, Y., Garaschuk, O., 2018. Spontaneous calcium transients in the immature adult-born neurons of the olfactory bulb. Cell Calcium. 74:43-52. doi:10.1016/j.ceca.2018.06.001 (***shared first authorship**)

Liang, Y., **Li, K.**, Riecken, K., Maslyukov, A., Gomez-Nicola, D., Kovalchuk, Y., Fehse, B., Garaschuk, O., 2016. Long-term *in vivo* single-cell tracking reveals the switch of migration patterns in adult-born juxtaglomerular cells of the mouse olfactory bulb. Cell Res. 26, 1–17. doi:10.1038/cr.2016.55

Declaration of contribution

The dissertation work was carried out in the Institute of Physiology, Department of Neurophysiology, at the Eberhard Karls Universität Tübingen under the supervision of Professor Olga Garaschuk. The study was conceived by Professor Olga Garaschuk. Mr. Xin Su contributed to Sholl analysis. I accomplished anything else (~95%) in this study. I hereby declare that I have produced the work entitled "Endogenous activity regulates the early development of adult-born neurons in the mouse olfactory bulb", submitted for the award of a doctorate on my own, have used only the sources and aids indicated and have marked passages included from other works. I swear upon oath that these statements are true and that I have not concealed anything. I am aware that making a false declaration under oath is punishable by a term of imprisonment of up to three years or by a fine.

Tübingen, 13.06.2018

Signature:

Acknowledgment

Curriculum vitae

EDUCATION AND EMPLOYMENT
- Universität Tübingen, Germany   2014 -- 2018
  Ph.D., Experimental Medicine: Neurophysiology
  Dissertation: Endogenous activity regulates the early development of adult-born neurons in the mouse olfactory bulb
- Simcere pharmaceutical R&D center, Nanjing, China   2010 -- 2013
  Novel drug innovation for Alzheimer´s diseases *in vitro* targeting GSK-3β and BACE-1
- Nanjing Normal University, China   2007 -- 2010
  M.Sc., Cell Biology.
  Thesis: The role of NRAGE in NGF-stimulated neurite outgrowth
- Weifang University, China   2003 -- 2007
  B.Sc., Biology

AWARDS AND HONORS
- Honorary Assistant Research Scientist, by Nanjing City Hall   2013
- Annual outstanding individual in Simcere R&D center   2012
- Hengli development scholarship in Nanjing Normal University   2009
- Excellent bachelor thesis in Weifang University   2007
- Weifang University scholarship   2006

PUBLICATIONS
- **Li K**, Su X, Kovalchuk Y, Garaschuk O. Endogenous but not sensory-driven activity regulates the early development of adult-born neurons. (*manuscript in preparation*)
- Maslyukov A*, **Li K***, Su X, Kovalchuk Y, Garaschuk O, 2018. Spontaneous calcium transients in the immature adult-born neurons of the olfactory bulb. Cell Calcium, 74:43-52. (***shared first authorship**)
- Brawek B*, Liang Y*, Savitska D, **Li K**, Fomin-Thunemann N, Kovalchuk Y, Zirdum E, Jakobsson J, Garaschuk O, 2017. A new approach for ratiometric *in vivo* calcium imaging of microglia. Scientific Reports; 7(1):6030.
- Askew K, **Li K**, Olmos Alonso A, et al., 2017. Coupled proliferation and apoptosis maintain the rapid turnover of microglia in the adult brain. Cell Reports; 18(2):391-405.
- Liang Y, **Li K**, Riecken K, Maslyukov A, Gomez-Nicola D, Kovalchuk Y, Fehse B, Garaschuk O, 2016. Long-term *in vivo* single-cell tracking reveals the switch of migration patterns in adult-born juxtaglomerular cells of the mouse olfactory bulb. Cell Research; 26:805-821.
- Feng Z, **Li K**, Liu M, Wen C, 2010. NRAGE is a negative regulator of nerve growth factor-stimulated neurite outgrowth in PC12 cells mediated through TrkA-ERK signaling. J Neurosci Res.; 88(8):1822-8.